Universidade de São Paulo
Instituto de Física

Análise da troca de gases traço entre a atmosfera livre e a camada limite planetária na Amazônia

Guido Giovanelli Haytzmann

Orientador(a): Prof. Dr. Luiz Augusto Toledo Machado

Dissertação de mestrado apresentada ao Instituto de Física da Universidade de São Paulo, como requisito parcial para a obtenção do título de Mestre(a) em Ciências.

Banca Examinadora:
Prof. Dr. Luiz Augusto Toledo Machado - Orientador (Universidade de São Paulo)
Prof. Dr. Micael Amore Cecchini (Universidade de São Paulo)
Prof. Dr. Jordi Villa-Guerau de Arellano (Universidade de Wageningen)

São Paulo
2024

FICHA CATALOGRÁFICA
Preparada pelo Serviço de Biblioteca e Informação
do Instituto de Física da Universidade de São Paulo

Haytzmann, Guido Giovanelli

Análise da troca de gases traço entre a atmosfera livre e a camada limite planetária na Amazônia. / Trace gas exchange between the free troposphere and the planetary boundary layer in the Amazon. São Paulo, 2024.

Dissertação (Mestrado) - Universidade de São Paulo, Instituto de Física. Depto. de Física Aplicada.

Orientador: Prof. Dr. Luiz Augusto Toledo Machado

Área de Concentração: Física Atmosférica.

Unitermos: 1. Amazônia; 2. ATTO; 3. Nuvens; 4. Gases; 5. CLP.

USP/IF/SBI-027/2024

University of São Paulo
Physics Institute

Trace gases exchange between the free troposphere and the planetary boundary layer in the Amazon

Guido Giovanelli Haytzmann

Supervisor: Prof. Dr. Luiz Augusto Toledo Machado

Dissertation submitted to the Physics Institute of the University of São Paulo in partial fulfillment of the requirements for the degree of Master of Science.

Examining Committee:
Prof. Dr. Luiz Augusto Toledo Machado - Supervisor (University of São Paulo)
Prof. Dr. Micael Amore Cecchini (University of São Paulo)
Prof. Dr. Jordi Villa-Guerau de Arellano (Wageningen University and Research)

São Paulo
2024

Agradecimentos

Acredito que seja mais difícil começar a seção de agradecimentos que começar a própria dissertação. De qualquer forma, eu vou começar agradecendo profundamente aos meus pais Ana Claudia e Carlos, e a Deus, pois sem eles não seria possível estar escrevendo este texto. Obrigado pai e mãe, por terem me apoiado e incentivado incondicionalmente até aqui. O amor e carinho de vocês é a coisa mais importante na minha vida.

Em segundo lugar, tenho que agradecer meu orientador Luiz Augusto Toledo Machado por ter me ajudado tanto durante todo o mestrado, e ter sido presente mesmo quando isso parecia impossível. Tenho certeza que levarei comigo os apredizados que tive com você para muito além da vida acadêmica.

Agradeço imensamente a você Ju, pelo companherismo, apoio e incentivo durante todo esse processo. Aproveito aqui para agradecer a toda a minha família, em especial minhas 2 avós, que seja da terra ou do céu, iluminam minha caminhada. Junto da família de sangue, agradeço toda minha família de coração por estarem comigo sempre. Sem vocês, nada disso faria sentido.

A todos os colegas do Laboratório de Física Atmosférica (LFA), minha gratidão pelo ambiente trabalho excelente, do qual me sinto feliz de fazer parte. Agradeço pelas conversas, ajudas, trocas de conhecimentos e pelos bons momentos.

A todos os membros da campanha CAFE-BRAZIL, meu muito obrigado por terem feito parte desse momento tão especial, a partir do qual me conectei fortemente com o trabalho do mestrado.

Agradeço imensamente a todos os membros do MAQ na Universidade de Wageningen por terem me recebido tão bem. Agradecimento especial aos professores Jordi Vila, Oscar Hartogensis e Luiz Machado por terem feito tudo acontecer. Aproveito esse momento para agradecer a todos os amigos que conheci em Wageningen. Vocês me acolheram e fizeram com que eu me sentisse em casa.

A toda equipe do Laero Toulouse e em especial ao Thibaut Dauhut, minha gratidão por terem me recebido tão bem. Guardo meus dias em Toulouse com muito carinho.

A todos os professores que passaram pela minha vida e contribuiram com minha formação, meu muito obrigado. Em especial ao Prof. Marcelo Barão, que dispertou meu interesse pela física, e ao Prof. Dr. Henrique de Melo Jorge Barbosa, que dispertou meu interesse pela física Atmosférica.

Muito obrigado a todos que contribuiram compartilhando os dados utilizados neste projeto.

Agradeço a todas as pessoas que de alguma forma contribuiram para que eu pudesse chegar até aqui.

O presente trabalho foi realizado com apoio do CNPq, Conselho Nacional de Desenvolvimento Científico e Tecnológico - Brasil.

Resumo

As emissões antropogênicas de gases de efeito de estufa estão causando o aumento da temperatura da Terra em um ritmo sem precedentes. Neste cenário, a floresta amazônica destaca-se pelos seus serviços ambientais prestados, como o armazenamento de carbono e a regulação dos ciclos biogeoquímicos globais. É, portanto, vital compreender os processos-chave que mantêm a floresta viva. Cientistas demonstraram que o solo da Amazônia depende do transporte de longa distância de nutrientes para suprir as necessidades da vegetação, como é o caso do fósforo. Esse transporte ocorre através de rios atmosféricos na troposfera livre. No entanto, pouco se sabe sobre como esses rios atmosféricos penetram na camada limite planetária (CLP). Este estudo tem como objetivo dar um primeiro passo para preencher esta lacuna de conhecimento, investigando a troca de gases traço entre a troposfera livre e a CLP na região amazônica. A investigação foi apoiada por vários conjuntos de dados obtidos na torre ATTO (Amazon Tall Tower of Observations), sobre concentrações de gases e parâmetros meteorológicos em diferentes alturas acima e dentro da copa da floresta. O estudo também utilizou o recém estabelecido sítio da Campina, que está equipado com uma vasta gama de radares e medições in-situ de parâmetros relacionados com as nuvens. A combinação de medições de perfis verticais de gases e da dinâmica atmosférica proporciona uma visão única da variabilidade das concentrações de gases na região amazônica. Duas campanhas recentes foram utilizadas para estudar a variabilidade dos gases: CloudRoots durante a estação seca e CAFE-BRASIL durante a estação chuvosa. Primeiro, foi realizada uma caracterização geral das nuvens convectivas rasas, congestus e profundas durante as estações seca e chuvosa. Foram observadas diferenças significativas nas características das nuvens entre as duas estações. As principais diferenças são as nuvens mais profundas durante a estação das chuvas e o papel do vapor de água precipitável (PWV), que define a atividade das nuvens durante a estação seca, mas tem valores semelhantes para todos os tipos de nuvens durante a estação das chuvas. A variabilidade da concentração de gás durante os eventos de cobertura de nuvens foi então investigada para diferentes tipos de nuvens. Uma análise cuidadosa mostrou que as nuvens profundas têm a maior influência nas concentrações superficiais de gases traço, especialmente O_3 e CO_2. Um estudo de caso mostrou que as variações observadas nas concentrações destes gases durante um evento convectivo profundo são principalmente causadas pelo transporte de ar de altitudes mais elevadas para a CLP. Além disso, os resultados deste estudo indicaram diferenças relevantes nos processos que determinam as concentrações de CO e de carbono negro durante as duas estações. O padrão sinótico se mostrou crucial para a variabilidade dos gases vestigiais durante a estação seca. Por fim, as variações significativas dos gases que ocorreram desatreladas a precipitação foram investigadas utilizando simulações do modelo MesoNH, com intuito de avaliar a potencial contribuição das ondas de gravidade geradas por convecção no transporte de massas de ar da troposfera livre para a CLP. Os resultados indicam que as ondas de gravidade induzem flutuações no campo de vapor de água na CLP. Este efeito pode estar relacionado às flutuações das concentrações de gases traço à medida que as linhas de tempestade se aproximam.

Palavras-chave: Amazônia, Nuvens, ATTO, Gases, CLP

Abstract

Anthropogenic emissions of greenhouse gases are causing the Earth's temperature to rise at an unprecedented rate. In this scenario, the Amazon rainforest stands out for its essential environmental services, such as carbon storage and regulation of global biogeochemical cycles. It is, therefore, vital to understand the key processes that keep the forest alive. Scientists have shown that Amazonian soils depend on the long-range transport of nutrients, such as phosphorus, to meet the needs of vegetation. This transport occurs through atmospheric rivers in the free troposphere. However, how these atmospheric rivers penetrate the planetary boundary layer (PBL) remains unclear. This study aims to take a first step towards filling this knowledge gap by investigating the exchange of trace gases between the free troposphere and the PBL in the Amazon region. The investigation was supported by several datasets from the Amazon Tall Tower Observatory (ATTO), which provided data on gas concentrations and meteorological parameters at different heights above and within the rainforest canopy. The study also used the recently established Campina site, which is equipped with a wide range of radars and in-situ measurements of cloud-related parameters. The combination of measurements of vertical gas profiles and atmospheric dynamics provides a unique insight into the variability of gas concentrations in the Amazon region. Two recent campaigns have been used to study the gas variability: CloudRoots during the dry season and CAFE-BRAZIL during the wet season. First, a general characterization of shallow, congestus, and deep convective clouds during the dry and wet seasons was performed. Significant differences in cloud characteristics were observed between the two seasons. The main differences are the deeper clouds during the rainy season and the role of the precipitable water vapor (PWV), which defines the cloud activity during the dry season but has similar values for all cloud types during the wet season. The variability of the gas concentration during cloud cover events was then investigated for different cloud types. A careful analysis showed that deep clouds have the greatest influence on surface concentrations of trace gases, especially O_3 and CO_2. A case study showed that the observed variations in these gas concentrations during a deep convective event are mainly caused by air transport from higher altitudes to the PBL. The results of this study indicated relevant differences in the processes driving CO and black carbon concentrations during the two seasons. The synoptic pattern is crucial for trace gas variability during the dry season. Finally, variability during non-rain events was investigated using model simulations from MesoNH to assess the potential contribution of convection-generated gravity waves in transporting air masses from the free troposphere into the PBL. The results indicate that gravity waves induce fluctuations in the water vapor field in the PBL. This effect could explainfluctuations in trace gas concentrations as squall lines approach.

Keywords: Amazon, Clouds, Gases, ATTO, PBL

List of Figures

Contents

1 Introduction

Heat waves, droughts, floods, and extreme weather events, in general, have increasingly impacted the world's population in recent years. Zhang et al. [2013] showed that the rising frequencies of extreme weather events correlate with Earth's increasing temperature. The United Nations considers climate change to be one of the major challenges for the twenty-first century. The International Panel of Climate Change IPCC [2022] claims that more than 3 billion people live in highly vulnerable regions to climate change. Scientists have demonstrated that the main cause of global warming is the anthropogenic emissions of greenhouse gases (GHG). According to IPCC, water vapor is the most important greenhouse gas; second is Carbon Dioxide (CO_2), which is the most important anthropogenic GHG, followed by Methane (CH_4). CO_2 is relevant to the greenhouse effect due to its substantial fossil fuel combustion and deforestation emissions. In addition, CO_2 has a long residence time in the atmosphere, causing emissions from the past to still play a role in present days. Methane (CH_4), is emitted mostly by agriculture activities and natural gas distributions Karakurt et al. [2012]. Therefore, monitoring the concentrations of these gases and studying their behaviors at numerous locations is of utmost importance for Climate Science.

Certain natural ecosystems stand out for their essential environmental services in the current global warming scenario. An important example is the Amazon rainforest due to its crucial role in carbon storage Malhi et al. [2006], regulating the Earth's biogeochemical, hydrological, and energetic cycles Artaxo et al. [2013], combined with the fact that it contains one of the greatest biodiversity in the planet. Despite its great relevance for maintaining life on Earth, human actions have harmed it with deforestation, mining, burning, and global warming. Sampaio et al. [2007] points out that the Amazonian ecosystem might be walking to a tipping point, from where the forest alone consumes itself to death. As a result, forests could move from carbon sinks to carbon emitters, and Gatti et al. [2021] shows this process is already happening in parts of the Amazon. Naturally, the transition of the forest from sink to source of carbon would have strong implications for climate change. Thus, it is fundamental to understand and model the processes that control the carbon cycle in the region. More than that, comprehending the forest by understanding the important processes that keep it alive has become an essential field of study. For this reason, a collective scientific effort aims to collect quality data in the region. The outcomes of this effort are multiple experiments, such as large-scale biosphere-atmosphere experiment in Amazonia (LBA) Nobre et al. [1996] and several data campaigns, such as the GoAmazon (2014) and ACRIDICON-CHUVA (Martin et al. [2016], Machado et al. [2018a], Wendisch et al. [2016]). Another great accomplishment for the studies of the Amazon in the last few years was the installation of the Amazon Tall Tower of Observation (ATTO) in 2015, which is located 150 km away from Manaus and is 325 m tall Andreae et al. [2015]. ATTO has monitored meteorological, chemical, and biological parameters, such as aerosol concentration, fluxes, size distributions, aerosols, greenhouse gases, volatile organic compounds (VOCs), and weather complementary data.

Scientists have discovered that Aerosol Atmospheric rivers (AAR), as defined in Chakraborty et al. [2021a], hold great importance for the health of the Amazonian ecosystem. That is because the forest's soil lacks nutrients and minerals. Yu et al. [2015] and Ben-Ami et al. [2010] have demonstrated that African dust deposition into the Amazon Basin can pro-

vide a significant amount of minerals and phosphorus, a key nutrient for the rainforest. In addition to that, it has been shown that the long range transport of Saharan dust and other aerosols from Africa to the Amazon Chakraborty et al. [2021b], are a important source of clouds condensation nuclei (CCN) in the region Holanda et al. [2020]. Atmospheric currents are also important for the humidity transport from the Amazon rainforest to southeast Brazil Salati et al. [1979]. Nevertheless, it is still unclear to science how these atmospheric rivers penetrate the planetary boundary layer (PBL). The first step to understanding that process is to investigate further **the relevant mechanisms for exchanging gases and particles between the free troposphere and the planetary boundary layer**.

To understand the exchange of gases and particles between the free troposphere and the PBL, it is necessary to incorporate the cloud reactor, where the major player is the vertical motion that drives the interaction between these two layers. Thus, any mechanism involved in this exchange must be linked to convection, especially up and downdrafts. Therefore, clouds are strong candidates to play a leading role in this process, as they are important vertical mixing agents of the atmosphere. For this reason, in the next paragraphs, a brief discussion will be presented on the relevance of clouds for the Earth's climate, particularly in the Amazon region.

Clouds are vital for the maintenance of life on Earth, not only because of their role in the water cycle but because they reflect part of the sun's radiation back to space and help cool the planet Ramanathan et al. [1989]. The science of aerosols and their direct and indirect effect on the planetary radiative budget has developed intensely in the past decade because clouds and aerosols interactions were the greatest source of uncertainties for future climate projections, according to the IPCC report of 2013 Stocker et al. [2013]. The Amazon region has been an essential place for clouds and aerosol science since its environment is very complex and propitiates the right conditions for studying the gas-aerosol-raindrops interactions Franco et al. [2022], Cecchini et al. [2016], which still is a topic with many questions to be further investigated. One factor that makes the Amazon the ideal environment for studying this topic is that the region has two well-defined seasons with different aerosol characteristics and sources. The wet season (January - May) is characterized by pristine atmospheric conditions Pöhlker et al. [2018] and high rates of precipitation. In this period, natural aerosols are predominant, such as pollen, fungus spores, and Secondary Organic Aerosols (SOA), which are originated by the oxidation of Volatile Organic Compounds (VOC) as described in Karl et al. [2009]. Even though the human impact is reduced during the wet season, it cannot be disregarded. Holanda et al. [2023] demonstrated that the long-range transport of air from African biomass burnings was the region's main source of Black Carbon during this period. Hence, describing how black carbon penetrates the planetary boundary layer during the wet season can provide valuable insights into how important nutrients and minerals go through the same process. On the other hand, the dry season (June - October) is characterized by polluted atmospheric conditions, low rain rates, occasional thunderstorms, and intense biomass-burning activity, which is the main source of the aerosols in this period. A further comprehension of how the Amazonian ecosystem behaves and responds to the different conditions from the different seasons holds great scientific significance, especially for understanding and modeling the environment under both heavy and mild human interference.

Recent studies pointed out that aerosols don't only affect but are also affected by the life cycle of clouds, especially storm clouds Machado et al. [2021]. Gases and aerosols

are transported by the up and downdrafts from the free troposphere to the boundary layer and the other way around. This turbulent process inside clouds propitiates the perfect conditions for new particle formation (NPF) Bardakov et al. [2022]. Model simulations have described how updrafts and downdrafts change particles and VOC concentration in the outflow of deep convection clouds Bardakov et al. [2021]. Another aspect of the presence of clouds relevant to the atmosphere's chemistry is that it decreases the incidence of radiation. Hence, it decreases the rate of photolysis of some chemical species and the rate of Photosynthesis Vilà-Guerau de Arellano et al. [2020], affecting the absorption of CO_2 by the vegetation. Nevertheless, different stages of clouds may have varying impacts on boundary layer conditions. This is due to different factors related to each cloud type, such as their unique up and downdraft patterns, the heights reached by the cloud top, and the mechanisms providing multiple atmospheric layers interaction, as illustrated in Figure 1. Besides, other cloud mechanisms can directly or indirectly affect the gas concentration, such as the thunderstorm lightning concentrations that modify the NO_x and Ozone (O_3) concentrations Brune et al. [2021]. A study evaluating how the different cloud types affect the trace gas surface concentration in the Amazon is missing and is this study's aim. Furthermore, on different cloud types, in the past years, scientists have been trying to understand what processes are important for activating the transition from shallow to deep convection in the Amazon, as in Zhuang et al. [2017] and Henkes et al. [2021]. Characterizing the behavior of several parameters, such as raindrop velocities, cloud top height, and precipitation rate from shallow and deep convection clouds, is essential for modeling this transition. This characterization was still incomplete, and is another goal of this study.

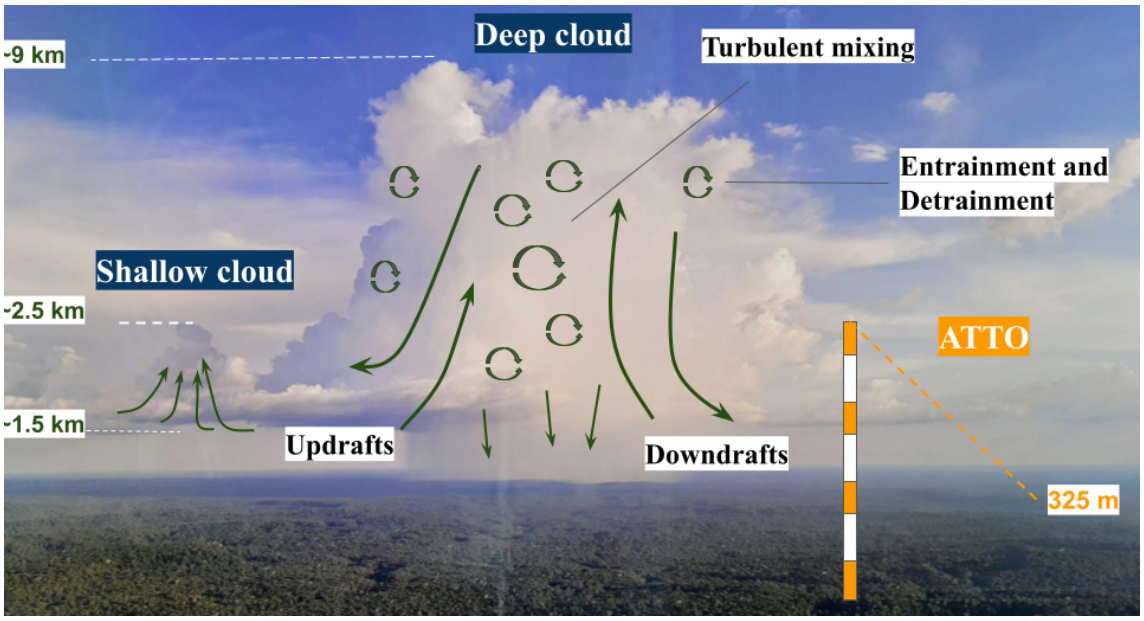

Figure 1: Illustration of the turbulent processes inside different cloud types. Adapted from https://turbli.com/blog/a-turbulent-world-thunderstorm-clouds/.

Several studies have demonstrated that thunderstorms produce atmospheric gravity waves Walterscheid et al. [2001], characterized by propagating oscillations of air masses. In other words, gravity waves are perturbations in the troposphere characterized by an al-

ternating pattern of up and downdrafts propagating radially from thunderstorms or squall lines. If these perturbations reach the PBL, they might break into it and inject air masses from the free troposphere inside the PBL. Consequently, if the gravity waves encounter atmospheric rivers, they might push the air inside the boundary layer. A first step in evaluating these hypotheses would be identifying gravity waves and verifying whether they can cause any variations in the boundary layer conditions. This study presents this analysis, employing computational models that will be further discussed in the next paragraphs.

Scientific experiments and instruments are very expensive, requiring a long and intense effort to work perfectly. Throughout the last few decades, computational modeling has greatly improved and became extremely important for climate science due to its ability to simulate several parameters' time evolution from a system by considering the initial and boundary conditions and the theoretical laws. In this study, computational modeling was useful to help identify convective-generated gravity waves, infer whether they can break the stable top layer into the PBL, and get insights into whether they can play a role in the exchange of gases and particles between the free troposphere and the PBL. For that, a model with high spatial and temporal resolution was necessary for simulating clouds, rain, and the environment of the Amazon rainforest. Multiple models can perform that analysis. In this study, through cooperation with the CNRS, the MESO-NH was selected as it is a well-suited tool to investigate the atmospheric dynamics in the tropics, especially the cloud organization, the associated circulations, and gravity waves generated by convection. The model will serve as a complementary analysis of the data.

As discussed above, understanding what are the important mechanisms involved in the exchange of air masses between the free troposphere and the PBL in the Amazon is necessary to clarify many aspects of the interactions of the forest with its atmosphere, which is essential for forecasting the future of the Amazon and hence of the Earth's climate. Aiming to obtain a deeper comprehension of this topic, this study analyzes the behavior of surface concentrations of CO, CO_2, CH_4, O_3, and Black Carbon (BC) in the Amazon under different cloud types. In addition, this study analyzes the peaks of variations of the aforementioned compounds and separates them into two situations: the ones that did and did not occur simultaneously with rainfall. The first situation is used to reinforce the role of clouds as vertical mixing agents of the atmosphere, whilst the second one is useful to study other dynamic mechanisms responsible for transporting gases and particles from the free troposphere to the surface, such as the gravity waves.

Carbon Dioxide and Methane were selected for this study because of their importance as greenhouse gases (GHG). Both gases have their main sources within the canopy heights in the studied region. For CO_2, it is the respiration process, and for Methane, it could be the emissions from the flooded areas in the forest or other fauna and flora activities. O_3 was selected due to its important role in the oxidation of VOCs to form SOA, and its vertical profiles are opposite to the last two compounds. O_3 has its source in the free troposphere, and it is rapidly consumed in chemical reactions near the forest, causing its concentrations to be higher at higher altitudes. Analyzing the variations in the concentrations of compounds with different vertical profiles is essential for investigating the vertical transport of air masses in the atmosphere. Finally, CO and BC were selected to be part of the analyses for being biomass-burning tracers. Black carbon itself can be especially useful to infer whether the air masses penetrating the boundary layer are local (dry season) or from long-range transport (wet season).

The data used in this study were measured during the CloudRoots and CAFE-BRAZIL campaigns at the ATTO site. The CloudRoots campaign happened in August 2022 (dry season) and was an effort to understand better the role of clouds in the Amazon's energy, water, and carbon cycles. One of the most important aspects of CloudRoots is its interdisciplinarity, as it aims to combine studies of evolving photosynthesis from the vegetation, variation of gas concentrations, heat transport, and cloud microphysics. The CAFE-BRAZIL (Chemistry of the Atmosphere Field Experiment in Brazil) occurred from December 2022 to January 2023 (wet season). It combined data from the High Altitude and Long Range Aircraft - HALO (https://halo-research.de/) with the ATTO complex measurements. The campaign aimed to investigate new particle formation, especially during deep convection events.

Due to the importance of comprehending the interactions between the Amazon rainforest and its atmosphere, many studies have been published in the last decades. Some focus on the importance of clouds Ouwersloot et al. [2013], and others focus on atmospheric chemistry Nascimento et al. [2022]. Other studies only analyze experimental data or focus on modeling. This study combines cloud, thermodynamics, and dynamics with the atmosphere's chemistry, using experimental and computational analysis provided by the CloudRoots and CAFE-BRAZIL campaigns and the MesoNH model simulations. With this synergy combination of data and tools, it was possible to characterize the main cloud types in Amazonian, their effect on trace gas concentration before, during, and after the cloud, the day and nighttime effect, the effect in different heights and the potential gravity wave production by storms and its effect on the interaction between boundary layer and free atmosphere.

2 Objectives

This study aims to improve the understanding of clouds and their effect on the atmospheric processing of the Amazonian biogeochemical reactor. Additionally, it explores how the free troposphere and the planetary boundary layer (PBL) exchange gases and particles. The specific objectives are:

- **S.O. 1 -** Study the main dynamic and thermodynamic characteristics of the shallow, congestus, and deep convective clouds.
- **S.O. 2 -** Study how different cloud types affects the concentration of CO_2, CO, CH_4, O_3, Black Carbon near the surface.
- **S.O. 3 -** Evaluate the contribution of up and downdrafts associated with clouds in transporting the aforementioned gases and particles from the free troposphere into the PBL and vice-versa.
- **S.O. 4 -** Examine peaks of variations of CO_2, CO, CH_4, O_3 and Black Carbon during the wet and dry season and determine their main causes.
- **S.O. 5 -** Evaluate the potential effect of atmospheric gravity waves produced by deep convective clouds in transporting gases and particles from the free troposphere to the PBL and vice-versa.

Combining these objectives, this study seeks to achieve a clearer comprehension of the Amazon Forest cycles involving, clouds, trace gases, and particles, which are fundamental for the maintenance of the forest's life.

3 Methodology

This section will present the instrumentation and the research strategy utilized in this study to accomplish the objectives.

3.1 Instrumentation

The ATTO complex provided all the experimental data used in this study. It includes the ATTO tower (325m), two secondary smaller towers, and the Campina site. The secondary towers are named Instant and Triangular Tower (81m), about 500m from ATTO. All towers monitor gases and particle concentrations and weather parameters. The Campina Site is located 4 km from ATTO, where the cloud instruments are settled.

3.1.1 ATTO tower

As mentioned before, the ATTO tower is a 325 meters tall tower, located 150 km away from Manaus, in the Uatumã Reserve, a highly conserved area in the heart of the Amazon Forest. It was built with the goal of long-term monitoring the concentrations of GHG, aerosols, and meteorological conditions, aiming to provide the ideal database to analyze how sensitive the forest is to climate change.

Figure 2: ATTO Tower. Adapted from https://www.attoproject.org/media/gallery/.

In this particular study, measurements of ozone and black carbon concentrations were taken at the ATTO tower. Ozone is sampled in 3 different height levels (80, 150, and 320m) by the instrument TEI 49i, which infers the O_3 concentrations by analyzing the absorption of ultraviolet radiation by air volume; the detection limits are 0.5 ppb. The instrument measures ozone concentration at a specific level every 10 seconds and switches the height level every 5 minutes. That is because there aren't instruments at every height

level, in fact there are inlets at every height level that transport the air from the different heights to the instruments that stay at the ground inside refrigerated containers. The Black Carbon measurements were taken at 320m by the Multi-Angle Absorption Photometer (MAAP). This instrument analyses the scattering of a beam of light (637 nm) at a glass fiber filter used to sample aerosol particles, making use of photometers disposed of in different scattering angles, which makes it possible to infer Black Carbon concentrations utilizing physics laws that describe radiative scattering as explained in Franco [2021].

3.1.2 Instant tower

The Instant Tower is an 81m tall tower located around 500m from ATTO. Carbon Dioxide (CO_2), Carbon Monoxide (CO), and Methane (CH_4) are monitored throughout this tower at multiple heights (4, 24, 38, 51, and 79m). The instrument responsible for the measurements of the concentrations of these gases is the Picarro G2401; it works based on the cavity ring-down spectroscopy technique (CRDS), and its functioning was explained by Winderlich et al. [2010].

3.1.3 Campina

The Campina site is an open sky cloud laboratory. It is located 4 km from the ATTO tower and is where the Cloud-related instruments are installed, as presented in Figure 3. Due to the close distance between Campina and ATTO, it was considered that Campina clouds represent statistically the mesoscale cloud field characteristics, meaning the cloud cover at ATTO and Campina should not differ significantly. The selection of the location of the Campina site was based on the fact that the trees in its surroundings are lower than 12 m, allowing the operation of remote sensing instrumentation.

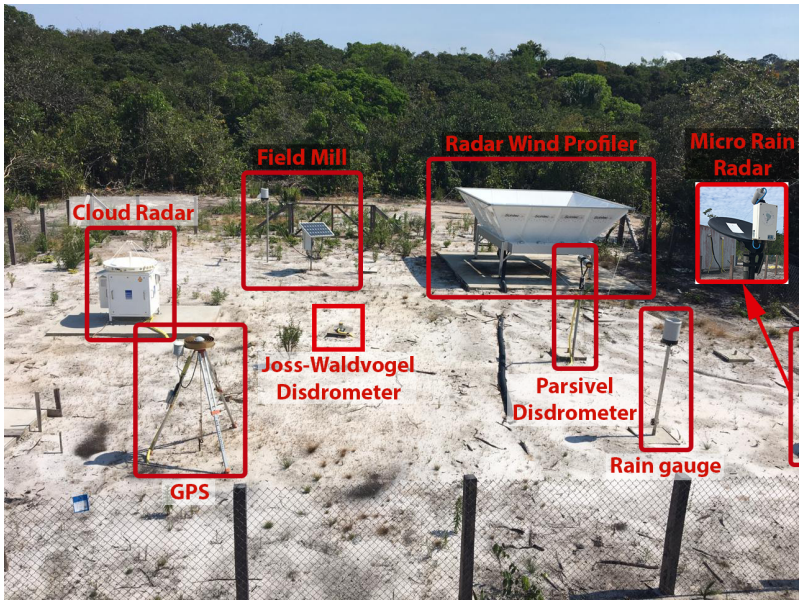

Figure 3: Image of the instrumentation installed at the Campina site. Adapted from https://www.attoproject.org/cloud-radar-measuring-from-a-hole-in-the-forest/.

The cloud radar Mira-35C (Figure 4), the Joss-Waldvogel Disdrometer, and the GPS

were the instruments from Campina used in this study. MIRA-35C is a vertically pointing radar; its frequency is in the Ka-Band (35 GHz), designed to detect cloud droplets and ice profiles. MIRA-35C provides a vertical profile, ranging from 0 to 18 km of the reflectivity and Doppler velocity of the targets. Measurements are taken every 5 seconds with a vertical resolution of 30 meters; in other words, it provides reflectivity and Doppler velocities matrices. In the Mira-35C dataset, the columns represent different heights, and the lines represent different instants of times. To avoid noise and insect effects on the data and detect only cloud droplets and ice, a filter of reflectivity was applied so that only reflectivity data higher than -30 dBZ are considered. It must be mentioned that the Doppler velocities do not represent the velocities of the air masses. Since Mira-35C is a cloud radar, it measures the Doppler velocities of the droplets, which represent terminal velocities combined with the vertical motion of the parcels. It is important to emphasize that this study used the Doppler velocities data only in the Warm Layer of the atmosphere, defined by Unfer [2023] as the atmospheric layer located in between the mean cloud base height and the bright band, which was calculated to be in between 4000 and 4500m, this is essential to avoid errors in the measurements, usually associated to the bright band. The reasons for analyzing the velocities only in the warm layer are because the bright band strongly attenuates the radar signal and because the warm layer is the closest to the surface, so the convection in this layer should have the greatest impact in the surface conditions. In addition, it avoids the ice particles, where the density and refraction index is unknown. MIRA 35-C also provides data on the cloud top height, which is essential to investigate cloud depths and heights.

Figure 4: Photo from Mira 35-C, the cloud radar located at the Campina site. Adapted from https://www.attoproject.org/cloud-radar-measuring-from-a-hole-in-the-forest/.

Another important parameter regarding atmosphere science is the Precipitable Water Vapor (PWV), the air column's integrated mass of water vapor. The GPS provides a value of PWV every ten minutes based on the tropospheric-induced signal delay due to the water vapor content. Finally, the last cloud-related variable analyzed in this study was the rain rate supplied by the Joss-Waldvogel disdrometer. These measurements were used to obtain the integrated rain droplet distribution for each cloud classification.

3.1.4 Scintillometer

The scintillometer is a precise arrangement between a transmitter and a receiver of an electromagnetic wave, but unlike radar, the irradiation is only in one direction, from the transmitter to the receiver, nearly 500m apart. The transmitter was at the ATTO tower, while the receiver was at the Instant tower. This instrument aims to measure the variability of moisture and sensible heat flux. To obtain these variables, the receiver measures the path-averaged refractive index of the air, which represents the turbulent strength of the atmosphere, which is directly related to the ability of the atmosphere to transport humidity and sensible heat. Meijninger [2003]

3.1.5 CloudRoots

The cloudroots campaign (Vila-Guerau de Arellano et al. [2024]) was set at the ATTO complex during August 2022 in the Amazon dry season, when the antropogenic effect is the strongest in the region due to biomass burning activities. The main goal of the campaign was to investigate and quantify the links between photosynthesis, turbulence, and clouds as a continuum: from the leaf to the cloud and from the cloud to the regional cloud distribution, covering all the relevant spatiotemporal scales, as described in the campaign website (https://cloudroots.wur.nl). Cloudroots collected a very unique database with great interdisciplinarity, containing measurements from stomatal aperture up to aircraft measurements.

3.1.6 CAFE-BRAZIL

The CAFE-BRAZIL campaign was also set at the ATTO complex (as one site of the general field experiment). It lasted from December 2022 until January 2023, during the wet season. In this period, the anthropogenic effect in the region was minimal, and the processes that ran the element cycles were predominantly natural. This campaign's main objective was to investigate new particle formation. During the campaign, a unique and comprehensive dataset was collected, including several hours of aircraft measurements combined with multiple radiosondes and measurements from the ATTO complex.

3.2 Research Strategy

This section will explain the research strategy used to answer all the specific objectives presented in section 2.

3.2.1 Specific Objectives 1 and 2

The methodology used to accomplish S.O.1 and S.O.2 are very similar, therefore they are presented together. First, it is necessary to identify and classify clouds as shallow, cumuliform, and deep, or a different type. These cloud types are predominant in the Amazonian region and are more associated with the exchange between the free-atmosphere and boundary layer. The classifications allow to describe the main characteristic of these three cloud types, such as droplet mean velocities, rain rate, precipitable water vapor (PWV), cloud top height, and cloud duration. In addition, cloud classification also enables to describe the variability of the gas concentration and particles under the presence of different cloud types. Finally, it is important to separate day and night cases of clouds for a deeper investigation since the gas concentration follows the diurnal cycle, with different sources and sinks. The details of these procedures will be explained in the following paragraphs.

In the first part of this study, a computational routine for identifying and classifying clouds using MIRA-35C data was implemented based on Giangrande et al. [2017]. The routine consists of 3 basic steps:

- Identifying and enumerating all the clouds in a period of 24 hours.

This is probably the most challenging and important part of the routine. Initially, the code must identify all the continuous clusters of reflectivity, and these will be considered as clouds. It means that if the code detects a cloud droplet at a given height H at time T, if in T+1 it identifies a droplet at height H, H+1, or H-1, the code will consider these data to be components of the same cloud. When the code identifies a cloud, it saves the instant of time of the beginning T_i and of the end T_f of the detection. It gives each cloud an identification number to return a matrix with the same size as the reflectivity one. Still, for every data cluster, it replaces the reflectivity values with the number of that cloud, allowing us to deal individually with them in the future.

- Filtering very small clouds that are not useful for this work.

This study focuses on the impact of clouds on the exchange of gases and particles between the PBL and the free troposphere. For that purpose, it was established to concentrate the efforts on analyzing clouds that were not too small to affect gas concentration, so the clusters whose duration was lower than five minutes and whose depth was smaller than 60 meters were discarded.

- Classifying the clouds based on the cloud top and base height.

In this step, the routine uses the enumeration matrix to detect the height levels of each cloud top. This allows the code to access the cloud base and top height, which is what the classification is based on, and the cloud depth, as shown in table 1. In this study, only shallow, Congestus, and deep clouds were taken into account since the focus of the investigation is the effect on clouds near the surface, and these are the clouds with the base located closest to it (below 3 km). An example of a typical wet season day classification is presented in Figure 34 in the appendix 7.

The procedure used to evaluate the impact of the three different cloud types in the concentrations of gases and particles near the surface and analyze the evolution of the cloud

classification	cloud base height	cloud top height	minimum cloud depth
Shallow	$<$ 3 km	$<$ 3 km	60 m
Congestus	$<$ 3 km	3$<$top$<$8 km	1.5 km
Deep	$<$ 3 km	$>$ 8 km	5 km

Table 1: Definition of the classification rules based on the cloud base height, top, and depth.

characteristics during the cloud detection was defined as: Initially gathering all the T_i and T_f from a certain cloud type, then saving the gas concentrations and the cloud parameters within the interval [T_i,T_f] of the clouds. After this step, these data are normalized into a one-dimensional list of scalars with ten elements. Each element of the lists represents the time average of the parameter between T_n and T_n + (T_f-T_i)/10, being n a natural number between 1 and 9. Consequently, the final list represents the average time evolution of the parameters during cloud detection. For instance, if the input is a 100-element list ranging from 1 to 100, the output will be the following 10-element list:

5.5	15.5	25.5	35.5	45.5	55.5	65.5	75.5	85.5	95.5

This process is repeated for every cloud, so there is a 10-element list representing the average evolution of a certain parameter while detecting every cloud of a certain cloud type. Hence, it is possible to obtain the average among all lists, as they are the same sized, and the result will represent the average time evolution of the parameters under the time of coverage of a certain cloud type.

3.2.2 Specific Objective 3

To answer S.O.3, a case study of a deep convection cloud during the CloudRoots campaign on the fourteenth of August of 2022 was performed. The initial step of the investigation was to understand how the deep cloud affected the meteorological conditions in the region. To accomplish that, the evolution of potential temperature, specific humidity, and variance of the vertical wind speed and turbulent kinetic energy (TKE) were analyzed in a window of two hours around the maximum precipitation rate detected during the deep case. Then, the results were compared to the average evolution of the same parameters calculated at the same time interval in an aggregate of all days of CLoudRoots in which the predominant cloud types were shallow convective ones. The classification of the predominant cloud cover is presented in the article Vila-Guerau de Arellano et al. [2024].

Next step of the case study was to identify the occurrence of a Downdraft. A Downdraft is defined as a downward direction air movement forced by the evaporation of rain. Therefore, the meteorological parameters that should characterize it are: the Variance of Vertical Wind Speed, the Turbulent Kinetic Energy, Precipitation Rate and Potential Temperature, since air is injected from higher altitudes into the PBL. The last part of the case study consisted of checking whether the concentrations of CO_2 and O_3 presented any variations at the moment of the occurrence of the downdraft.

3.2.3 Specific Objective 4

The research strategy used to investigate specific objective 4 comprises three main steps. First is identifying peaks and oscillation peaks of CO_2, CO, CH_4, O_3, and Black Carbon concentrations. Next is saving the instants of time designated as P_i, the beginning of the peak, and P_f, the end of the oscillation. The final step is verifying if there is any precipitation within the interval of detection of the peak.

A computational code was developed to identify the peaks. The code receives the temporal series of any variable (X), the time series jd, the time range Δjd in which the oscillations are being searched, and the percentile α that designate which variations are the targets of the study. In the end, it returns a new temporal series where all values that do not belong to an oscillation are marked as not a number (NAN) and two lists with the values P_i and P_f of every oscillation.

Before explaining the functioning of the code, it is convenient to explain the concept of a moving interval, which involves taking a fixed time interval, Δjd, and moving it along the entire time series jd. For instance, if jd represents a time series of one hour with time steps of one minute, and the time interval Δjd is set to 5 minutes, the initial interval would cover from 1 to 5 minutes, the second interval from 2 to 6 minutes, and so forth. This process continues until the last interval, ranging from 56 to 60 minutes, resulting in 56 intervals.

The routine operation consists of obtaining a list with the differences ΔX between the maximum and the minimum values inside the moving intervals Δjd. Next, the function finds the α percentile of the differences ΔX that will be the base for identifying the oscillations. To identify the oscillations in the concentrations of the previously mentioned compounds, the code was programmed to find the differences within the moving interval of 3 hours and designate the 5% highest differences as the peaks.

After identifying the peaks, the P_i's and P_f's must be adjusted. That is because the Δjd is 3 hours. The compounds have their temporal series of concentrations with a time step ranging from 15 to 30 minutes, which can lead to different moving intervals to have the same difference ΔX and hence the P_i's might be settled too early and the P_f's too late. To illustrate that picture, lets suppose a stable concentrations before and after a sudden increase from a time step to another. The difference between maximum and minimum will be the same in all the moving intervals that contain this increase. Hence, P_i will be the first and P_f the last among them. To avoid this error it must checked if the ΔX calculated at P_i is equal to the one calculated at P_i + 1 time step, if so, than P_i must be relocated to P_i + 1 time step. P_f is resettled in an analog way. If ΔX calculated at P_f equals ΔX calculated at P_i - 1 time step, then P_f must be relocated to P_f - 1 time step. With these adjustments, it is possible to rely on the accuracy of P_i's and P_f's, and the code can move on to the next step.

After properly defining all P_i's and P_f's, the code classifies the oscillations into three distinct cases: Peaks, Valleys, or Oscillations. Figure 5 illustrates examples of each of the three different types of oscillations. Figure 5a displays an example of a peak, 5b illustrates an oscillation, and Figure 5c presents an example of a valley in the concentrations. This classification is based on the following criteria: a peak is identified when concentrations initially rise and subsequently fall; a valley is identified by an initial decrease followed by an increase in concentration; and finally, an oscillation is characterized by concentrations either rising or falling at least twice, with the opposite trend occurring in between. For

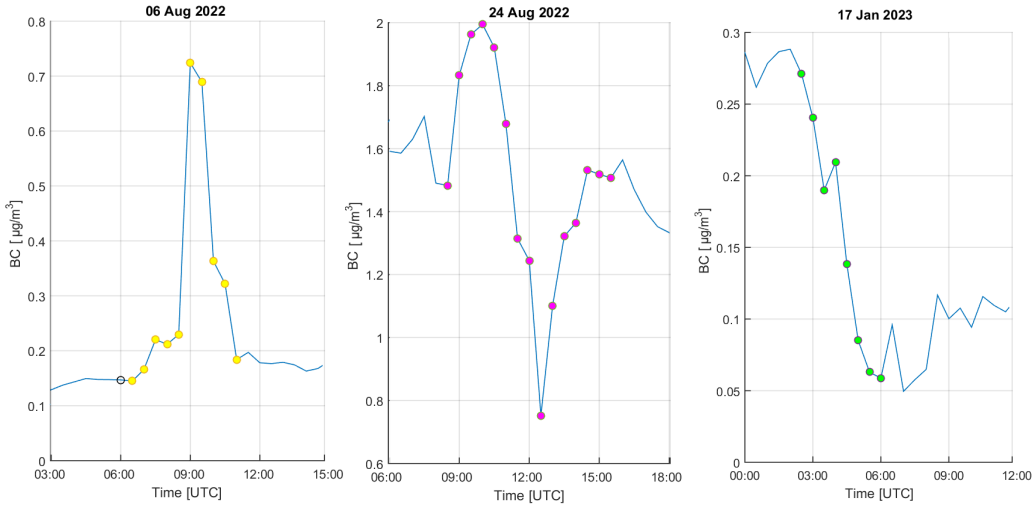

Figure 5: Examples of the three types of variations detected in the concentration of Black Carbons. a) Illustrates an example of a peak; b) Illustrates an example of an oscillation; c) Illustrates an example of a valley.

instance, when concentrations first rise, then fall, and in the end rise again. It is important to mention that the code characterizes concentration trends as either rising or falling when they strictly increase or decrease for at least one hour. This approach may lead to misclassifications of oscillations, as sometimes the concentrations present a net increase after one hour, even with a time step that decreases from the previous one within that time, causing the code to miss that increase. Nevertheless, it should be pointed out that this study will only focus its analyzes on peaks and oscillation cases, and only oscillations that begin with the increase in the concentrations. The last part of this procedure consists of checking whether precipitation was detected within the times of significant variations in the concentrations.

3.2.4 Specific Objective 5

Model simulations from MesoNH were used to evaluate the potential effect of atmospheric gravity waves produced by deep convective clouds in the transport of gases and particles from the free troposphere to the PBL and vice-versa.

MesoNH, described in Lac et al. [2018], is an atmospheric research model developed by LAERO (CNRS, Université de Toulouse, IRD) and CNRM (CNRS and Météo-France) since 1993. It simulates the atmosphere's non-hydrostatic dynamics and thermodynamics following the Navier-Stockes equations. It considers the radiation energy transfers and the cloud water phase changes thanks to parametrizations shared with operational centers, ECMWF, and Météo-France. It runs over limited-area mesoscale domains with grid spacing ranging from tens of kilometers to meters thanks to cutting edge turbulence representations and advection schemes. As a community model, its capabilities increase year after year with continual implementation of user developments.

Meso-NH is a well suited tool to investigate the atmospheric dynamics in the tropics, especially the cloud organisation, the associated circulations, as well as gravity waves

generated by convection. Open boundary condition capability allows us to force it from large scale operational analyses and simulate realistic convective situations which are comparable to field observations, for better assessment of the simulated processes/circulations and their role.

The model was run in this investigation on 18 January 2023, one day from the CAFE-BRAZIL field campaign. Note that this day is also one of the selected days for a model intercomparison study, when several mesoscale models will simulate these days to compare their ability to reproduce the observations and determine how close they are to represent the processes at play.

For the current study, an 800km-wide Amazonian domain encompassing the ATTO-Campina site, Manaus airport, and the upwind region in the Northeast was chosen to capture the life cycle of the convective systems that affected the ATTO-Campina site. The atmospheric evolution was simulated for 24h, starting from 00 UTC (20 UTC the day before in local time). Convective development was validated via comparison with satellite brightness temperature measurements of cloud tops.

The primary objective of utilizing MesoNH simulations was to investigate the potential contribution of gravity waves in transporting air masses from the free troposphere into the Planetary Boundary Layer (PBL). The initial step involved identifying gravity waves within the simulation outputs to achieve this. This investigation applied wavelet analysis to the vertical velocity (W) map at the pressure level corresponding to the PBL. The wavelet analysis involves Fourier transformation, converting the spatial representation from meters to frequencies. Gravity waves are expected to manifest as peaks of energy associated with specific frequencies. The PBL pressure level was determined as the first level above the canopy, where potential temperature exhibits a sudden change. After detecting the gravity waves, it was checked whether variations in the water vapor mixing ratio inside the PBL were detected at the locations where the gravity waves were active.

/

4 Results and Discussion

This section will present and discuss the results obtained in this study.

4.1 CloudRoots and CAFE-BRAZIL - Clouds Characteristics

This subsection will present the behaviors of the shallow, Congestus, and deep convection cloud characteristics during the CloudRoots Experiment, showing the typical behavior for the dry season and for the CAFE-BRAZIL Experiment, describing the typical cloud behavior for the wet season.

Figure 6 illustrates the distributions of cloud top height, detection time duration, mean vertical velocities of droplets, maximum rain rate, mean PWV, and instant of time of the beginning of detection (T_i) observed during the CloudRoots campaign. The first important aspect to be noted is related to the low convective activity during the dry season, reducing the number of clouds in each classification. It also should be considered that the CloudRoots duration was only 20 days and CAFE-BRAZIL 2 months. Nevertheless, during CloudRoots 7 shallow (blue distributions), 30 Congestus (red distributions), and 8 deep convection clouds (green distributions) were identified; it should be highlighted that due to the limited occurrence of deep and shallow clouds during this period, the distributions of these cloud types may have a smaller statistical significance. At this point, it is important to mention that for calculating the statistics of cloud characteristics, all shallow and congestus clouds detected within the interval of 30 minutes arround the detection of a deep cloud were disregarded, which also contributes to the number of detected shallow clouds being so small.

The first distribution in Figure 6A concerns the Cloud top height. The distributions from different classifications don't overlap at any altitude, which is expected, as the definition of the cloud types is based on their cloud top height. Nevertheless, deep convection cloud tops are mostly situated between 13 and 18 km, while Congestus clouds predominantly exhibit tops between 4 and 6 km, and shallow tops are typically found at altitudes ranging from 1 to 2 km.

The distribution of the duration of detection time of each cloud type is presented in Figure 6B. The detection should not be considered as the lifetime of the clouds because it is an Eulerian system where the clouds are moving, and the sensor is fixed; hence, the detection time is correlated with the cloud's horizontal extension and the speed of cloud propagation. The greatest part of shallow clouds do not stay in Mira's view longer than 10 minutes; it presents the shortest detection times among these clouds. Congestus clouds are mostly detected for around 15 minutes, and the occurrence of longer detection decays rapidly until close to 100 minutes. Finally, deep clouds have a peak duration between 100 and 200 minutes. As previously mentioned, the detection duration should be somehow proportional to the horizontal extensions of the cloud types and propagation speed. Hence, it makes perfect sense that deep clouds have the longest detection times and shallow ones have the shortest. Considering an average deep cloud displacement of 10 $m.s^{-1}$ Anselmo et al. [2021], and using the typical deep convective cloud duration of 150 minutes, the

population of deep clouds can be estimated as typically 90 km wide, in agreement with the observation of Machado et al. [2018a].

The distribution of the mean vertical velocity of each cloud type is presented in Figure 6C. These data were obtained from the Mira radar, and the vertical velocity was calculated inside the warm layer, as defined in section 3. These calculations allow us to avoid the bright band that produces wrong speeds and avoid the ice layer with lower speeds. Based on the distributions, it is possible to affirm that most shallow clouds have a positive average velocity of their droplets ranging from 0 to 5 meters per second. The shallow convection normally has no rainfall. Most Congestus and deep clouds have an average negative velocity ranging from 0 to -5 meters per second, although some Congestus clouds do present a positive mean velocity. These are probably the clouds in the initial stage of a congestus, when it is still characterized by predominant conditions of updrafts. The deep and Congestus clouds have a strong convective activity, forming raindrops, and the raindrops have a terminal velocity that is a function of the radius size (Atlas et al. [1973]). Therefore, the measured speed combines the air's vertical velocity and the raindrop's terminal velocity, especially in the warm layer.

The maximum rainfall distribution describes the rainfall pattern (6D). As expected, the distributions for shallow convection show no rain activity. Distributions indicate that deep convective clouds generally present higher values of maximum precipitation rate than any other cloud type. However, there are clouds with a smaller rain rate than congestus clouds. The reason for that is probably associated with the large cloud structure of the deep convection with a large stratiform cloud deck and less efficient rain producer than the Cumuliform, where most of the rain is associated with convective clouds and a more efficient rain producer processes, where the cloud droplet is formed and precipitated, contrarily to the deep convective clouds where the part of the raindrop is advected to the outflow.

The precipitable water vapor (PWV) distribution is presented in Figure 6E. As expected, the mean PWV is larger for deep clouds, followed by cumuliform and shallow clouds. Deep convective clouds peak around 55 mm, and cumuliform clouds around 50 mm are closer to the deep convective clouds. As already discussed, some cumuliform clouds could have high water content, but most of the distribution has much smaller water content than the deep convective clouds. Shallow clouds have values smaller than 45 mm. This clear distinction in the PWV indicates that this might be a crucial factor for triggering deep convection during the dry season.

The distribution of T_i (daytime of the beginning of detection of the cloud), is presented in Figure 6F. One can note that shallow clouds were most commonly detected in the early morning when convection was activated by the presence of the sun. At the same time, Congestus and deep clouds presented a strong peak during the early afternoon when deep clouds were also mostly detected during the early afternoon and night. Usually, it is expected that shallow clouds occur during the morning hours. They develop into Congestus in the early afternoon and finally achieve their final stage as deep convection in the late afternoon. However, the results do not illustrate that pattern. The typical behavior of the dry season shows days of shallow, days of cumuliform, and a few days of deep. This evolution behavior is much more frequent during the rainy season.

Figure 7 presents similar results from the former Figure but for the clouds detected during the CAFE-BRAZIL campaign. CAFE-BRAZIL was set during the wet season,

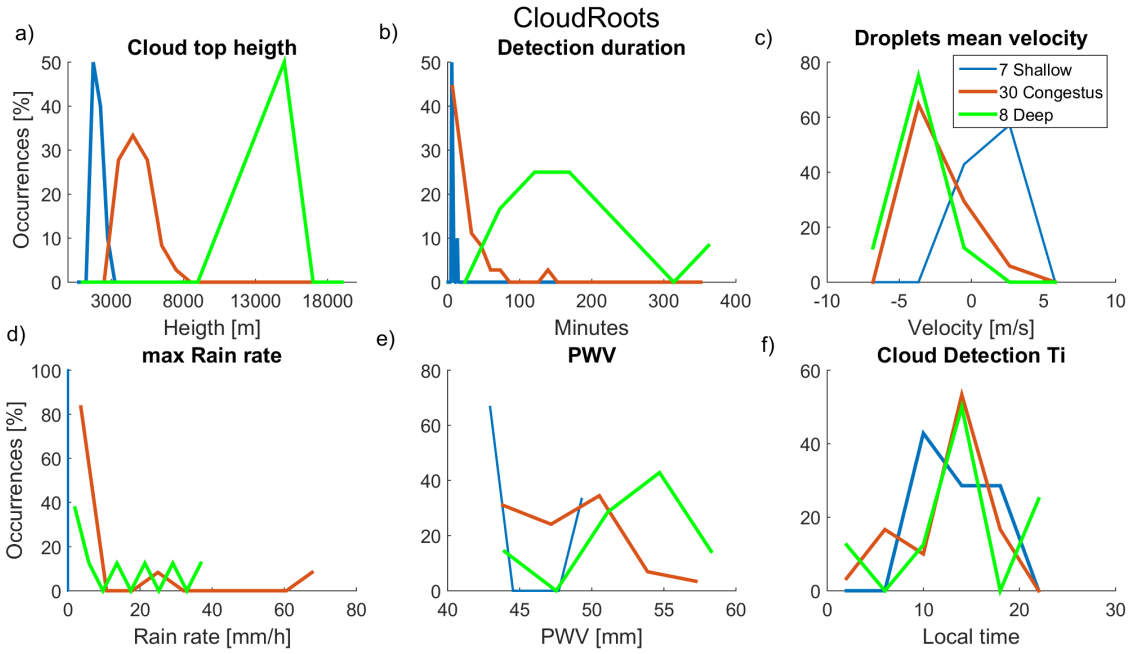

Figure 6: Distribution of cloud characteristics of three different cloud types: shallow, congestus, and deep. Cloud top height a), detection duration b), droplets mean velocity c), and cloud detection T_i f) are provided by the cloud radar MIRA-35C, as well as the cloud classifications. PWV e) and max rain rate d) are provided by the GNSS station and the JOSS disdrometer respectively. The experimental data used in this Figure were collected during the CloudRoots campaign. 7 shallow, 30 congestus and 8 deep clouds were used in the calculation of the ditributions.

covering December 2022 and January 2023. Therefore, a considerably larger number of clouds was detected. The number of clouds detected was 182 shallow, 148 Congestus, and 53 deep convective clouds. Due to the larger number of clouds detected, the distributions of CAFE-BRAZIL are more representative and significant than the ones from CloudRoots.

The distributions regarding the cloud top heights (Figure 7 A) do not differ significantly from the one presented for CloudRoots. However, after a meticulous analysis, some differences can be clearly observed. For instance, deep convective clouds presented a peak of maximum occurrence around 15 km during CloudRoots, and for the wet season, it occurs around 13 km. This finding agrees with Biscaro et al. [2021] that observed that dry season clouds tend to be stronger/deeper than those in the wet season. The higher CAPE values during the dry season explain the more intense vertical development as in Williams et al. [2002]. The same feature is observed for the cumuliform clouds. This is probably related to the quick passage, during the wet season, from cumuliform to deep, contrarily to the dry season, when subsidence avoids the evolution to deep, and the cumuliform cloud stays for longer, growing cloud top slowly during the day. However, shallow clouds during the wet season have slightly higher cloud tops. This is probably related to the large amount of water vapor available during the wet season, allowing shallow clouds to develop deeper.

Figure 7B shows the cloud duration distribution. The shapes of the distributions are

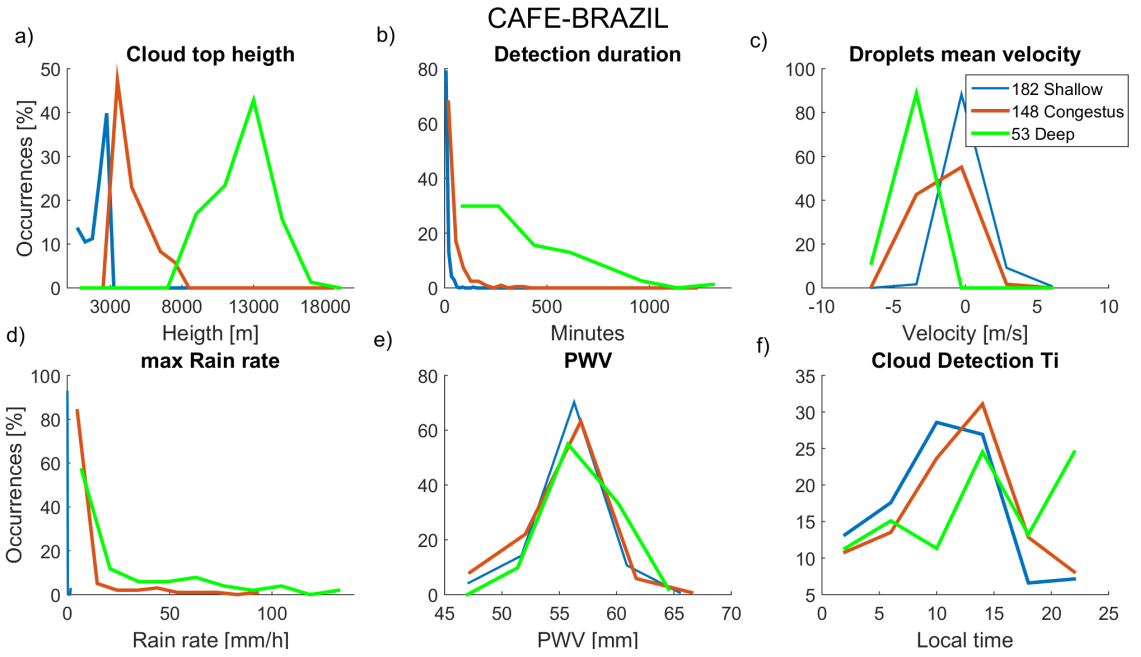

Figure 7: Distribution of cloud characteristics of three different cloud types: shallow, congestus, and deep. Cloud top height a), detection duration b), droplets mean velocity c), and cloud detection T_i f) are provided by the cloud radar MIRA-35C, as well as the cloud classifications. PWV e) and max rain rate d) are provided by the GNSS station and the JOSS disdrometer respectively. The experimental data used in this Figure were collected during the CAFE-BRAZIL campaign. 182 shallow, 148 congestus and 53 deep clouds were used in the calculation of the distributions.

quite similar between shallow and congestus. However, the values are different as congestus cloud detection duration is considerably longer than shallow ones, meaning that its horizontal extension is larger, as expected. The most important feature in this Figure is the duration of deep convective clouds; they could reach a thousand minutes, and considering a propagation speed of 10 $m.s^{-1}$, the cloud size could reach a size of around 500 km. It is well known that larger systems are formed during the wet season Machado et al. [2018b]. The same feature is observed for the shallow and cumuliform clouds. Their detection time is longer during the wet season, indicating larger horizontal extensions and possibly a longer lifetime, as there is a relationship between size and duration Machado and Laurent [2004]. Apparently, the cloud duration distribution could be parameterized by an exponential decay curve, with the decay rate being the highest for shallow clouds and the smallest for deep clouds, and the decay rate is smoother for the wet season than the dry.

Figure 7c shows the droplet's mean velocity distributions, which present different behaviors from the dry season. The distributions for the wet season depict a more significant distinction among different cloud types than during the dry season. Deep clouds have nearly the same distribution as in the dry season. On the other hand, now it was observed both positive and negative values of the droplets mean vertical velocity in shallow clouds, indicating that even the shallow clouds have raindrops in the wet season, reducing the estimated mean velocity. The Congestus during the dry season presented a similar distri-

bution as the deep clouds. However, in the wet season it is distinct, and the distribution is situated in between the deep and the shallow clouds, which is expected as it is the middle stage of the life cycle of a convective cloud that develops from shallow to deep.

The rain rate also differs from the distribution of CloudRoots. In Figure 7D) it can be seen that Deep clouds have the largest rain rate, followed by cumuliform, and shallow clouds have nearly no rainfall. During a deep cloud, one can note the rain rate reaching 120 mm.h^{-1}. The larger population of clouds sampled during the CAFE-BRAZIL gives a more robust analysis of the clouds.

Figure 7E presents the distributions of PWV for the wet season. One can note that the PWV distribution is similar among the different cloud types. As moisture is eagerly available during the wet season, humidity does not show to be a limited factor in choosing the cloud type, contrarily in the dry season, when PWV is a crucial factor controlling the convection.

The distributions of T_i (Figure 7F) describe a succession of cloud development from shallow toward deep convective clouds. Shallow clouds begin mostly during the morning hours, followed by Congestus in the early afternoon, and end up with deep clouds, which begin mostly between the early afternoon and middle of the night. This evolution differs from the dry season when the convection is more associated with days of shallow, days of cumuliform, and days with deep. The wet season is more frequent, the pattern of a cloud's development from shallow to deep along the day.

4.2 CloudRoots and CAFE-BRAZIL - Cloud Characteristics Evolution

The results presented in this section show the average evolution of the cloud characteristics during cloud detection. This analysis uses the normalized detection time explained in section 3, where *0* corresponds to the beginning of the detection and *1* to the moment the cloud leaves the view of the radar. Figure 8 illustrates the average evolution of the velocities of the hydrometeors inside the warm layer, the cloud top height, the rain rate, and the PWV during cloud detection regarding shallow, congestus and deep clouds detected along the CloudRoots campaign. Figure 8A describes the vertical velocities of the water droplets. For shallow clouds, they are close to zero at the borders of the clouds, and they reach positive values towards the middle of the detection. This indicates that these clouds have small updrafts and a bigger population of cloud droplets than raindrops since no negative values appear in the evolution. For congestus, the velocities do not present a significant variation; they are close to -2 meters per second during most of the detection but are slightly smaller in the middle of detection. This is associated with large raindrops with maximum rain activity in the middle part of the cloud horizontal extension when the cloud reaches the maximum rain rate, as shown in 8C. Deep clouds have the smallest values of velocities, which makes sense considering they are the most developed clouds, so their droplets should be bigger and, hence, have the largest terminal velocities and larger downdrafts. The absolute velocities are larger in the beginning when there is the maximum rain rate, and another reduction is observed after the middle of the detection, a time when the rain rate was also reported. This effect should be associated with the time the clouds cross the radar; as the population is small, the results reproduce individual features of each cloud passage over the radar. This trend is probably biased due to the low number

of deep clouds detected during this campaign.

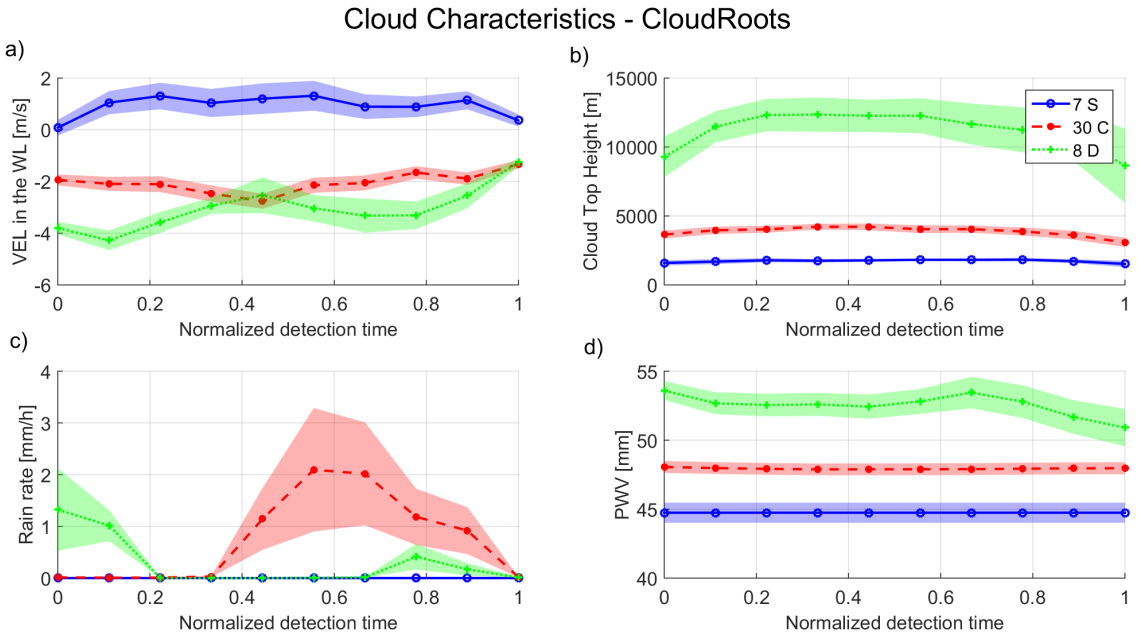

Figure 8: CloudRoots Average evolution of cloud characteristics throughout the cloud detection. The blue curves represent the evolution of the characteristics of shallow clouds, the reds are regarding the congestus clouds and the green ones illustrate the deep clouds. 7 shallow, 30 congestus, and 8 deep clouds were used to calculate the distributions. Confidence interval of 50%. The vertical velocities of the water droplets and the cloud top height were measured by the cloud radar MIRA-35C. Precipitation rates were obtained with the disdrometer Joss-Waldvogel disdrometer. The GNSS station performs PWV measurements. Condence interval of 50%.

Figure 8B presents the evolution of the cloud's top heights. The three different cloud types show similar evolution of cloud top, with more significant variation for the deep convection, the evolution could be described by symmetric parables centered at the middle of detection, where it presents the maximum cloud top height. Shallow cloud top heights evolution is within the range of 1.5 and 2.5 km, Congestus between 4 and 5 km, and deep clouds between 10 and 15 km.

Figure 8C shows the average rain rate for the three different cloud types. The results indicate that none of the shallow clouds presented any amount of rain, which corroborates the fact that almost no negative vertical velocities were detected in this type of clouds. Congestus clouds show a nice clear evolution during the detection, with increased precipitation in the middle, overcoming the amount of precipitation observed by deep convective clouds. However, as already mentioned, the effect of under-sampling shows more an individual characterization of the few clouds than a sample of the population, indicating that obtaining a sample of deep convection in the dry season requires more months and perhaps even years. The results indicate that Deep convection presents rainfall at the beginning or the end of detection time meaning that these clouds were measured during the passage of the stratiform clouds associated with the mesoscale convective system.

Figure 8D describes the evolution of the precipitable water vapor. There is a clear distinction between shallow and cumuliform and deep convective clouds. However, the

confidence interval is the smallest for the cumuliform clouds since they present the biggest population. Shallow and Congestus present a similar PWV evolution, whilst deep cloud values are considerably higher at the beginning and decrease at the end of detection. Henkes et al. [2021] shows that PWV is the primary factor controlling precipitation during the dry season. They demonstrate that the enhanced water vapor in the low level is at the origin of the main perturbation of the Boundary layer processes. They showed that the time taken to eliminate the nocturnal stable boundary layer has an important effect on the development of the convection. Lastly, it should be mentioned that the decrease in PWV during the detection of deep clouds is associated with the conversion process from water vapor to liquid water. as pointed out by Sapucci et al. [2019].

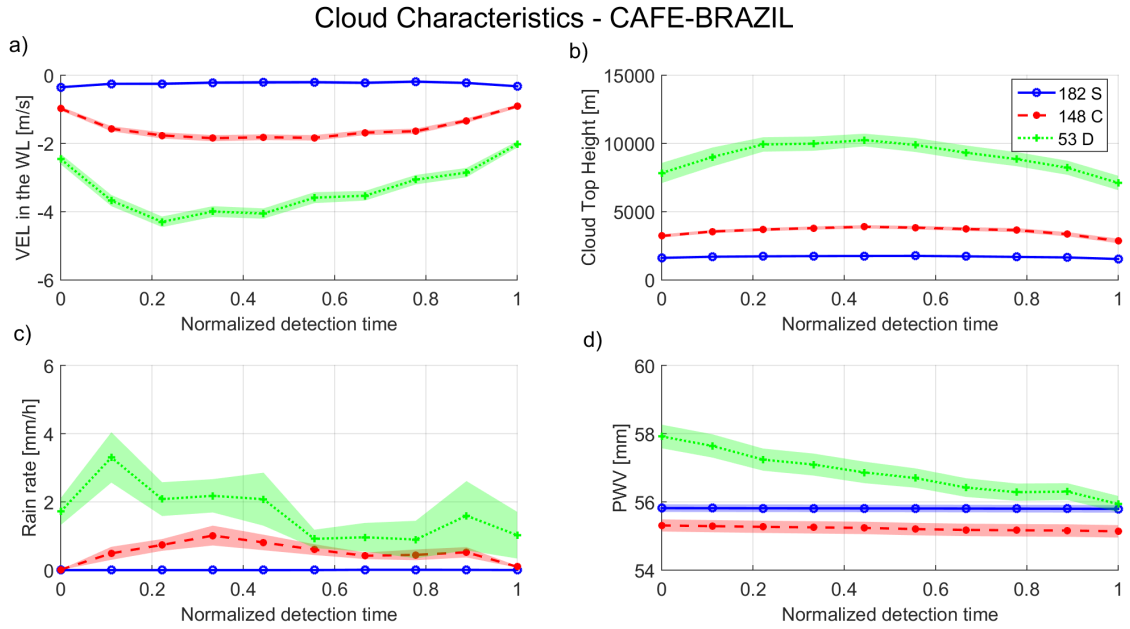

Figure 9: CAFE-BRAZIL Average evolution of cloud characteristics throughout the cloud detection. The blue curves represent the evolution of the characteristics of shallow clouds, the reds are regarding the congestus clouds and the green ones illustrate the deep clouds. 182 shallow, 148 congestus, and 53 deep clouds were used to calculate the distributions. Confidence interval of 85%. The vertical velocities of the water droplets and the cloud top height were measured by the cloud radar MIRA-35C. Precipitation rates were obtained with the disdrometer Joss-Waldvogel disdrometer. PWV measurements are performed by the GNSS station. Condence interval of 85%.

Figure 9 describes the evolution of the cloud characteristics, similar to those presented for CloudRoots, but for CAFE-BRAZIL, representing clouds in the wet season, with a much larger sample. Figure 9A, at first glance, one can note that the behavior along the normalized detection time is quite similar to the dry season. However, important differences can be observed. It is notable that the evolution is more symmetric in this Figure. This is probably because the cloud sample is larger during CAFE-BRAZIL, so there are better statistical representations in the composites. The evolution of the hydrometeors velocities of shallow clouds is a near horizontal parable with values close to -0.5 m/s, this time presenting negative values and, therefore, larger raindrops whose terminal velocities overcome the updrafts inside the shallow clouds. Congestus and deep cloud evolution

have a clear shape of parables, with Congestus ranging between -1 and -2 m/s and deep between -2 and -5 m/s, larger than during the dry season, probably because raindrop terminal velocities are much larger. This result represents what was expected: the more developed the cloud, the faster the droplets fall toward the surface.

Figure 9B shows the evolution of cloud top heights, which are quite similar to the ones for CloudRoots, but the cloud top heights are smaller during the cafe campaign for deep clouds. The cloud top height does not change considerably during the detection time for shallow and cumuliform. This could be related to this season's quick change from shallow to cumuliform to deep clouds.

Figure 9C shows deep clouds having the largest rain rate, and shallow clouds have nearly no rain. The shape of the curve of the deep cloud is not symmetric. The rain rate oscillates during the detection, which could be associated with the invigoration of the convection inside the mesoscale convective system. The Congestus clouds have the evolution of the rain rate increasing up to the middle of detection, followed by a reduction at the end.

Figure 9D shows the PWV, also similar to the one from CloudRoots for shallow and Congestus, but this time, PWV from deep clouds decreases throughout the entire detection time. It is probably associated with the more intense conversion from water vapor to liquid water since the initiation of the cloud.

4.3 CloudRoots and CAFE-BRAZIL - Gas, Black Carbon concentrations and Turbulence Evolution Before-During-After a Cloud Event

In this section it will be presented the analysis of the impact of the different cloud types on the concentrations of Ozone, Carbon Dioxide, Carbon Monoxide, Methane, Black Carbon, and the turbulent fluxes estimated by the scintillometer.

Figures 10 to 15 follow the same concept as the previous Figures, but considering the time window of 30 minutes before and after the detection time of each cloud. The Figures are displayed as follows: In the upper section of the Figure, the results from the CloudRoots campaign are displayed, whilst at the bottom are the results from CAFE-BRAZIL. For each campaign, three panels are presented. The left panel presents the mean evolution of the parameter in the interval of time defined between t_i-30min and t_i, where t_i is the first instant of time that the cloud was detected. The middle panel illustrates the mean evolution along the cloud detection time, again using the concept of normalized detection time. Finally, the panel on the right represents the parameter in the interval between t_f and t_f+30min, where t_f is the last instant of time the cloud was detected. All panels contain three different curves, each with its corresponding confidence intervals. These curves represent the evolution of the same parameter but under the cover of a different cloud type. The blue curve represents the mean evolution of the parameters under the cover of shallow clouds, the red under congestus clouds, and the green under deep clouds. The objective of these Figures is for the reader to trace a curve from the left panel to the right, gaining insights into how the specific cloud type affected the analyzed parameter.

As previously discussed, each type of cloud exhibits a distinct pattern of updrafts and downdrafts, with considerable variations in intensity ranging from shallow (weakest) to

deep clouds (strongest). Other than that, deep clouds access the atmosphere's most distant levels from the surface, up to levels close to the tropopause, where the atmosphere's chemical composition is very distinct from the surface. Hence, deep clouds are expected to have the strongest impact on surface conditions of gas concentrations.

One last aspect to mention before entering the results is that the number of each cloud type, especially shallow clouds, considered in the statistics will present differences among the Figures. That is because the instruments have a different time resolution, and some of the shallow clouds were detected in intervals of time in which no concentration levels were measured. In addition to that, on some days, specific instruments could be facing problems or being under maintenance, so clouds detected in those moments can not be considered in the statistics. It is also important to mention that for calculating the cloud characteristics, the shallow and congestus clouds detected in a window of half an hour around the detection of a deep cloud were disregarded, but those will be considered for the present investigation.

Figure 10 presents the Ozone's evolution before, during, and after the cloud event. It illustrates the impact of the different cloud types on Ozone concentrations at the height level of 80m. The results from CloudRoots campaign are shown in the upper section of Figure 10. It is important to mention that the results have a low statistical significance, especially for shallow and deep clouds, as only 3 shallow, 27 Congestus and 8 deep clouds were considered. As mentioned before, the difference between the number of shallow clouds in the statistics of this figure and Figure 6 is because the temporal resolution of Ozone measurements is 15 minutes. Some shallow clouds were not detected in an interval with no Ozone measurements, hence the smaller number of shallow clouds. The blue curve, which represents the impact of the shallow clouds on the concentrations of Ozone, remains nearly constant during the cloud detection, and it slightly decreases before and after the cloud detection. However, one should consider that the shallow clouds detection time is a few minutes, as illustrated in Figure 6, and the time resolution of the measurements of the Ozone concentrations is 15 minutes. Hence, the apparent stability of the concentrations during the cloud cover is mostly caused by the fact that there is only one concentration of data during the detection of most shallow clouds. However, the concentrations before and after are in the same order, leading to the conclusion that the shallow cumulus clouds have a very small impact on the ozone concentrations. Moving on to the impact of congestus clouds, represented by the red curve, it presents a slight concentration reduction before the cloud detection, stability in concentration during the detection time, yet slightly higher than before detection, and a gentle increase after the end of the detection. The concentration stability during the detection is more reliable than the shallow one. However, most of the congestus was undetected for 30 minutes. Consequently, the apparent stability could also be due to the low number of cases. This slight increase in ozone concentration is probably related to vertical transport, which slightly changes the concentration, even being small for congestus. Looking for the impact of deep clouds (the green curve) on Ozone concentrations, one can note an increase before the detection, an oscillation during the detection where concentration considerably increases, of about 5 ppb, and later a stable concentration with this higher ozone level. Deep convective clouds reach higher levels and have more intense downdrafts, which leads to the increase of Ozone through the vertical transport of air rich in ozone from higher altitudes to the surface. The increase in ozone associated with downdrafts will be discussed in more de-

tail in the following sections.

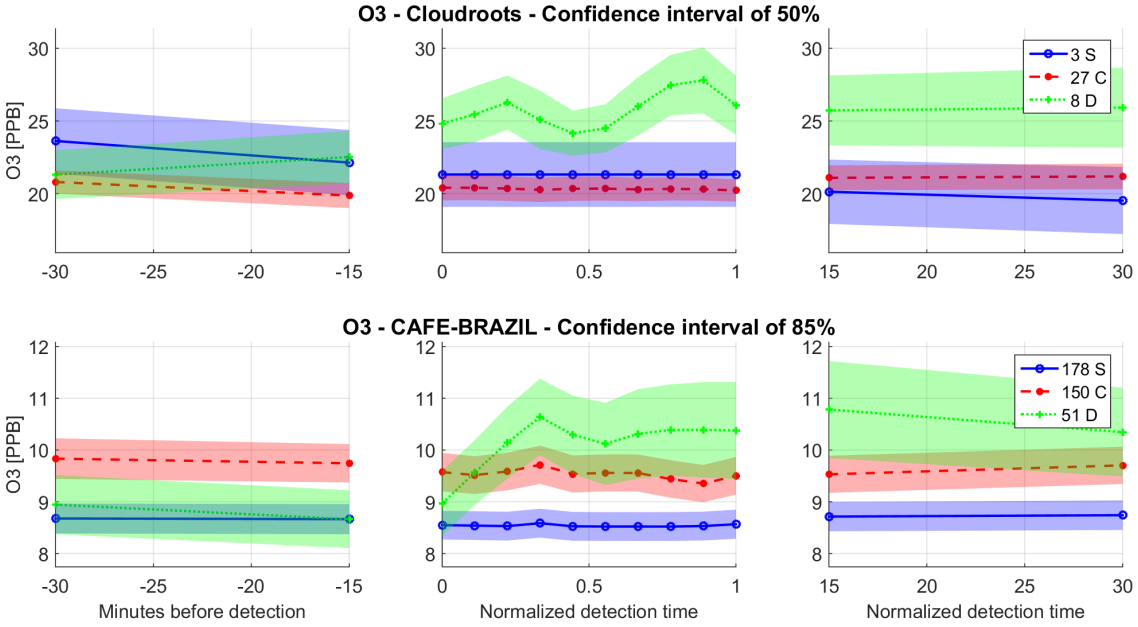

Figure 10: Evolution of Ozone concentrations from 30 minutes before until 30 minutes after cloud detection at the height level of 80m. The results from CloudRoots campaign are displayed on the upper section of the Figure and include 3 shallow, 27 congestus and 8 deep clouds, whilst the results from CAFE-BRAZIL are situated at the bottom and include 178 shallow, 150 Congestus and 51 deep clouds. The three different curves and their respective confidence intervals represent the evolution of the ozone concentrations but under the cover of a different cloud type. The blue curve is regarding Shallow clouds, the red Congestus clouds, and the green Deep clouds. Ozone measurements were performed by the instrument TEI 49i.

The cloud sample is more significant for the CAFE-BRAZIL campaign (bottom section of Figure 10), with 178 shallow, 150 congestus, and 51 deep cloud events. One can note that Ozone concentrations during CloudRoots are about three times higher than the values measured during the CAFE-BRAZIL campaign. That is explained by the fact that CloudRoots occurred during the dry and polluted season when several fires in the Region caused the Ozone concentrations to increase Galanter et al. [2000]. Regarding the impact of the clouds on the Ozone concentrations, for the shallow and congestus clouds, the result is similar to the dry season but with a larger modulation during the moment the cloud is acting. It is probably related to the more intense shallow and congestus clouds during the wet season. However, these clouds do not significantly affect Ozone concentrations; both curves remain approximately stable throughout the three panels. What calls attention in the wet season is that concentrations of O_3 are slightly higher under congestus clouds than shallow ones; meanwhile, during the dry season, this is not observed. During the dry season, the anthropogenic effect is very high, and the Ozone concentration is three-fold higher than in the wet season, hence the diurnal variations should be less relevant and the differences in the ozone levels among different cloud types should not be strong. On the other hand, during the wet season, human interference is minimal, and the difference in Ozone levels among the different clouds should be related to the diurnal cycle of the

cloud cover, illustrated in Figure 7 and the diurnal cycle of Ozone displayed in the appendix in Figure 39. As described in the appendix, typically shallow clouds occur in the early morning, whilst congestus usually happens in the early afternoon, and according to the daily cycle of Ozone, concentrations are higher in the afternoon than during the mornings. Finally, the most interesting aspect of this figure is the notable increase of Ozone under the presence of deep clouds. There is a difference of about 2 ppb between the Ozone concentrations before and after the cloud cover, suggesting the Ozone's transport from higher altitudes to the surface. It is important to mention that the evolution approach fits deep clouds best since they have the longest detection time and the largest horizontal and vertical extension, large enough when detected at Campina and simultaneously at the ATTO and instant towers.

Figure 11 illustrates the impact of the different cloud types on the concentrations of carbon dioxide (CO_2) at the height level of 79m. The results from CloudRoots, situated at the upper section of Figure 11, indicate that shallow clouds do not present a relevant impact on the CO_2 concentrations. However, a slight decrease is observed before and after the cloud detection. It could be explained by the fact during CloudRoots, most of the shallow clouds were detected during the morning hours, which is a photosynthetic active period and also a period in which the boundary layer height increases; hence, it is expected that concentrations of CO_2 decrease. The decrease isn't observed during cloud detection because only one concentration value was measured during the cloud detection. Also, the impact of congestus on the CO_2 levels, represented by the red curve, does not seem relevant. However, a small concentration increase is observed during the cloud detection. At last, a much more prominent increase can be seen for deep clouds on CO_2. This increase during the cloud activity is challenging to interpret. The complexity of this analysis is that it is difficult to infer the reason for this behavior only with this figure. If considering only the cloud mixing processes, a reduction in the concentrations would be expected because CO_2 levels above the canopy are smaller than inside. A more plausible explanation is related to the fact that these clouds often occur in the evening when CO_2 concentrations are increasing regardless of the cloud effect. Also, as the measurements are from the level of 79 m, the mixing produced by the convection might bring CO_2 air from inside the canopy to this level. A better discussion will appear in the next paragraph and sections. Before moving on to the analysis of CAFE-BRAZIL, it is interesting to note the difference in the concentration levels of CO_2 on the three curves, explained again by the diurnal cycle of the cloud types and the CO_2. The shallow clouds were detected in the early morning when concentrations of CO_2 were still high; later, the levels of CO_2 decreased until the afternoon when both congestus and deep clouds were mostly detected.

The results for CAFE-BRAZIL are presented at the bottom section of Figure11. The shallow clouds, as well as the CloudRoots campaign, do not seem to have a significant impact on the concentrations of CO_2. The concentrations remain stable before, during, and after the detection. For CAFE-BRAZIL 198 shallow clouds were considered, and they were detected throughout the day. The Congestus clouds seem to have a slight increase in concentration during detection. Still, the effect does not seem significant, as the concentrations settle back to the initial standard immediately after the detection. What stands out as the most interesting result of this Figure is the peak of CO_2 observed during the detection of deep clouds. Differently from CloudRoots, the increase of CO_2 during the cloud presence is not subtle or constant; it rapidly increases and decreases throughout

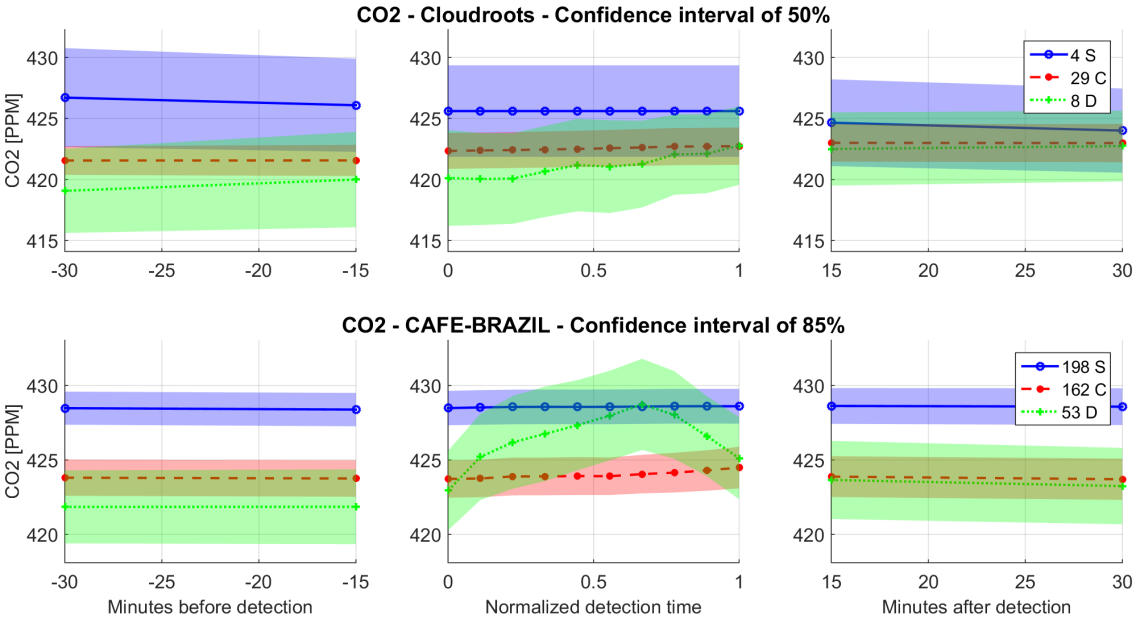

Figure 11: Evolution of CO_2 concentrations from 30 minutes before until 30 minutes after the detection of a cloud, at the heigh level of 79m. The results from CloudRoots campaign are displayed on the upper section of the figure and include 4 shallow, 29 congestus and 8 deep clouds, whilst the results from CAFE-BRAZIL are situated at the bottom and include 198 shallow, 162 congestus and 53 deep clouds. The three different curves and their respective confidence intervals represent the evolution of the CO_2 concentrations but under the cover of a different cloud type. The blue curve is regarding Shallow clouds, the red Congestus clouds, and the green Deep clouds. CO_2 measurements were performed by the instrument Picarro G2401.

the detection time. At this point, it might seem that this result contrasts with the previous result of the increase in ozone because the vertical profiles of CO_2 and ozone are opposite. CO_2 concentrations are highest at the ground level and decrease with height, whilst Ozone concentrations are higher at higher altitudes. So a downdraft should indeed increase the concentrations of Ozone, but at first sight, it should not increase the CO_2 levels. However, with careful analysis, one should note that on the one hand, the concentrations of Ozone increase and remain high even after the cloud detection, and on the other hand, the CO_2 concentrations increase and decrease during the detection, suggesting that there is not a downdraft injecting CO_2 from the free troposphere. It could be that when the downdraft reaches the surface, it might create some turbulence that would bring air from the canopy top to the level of 79m. The downdraft reaches the surface and spreads the air around it radially, which could cause upward vertical transport of air masses from the canopy levels to higher levels, such as where the sensors are located at 79m. As soon as the downdraft hits the sensor region, it would cause a subsequent decrease. Nevertheless, this hypothesis is very complex to test, but an initial investigation is presented in the next section. The day and night cases of Deep clouds were divided since the CO_2 has a strong diurnal cycle. If the hypothesis is that the increase is caused by air transport from the surface, the increase in CO_2 must be more relevant at night when the concentrations at the surface are highest.

Figure 12 is regarding the impact of the different cloud types on Black Carbon at the height level of 320 meters. In the CloudRoots section, it can be observed that the impact of shallow and Congestus clouds in the concentrations of Black Carbon is not as relevant as the one from deep clouds. During the detection of deep clouds, an immediate decrease in the concentrations of Black Carbon is observed, followed by an increase that brings it back to the same standards as before the beginning of detection. As Black Carbon is an aerosol, one of the causes that must be crucial for causing this reduction in the concentrations is precipitation. An interesting analysis is comparing the moments of reduction in the concentrations of Black Carbon with the precipitation rate evolution during the detection of deep clouds illustrated in Figure 8, and it is notable that the decrease moments are the same as precipitation peaks. One last aspect that should be pointed out is the considerable difference in the concentration levels during the detection of congestus clouds, which is about 60 percent of the values of shallow and deep clouds. The explanation for that difference is related to the fact that about half of the deep and shallow clouds were detected during a day when the concentrations of Black Carbon were higher.

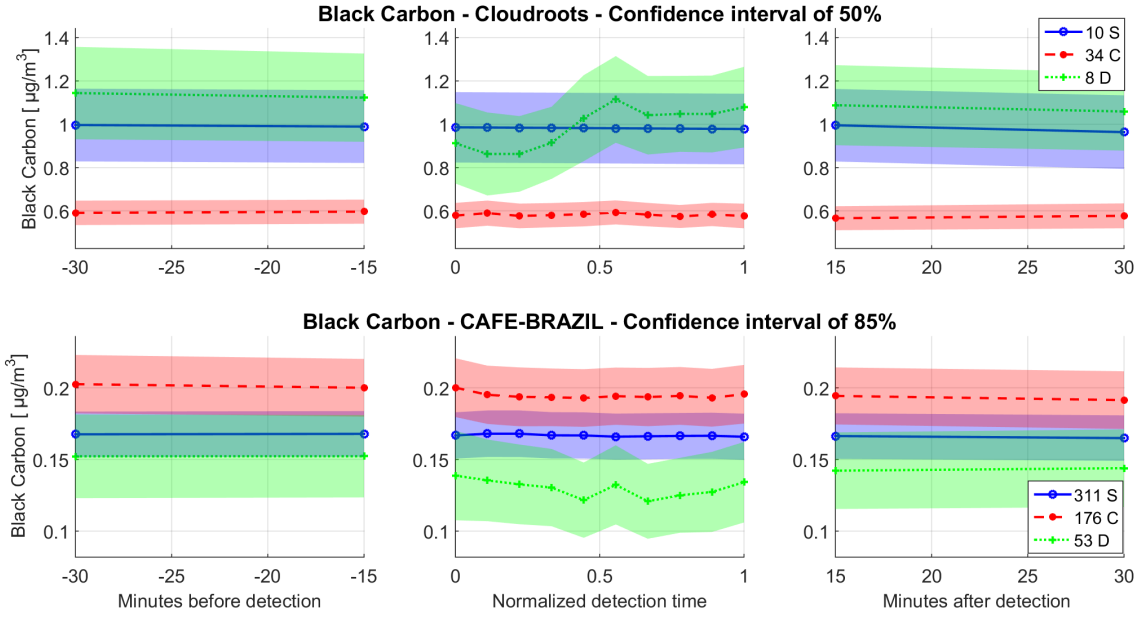

Figure 12: Evolution of Black Carbon concentrations from 30 minutes before until 30 minutes after detecting a cloud. The results from CloudRoots campaign are displayed on the upper section of the figure and include 10 shallow, 34 congestus and 8 deep clouds, whilst the results from CAFE-BRAZIL are situated at the bottom and include 311 shallow, 176 congestus and 53 deep clouds. The three different curves and their respective confidence intervals represent the evolution of the Black Carbon concentrations but under cover of a different cloud type. The blue curve is regarding Shallow clouds, the red Congestus clouds, and the green Deep clouds. BC measurements were taken at 320m by the Multi-Angle Absorption Photometer (MAAP).

Now, analyzing the bottom section of Figure 12, the first aspect that stands out as an interesting result is the lower level of Black Carbon concentrations during the CAFE-BRAZIL campaign. As discussed before, it is explained by the fact that the CloudRoots campaign occurred during the dry season, when biomass burnings are common in the

region, and Black Carbon is one of the most well-known biomass-burning tracers. Nevertheless, regarding the impact of the clouds on the concentrations of Black Carbon, the tendency observed before remains the same; deep clouds are the ones most affecting the concentrations. The impact of deep clouds in the concentrations of Black Carbon again seems to be correlated to precipitation since the reduction in the concentrations occurs when the precipitation rate is maximum, and the increase occurs when it is minimum, as displayed in Figure 9. Finally, the last aspect to be commented on is the difference in the concentration levels among the different cloud types, which has significantly decreased compared to CloudRoots. The highest BC levels were observed during the detection of Congestus clouds, which is not clear and needs further evaluation since most of them were detected in the early afternoon according to Figure 7, and that is the time of the minimum levels of BC, as shown in Figure 38. However, from another point of view, shallow convection occurs when there is no rain, favoring the fires, and does not reduce the concentration of BC.

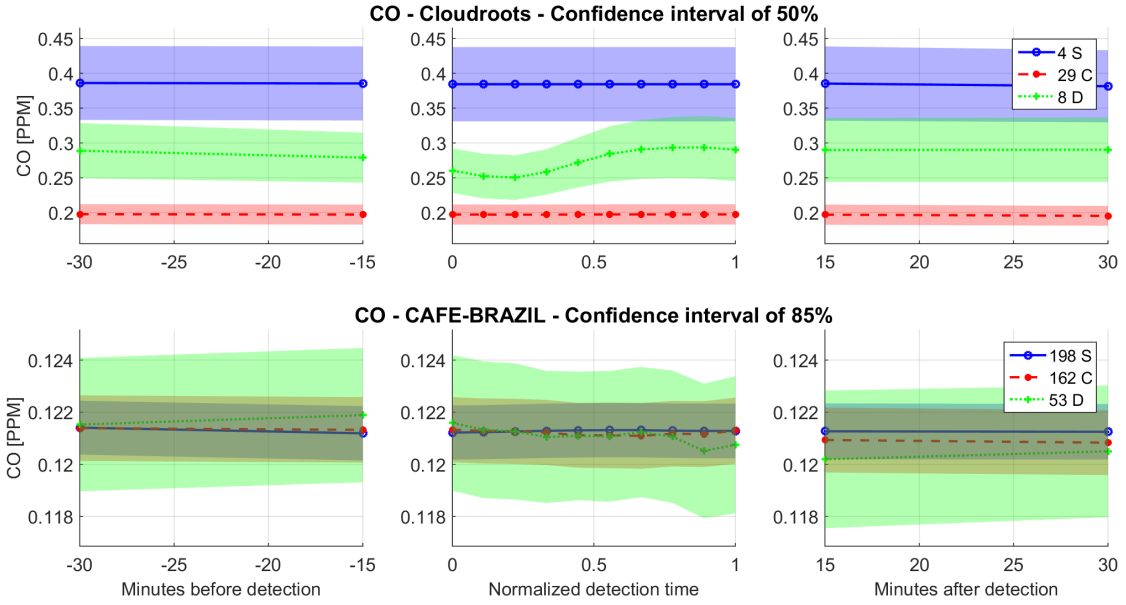

Figure 13: Evolution of CO concentrations from 30 minutes before until 30 minutes after cloud detection. The results from CloudRoots campaign are displayed on the upper section of the figure and include 4 shallow, 29 congestus and 8 deep clouds, whilst the results from CAFE-BRAZIL are situated at the bottom and include 198 shallow, 162 congestus and 53 deep clouds. The three different curves and their respective confidence intervals represent the evolution of the CO concentrations but under the cover of a different cloud type. The blue curve is regarding Shallow clouds, the red Congestus clouds, and the green Deep clouds. CO measurements were performed by the instrument Picarro G2401 at 79m.

Figure 13 depicts the impact of the different cloud types on the concentrations of Carbon Monoxide (CO) at the height level of 79 meters. CO, like Black Carbon, is an important biomass-burning tracer, meaning that even though CO is a gas and Black Carbon is a particle, it is expected to observe some similar aspects in both results. The first clear similarity is the disparity in the levels of concentrations of CO measured during the CloudRoots and CAFE-BRAZIL campaigns, which, as mentioned before, is explained by

the intense biomass-burning activity in the region during the dry season. When analyzing the CloudRoots, other similarities come up, such as the higher concentrations of CO measured during the detection of shallow and deep clouds compared to congestus clouds. It should be considered the reduced sample of shallow and deep clouds, causing the average value of concentrations to be highly affected by outliers, such as the detection of clouds on days of intense biomass burning in the region. The impact of shallow and congestus clouds on the concentrations of CO, as on Black Carbon, is not as relevant as the one from deep clouds. Concentrations of CO remain nearly constant throughout the detection of the Shallow and congestus, whilst during the deep clouds detection, an immediate decrease, followed by an increase back to the initial standards of concentrations of CO is observed, emphasizing the hypothesis that the surface conditions are mostly affected by the intense downdrafts and precipitation rates associated to Deep convection clouds.

Moving on to the CAFE-BRAZIL results from Figure 13, it is evident that the levels of concentrations of CO during the detection of the three different cloud types do not differ considerably from one to another. The concentrations of CO during the wet season do not seem to be strongly affected by the presence of any cloud types. One can note that deep clouds present the strongest effect on surface concentration when compared to shallow and congestus clouds. During shallow cloud detection, the concentration is approximately stable. During congestus events, levels of CO present a very subtle decrease, and during deep cloud events, the levels of CO decrease slightly, probably due to the more intense injection of clean air from higher altitudes transported through the downdrafts.

Figure 14 presents the impact of the different cloud types on methane (CH_4). During the CloudRoots campaign, it can be observed a clear similarity between the evolutions of methane and carbon monoxide (figure 13) under the cover of different cloud types. All the patterns observed on the impact of the different cloud types on CO were also observed on CH_4. i.e., stable concentrations under cover of shallow and congestus and the presence of a valley at the beginning of detecting the deep clouds. The only difference is that a slight increase in the CH_4 levels before and after shallow cloud detection was observed. In addition, both gases present a similar behavior related to the maximum concentration during shallow and the smallest during cumuliform. Lastly, it is important to mention that the similarities between CO and Methane are quite intriguing, as CO and Methane have different sources. CO's main source during the dry season is biomass burning activity. Meanwhile, the main sources of methane could be related to flooded forest areas, soil emissions, fauna and flora, and agricultural activities. Despite that, the diurnal cycle of these gases are similarly shaped and present maximum and minimum values simultaneously. Hence, it makes sense that the background levels follow the same order, maximum for shallow and minimal for congestus in both cases.

Regarding the CAFE-BRAZIL section of Figure 14, the results follow the same trend as for most of the previous gases: methane concentrations seem unaffected by the presence of shallow and congestus clouds. The most significant variation in the concentrations of CH_4 was observed during the detection of deep clouds. In the first half of the detection, the concentrations presented a subtle valley, and in the last quarter of the detection, another fall was observed. It can be seen that concentrations were highest during the detection of shallow clouds and lowest during deep clouds cover, which is reasonable since levels of CH_4 are highest during the morning hours, when shallow clouds were mostly detected, and lowest during the afternoon and early night when deep clouds were mostly

detected.

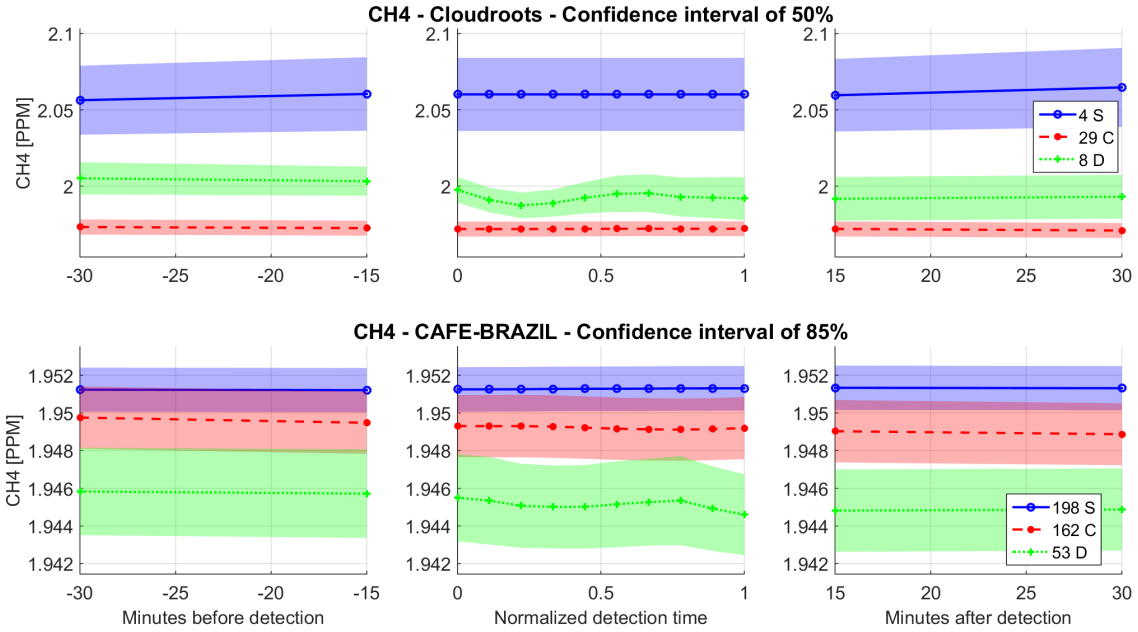

Figure 14: Evolution of CH_4 concentrations from 30 minutes before until 30 minutes after detecting a cloud. The results from CloudRoots campaign are displayed on the upper section of the figure and include 4 shallow, 29 congestus and 8 deep clouds, whilst the results from CAFE-BRAZIL are situated at the bottom and include 198 shallow, 162 congestus and 53 deep clouds. The three different curves and their respective confidence intervals represent the evolution of the CH_4 concentrations but under cover of a different cloud type. The blue curve is regarding Shallow clouds, the red congestus clouds, and the green Deep clouds. Methane measurements were performed by the instrument Picarro G2401 at 79m.

Figure 15 is the last of this type of analysis. This one differs from the others, as it illustrates the evolution of the scintillation measurements described in section 3.1.4, under different cloud types. The scintillometer data is related to the flux of air masses with different temperatures and, hence, air density fluctuation related to the turbulence. For example, at a moment of high solar incidence, causing the air near the surface to be heated and consequently raised due to its low density if this parcel crosses the optical path between the two parts of the scintillometer, it will cause scintillation. It hence will cause an increase in the values of CT^2, related to the variance of the air temperature between the two sensors, associated with the plumes of convection crossing the path between the two sensors. What is clear for both experiments is the fluctuation during the time the cloud is acting. Even shallow clouds show a small fluctuation, describing the ascending thermal plumes and the downdrafts acting; of course, it is increasingly important to the deep convective clouds. CAFE-BRAZIL data shows more fluctuation during the cloud event, probably associated with the longer time observed for the wet season cloud events. Before and after the cloud events, for the deep convective clouds, one can note stable behavior. However, one can note the increase before the cloud events for cumuliform clouds. The behavior before and after should be evaluated in more detail to understand

the process comprehensively. Some results could be associated with the preferred time each cloud was detected since most shallow clouds were detected during the morning and afternoon. Congestus was mainly detected in the afternoon when the air temperature is well mixed, as discussed in Vila-Guerau de Arellano et al. [2024], causing the vertical transport of air masses with different temperatures to decrease.

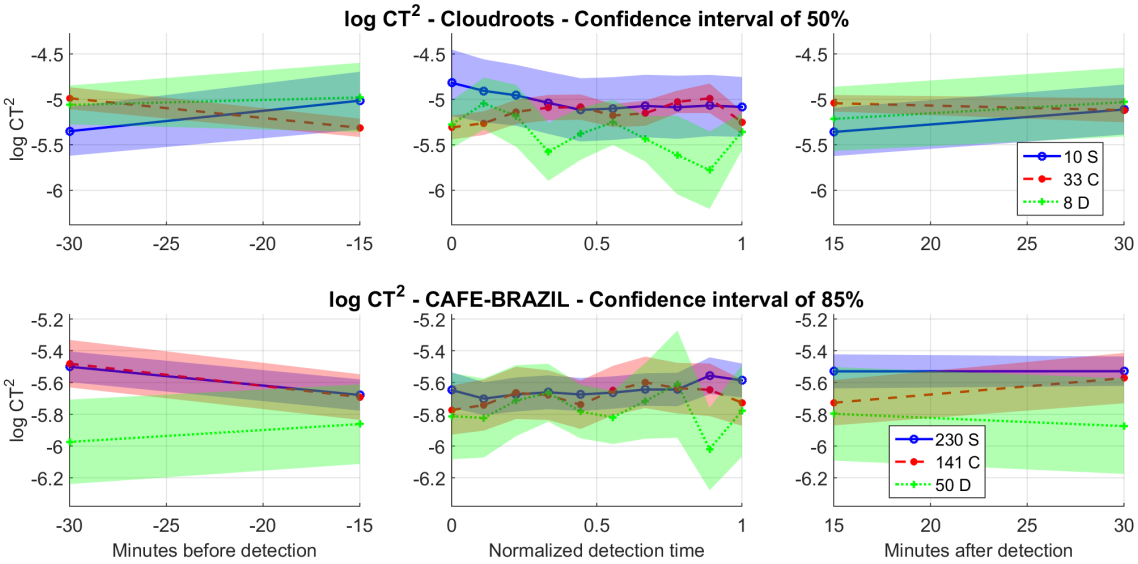

Figure 15: Evolution of scintillation (turbulence) from 30 minutes before until 30 minutes after detecting a cloud. The results from CloudRoots campaign are displayed on the upper section of the figure and include 10 shallow, 34 congestus and 8 deep clouds, whilst the results from CAFE-BRAZIL are situated at the bottom and include 230 shallow, 141 congestus and 50 deep clouds. The three different curves and their respective confidence intervals represent the evolution of the scintillation but under the cover of a different cloud type. The blue curve is regarding shallow clouds, the red congestus clouds, and the green deep clouds. CT^2 measurements were taken at 40m by the Scintillometer.

After analyzing all the figures from this section, it is clear that deep clouds are the ones most relevant to affecting the trace gas concentration near the surface. The hypothesis is that this impact is caused by updrafts and downdrafts associated with these cloud types, causing the injection of air masses from higher altitudes with different chemical and meteorological conditions or from the surface to the free atmosphere. This hypothesis will be investigated in the next sections.

4.4 The Impact of Deep Clouds on the Vertical Variability of Gas Concentrations

In this subsection, a detailed discussion will be presented on how deep clouds affect the concentration of CO_2 and O_3, aiming to clarify what are the mechanisms that cause the variations in the concentrations of these gases, illustrated in figures 10 and 11.

4.4.1 Day and Night Cases

In section 4.3, it was presented that deep clouds have a significant impact on the

concentrations of CO_2 and O_3. In addition, it was discussed that the causes for the variations in the concentrations of these gases should be distinct. The concentrations of CO_2 are highest at the surface and decrease with height, whilst Ozone concentrations increase with height. As a result, it was possible to conclude that the increase in the concentrations of both these gases can not be explained simply by the presence of Downdrafts since the air injected by Downdrafts comes from higher altitudes and is poor in CO_2. Therefore, the increase of CO_2, should be caused by the spreading and mixing of CO_2 from the surface. CO_2 has a strong diurnal cycle, as discussed before; during the day, the photosynthesis and the high PBL height cause the concentrations to be low, while at night, there is only respiration and no photosynthesis. In addition, the low height of the PBL collaborates with the concentrations of CO_2 to be maintained high. Hence, if the hypothesis of the increase in CO_2 under the presence of Deep clouds being caused by the spread of air from the surface is correct, it means that the increase should be stronger when the concentrations CO_2 on the surface are higher, in other words, during the night. For that reason, the Deep clouds were divided into day and night cases, and the results will be presented in the following paragraphs. Furthermore, the evolution of the concentrations of CO_2 was now analyzed at five different heights and the Ozone at two, enabling a more complete investigation. Only the results from CAFE-BRAZIL will be analyzed in this section due to the low occurrence of deep clouds during the CloudRoots campaign, so if divided into day and night cases, the statistics would not be significant.

Before entering the analysis of the results, it is necessary to explain the criteria used to divide the deep clouds into day and night cases. Locally, CO_2 is emitted as the result of respiration processes of the vegetation situated at the surface. On the other hand, photosynthesis works as a sink of CO_2. In addition to that, another process activated by radiation is the increase in the planetary boundary layer height, which propitiates a bigger volume for the gases to spread. As a result of that, the concentrations of CO_2 naturally decrease along it. When dividing the cases in day and night, the particular interest of the investigation is to check if the increase in CO_2, observed in figure 11, is caused by the spread and mixing of the surface air, rich in CO_2. Hence, it makes sense to divide the clouds into two cases: the ones that happened during the day when the CO_2 above the canopy is well mixed in the boundary layer, and there is radiation to activate photosynthesis, and the ones detected during the night when the boundary layer is characterized by the stability, high concentrations and stratified levels of CO_2. Based on this criteria, the day cases of deep clouds are the ones whose T_i and T_f are situated within the interval [8,17]h local time, and the night cases are situated within the interval [20, 5]h. In Figures 17 and 20, the interval of time designated as day is the one within the two vertical red dashed lines, and the night cases are the ones outside the vertical black dashed lines.

Figure 16 illustrates the evolution of CO_2 concentrations under the cover of deep clouds detected during a) the day boundary layer and b) the night boundary layer. The analysis includes measurements of CO_2 at five different height levels, two situated within the canopy heights (approximately 30m): 4m and 24m, represented by the black and blue curves, and three above the canopy: 38m, 53m, and 79m, represented by the green, red and purple curves. The first aspect to be noted in this figure is that during day cases, the concentrations of all heights, except at the ground level, are very similar; the difference from 24 to 79m is about 3 ppm. During the night, there is about a 25 ppm difference in

the concentrations of CO_2 measured at 24 and 79 meters. This is explained by the fact that the diurnal boundary layer is characterized by the mixing layer that homogenizes the vertical distribution caused by the turbulent mixing processes during the development of the convective boundary layer. The solar radiation heats the air close to the canopy, creating instability and forcing air parcels to be lifted, consequently causing vertical air mixing. On the other hand, during the night, there is no solar radiation. Consequently, the convective boundary layer is destroyed and gives place to the nocturnal boundary layer Fisch et al. [2004], which is around 300m in height Dias-Júnior et al. [2022], producing a larger difference in the concentrations of CO_2 between the different levels at night. Another aspect that stands out in this figure is the fact the concentrations of CO_2 measured at the 4m level are much higher and do not get well mixed with other heights. It could be caused by tree respiration and by soil emissions of CO_2 trapped in the canopy layer, preventing the air from this layer from mixing with the other heights.

Figure 16aA) presents the impact of day cases of deep clouds on the concentrations of CO_2 measured along the Instant Tower. It is important to mention that only six deep clouds, with an average duration of 2 hours and a half, were entirely detected during the day boundary layer period throughout the CAFE-BRAZIL campaign. When analyzing the figure, a decreasing tendency can be observed in all heights before and after the detection of the cloud, which is explained by the downdraft and the fact that photosynthesis is working as a sink of CO_2 during the day. Next, there is an oscillation in the CO_2 levels during cloud detection. At the 4m height, the concentrations during the detection were stable at the beginning, followed by a decrease in the levels and, in the end, an increase in concentration back to the initial standards. For the other heights, a decrease was observed until almost half of the detection time, followed by an increase in the concentrations and, finally, another decrease at the very end of the detection. However, one aspect in common for all heights is that the concentrations measured immediately after the cloud detection are lower than the ones measured immediately before.

Machado et al. [2024] discusses how rainfall events affect the concentrations of several gases on the surface. This article does not consider the evolution of the cloud event but the hours before and after the maximum rain rate. The article shows that during the day, the concentrations of CO_2 above the canopy slightly decreased before the maximum rain rate and increased afterward. This pattern seems to be observed during the cloud detection; however, in the article, the final concentrations of CO_2 are higher than the ones measured at the first profiles. There are three main considerations to be taken in account when both articles are compared: one is related to the sample; this article includes all months, so the dry and wet seasons. Secondly, the timing is 2 hours before and 2 hours after, and each rainy system has a different time duration, contrary to this study, where the time before and after is the effective time, without clouds. Finally, the referred paper works with rainfall, and this study uses cloud cover, so it provides different information. The fact that the concentrations of CO_2 after the rain even are higher than before in the article could be related to the diurnal cycle effect associated with the time of the rainfall event, mainly at the end of the afternoon, and considering the two hours after, it could capture the beginning of the night boundary layer and the end of the photosynthesis process. Meanwhile, the day cases considered in Figure 16 are entirely within the day boundary layer period. Hence, the photosynthesis combined with downdrafts injecting air poor in CO_2 should cause the levels of CO_2 to be lower after the detection. Nonetheless, even

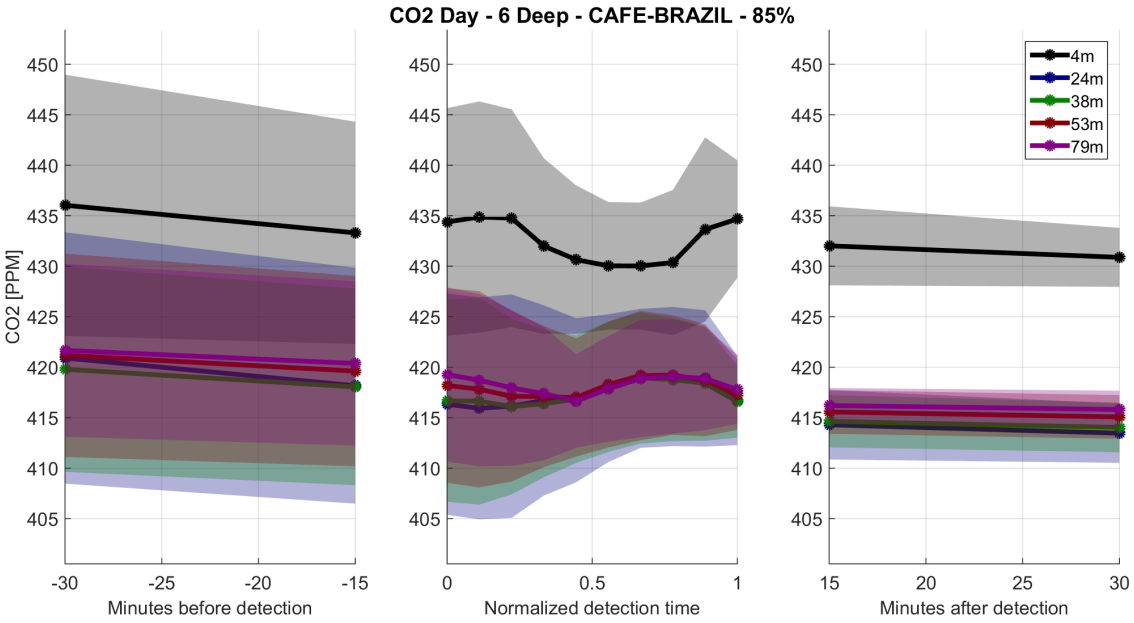

(a)

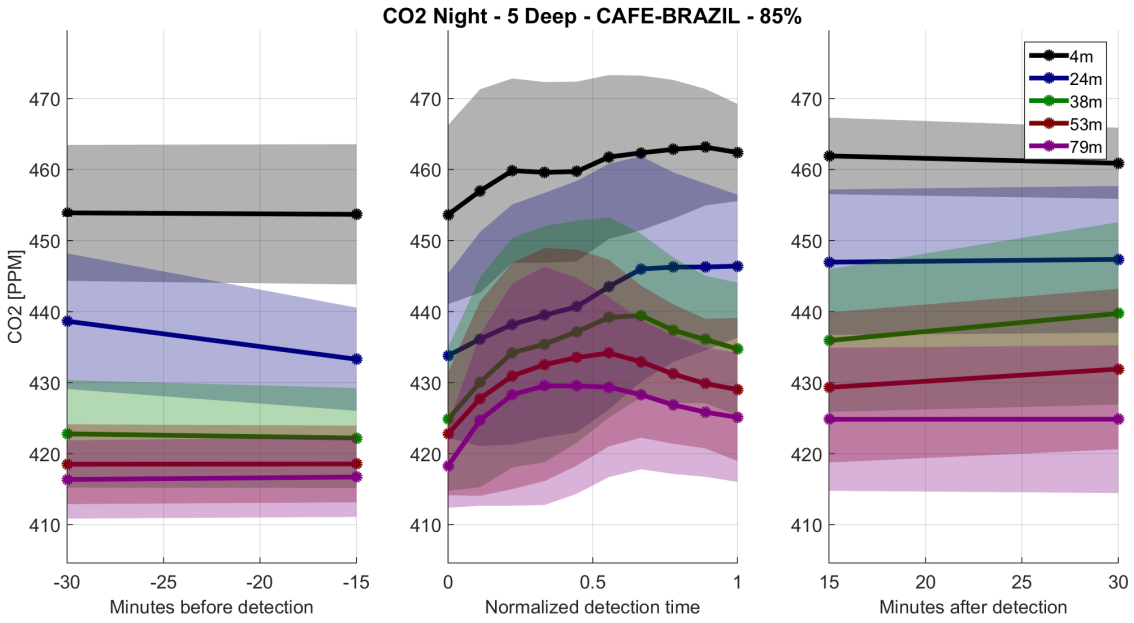

(b)

Figure 16: Evolution of CO_2 concentrations from 30 minutes before until 30 minutes after the detection of a deep cloud during: a) the day boundary layer (6 cases); b) night boundary layer (5 cases). The 5 different curves and their respective confidence intervals represent the evolution of the CO_2 concentrations in different heights. The black curve represents the height level of 4m; blue 24m; green 38m; red 53m and purple 79m. Day cases are the ones whose detection time is in between 8am and 17pm. Night cases are the ones whose detection time is in between 20pm and 5am. CO_2 measurements were performed by the instrument Picarro G2401 in the period of the CAFE-BRAZIL campaign.

considering these differences, there can be noted some similarities: the concentration inside the canopy is in phase with the contrations levels above, meaning that when one increase the other decrease, as described by Machado et al. [2024]. For a more complete analysis, the results from Figure 18 indicate the mean evolution of the rain rate during day and night cases of the deep clouds. The rainfall during the day occurs predominantly at the end of the cloud detection, and during the night, it occurs mostly at the beginning of the cloud detection. Combining the analyses from Figure 18 and 16a, it can be seen that during the day, there seems to be a correlation between the variations of CO_2 and the peaks of precipitation.

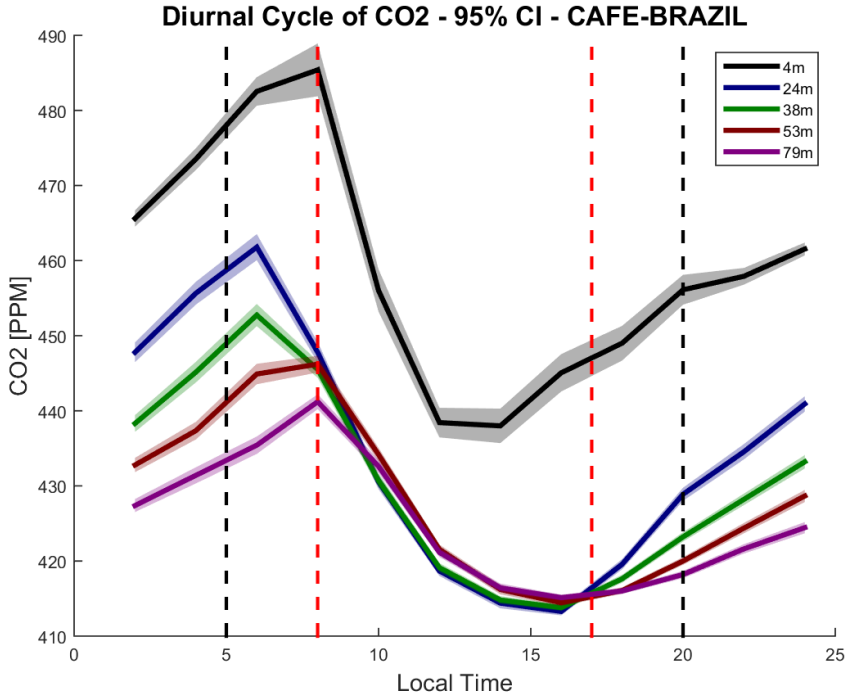

Figure 17: Diurnal cycle of CO_2 calculated for the CAFE-BRAZIL campaign in five different heights, each represented by a different curve. The black curve represents the height level of 4m; blue 24m; green 38m; red 53m and purple 79m. The two red vertical dashed lines mark the interval of time defined as the day boundary layer. Outside the two black vertical dashed lines is the period defined as the night boundary layer. CO_2 measurements were performed by the instrument Picarro G2401.

Other interesting features can be observed in Figure 16b. Only 5 Deep clouds with an average duration of 2.9 hours were detected at night. At this time, the PBL is stable, and CO_2 levels are stratified. Before the cloud detection, the concentrations at all heights except for the canopy level are stable. Meanwhile, at the 24m level, there is a considerable decrease of about five ppm in the concentrations, which could be caused by the limited sampling of clouds. The next factor that must be mentioned is that the levels of CO_2 after the cloud detection are higher than before at all heights. During the cloud cover, it can be seen that there is a clear increase in the concentrations at the first half of the detection at all heights. At the second half of the cloud's normalized detection time, the CO_2 decreases above the canopy and remains stable within the canopy heights.

The results of the levels above the canopy from the article Machado et al. [2024]

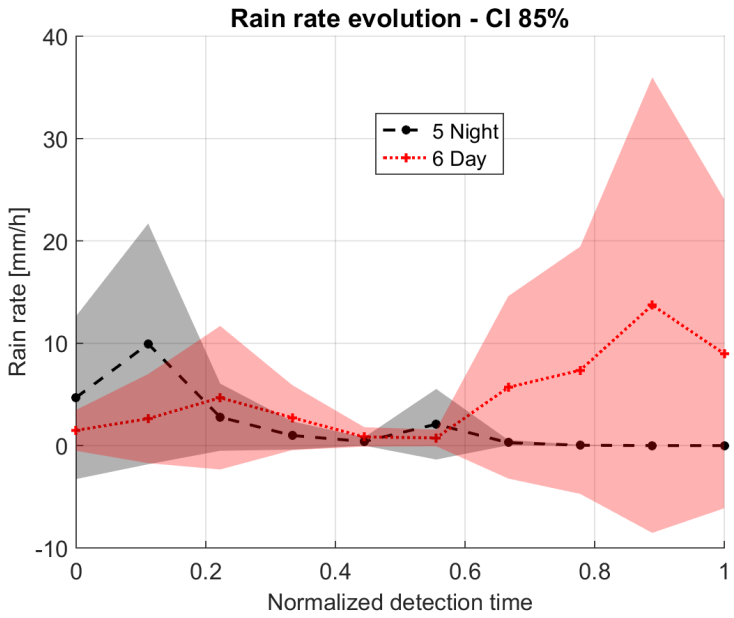

Figure 18: Precipitation rate evolution throughout the normalized detection time of 6 days and 5-nights cases of Deep convection clouds, represented by the red and black curves, respectively. Measurement of rain rate was performed by the JOSS-Waldvogel disdrometer during the CAFE-BRAZIL campaign.

coincide with the observations during cloud detection: an initial increase followed by a decrease in the concentrations. There could be two reasons for the initial increase in the concentrations at these levels: one of them is simply the natural increase expected during the night boundary layer period, as one can see in Figure 17, and the other one is that when the gust front arrives, it will spread clean air from the downdrafts at surface levels and push the air that was situated near the surface upwards, causing the concentrations above the canopy to increase. Meanwhile, according to Machado et al. [2024], the explanation for the decrease in the second half of the detection should be related to the fact that the rainfall affects the meteorological conditions, for instance, by decreasing temperature and increasing relative humidity and creates such an environment that suppress the soil and vegetation emissions of CO_2. This, combined with the downdrafts bringing poor CO_2 air from higher altitudes, should explain the decrease in the CO_2 levels in the second half of detection. For a better understanding of this process, it is necessary to include the results from Figure 18 in the analysis. The results displayed in Figure 18 indicate that during the night, all the precipitation happened within the first 60% of the detection time, with the peak at the very beginning of the detection. Now, combining the two results, it is possible to affirm that the maximum increase in the concentrations of CO_2 happened simultaneously with the maximum precipitation rate. After that, the rate at which CO_2 rises starts to decrease until the actual concentration values decrease above the canopy and stabilize within the canopy levels.

The results from Figure 16 corroborate the initial hypothesis mentioned in this subsection that the increase in CO_2 should be more pronounced during the night cases of Deep Clouds. This result suggests that the variation in CO_2 concentrations is caused by downdrafts, updrafts, and the mixing effect caused by the cloud dynamics. The complete

processes involved in the variations of CO_2 under the presence of Deep Clouds should consider gust fronts, downdrafts, precipitation, and the variations in meteorological conditions.

Figure 19 is similar to Figure 16, but describes the Ozone concentrations at the ATTO in two different height levels. The lowest level, 80 m (black curve), is near the same level as the highest level measured for CO_2. The other height level is at 150 m (blue curve). One can note an increase in concentration at 150 m at night, producing a peak concentration. A similar behavior is not observed at 80 m. This is probably associated with the effect of the residual boundary layer being affected by this height. The residual boundary layer has a concentration close to the concentration observed in the convective boundary layer.

Figure 19a represents the O_3 evolution under the day cases of deep clouds. It can be observed that both before and after cloud detection, ozone concentrations at the 150m level surpass those at 80m, which is expected, as it can be seen in Figure 20 that the 150m concentrations remain higher throughout the entire diurnal cycle. One can note that O_3 levels increased at 150m before the cloud detection and remained stable at 80m. Other than that, the results indicate that concentrations of O_3 measured during the cloud detection reach higher levels than those measured before or after. This effect should be related to downdrafts that inject air from higher altitudes, rich in Ozone. Finally, after the detection concentrations at 150m continue to rise, while at 80m they are falling. The decrease after deep convective clouds near the canopy could be related to the reactions with terpenes to form new particles Machado et al. [2023]. Interestingly, the difference in Ozone concentrations between these levels is considerably higher before the deep clouds event, suggesting that the turbulence caused by the up and downdrafts helps homogenize the Ozone concentrations in the PBL. An important pattern to note in this figure is that both curves follow the same trend during the cloud detection, meaning that when the concentrations at one height level rise, the concentrations at the other levels also increase and vice-versa. This pattern reinforces the hypothesis of the downdraft, as simultaneous variations in ozone concentrations at different height levels close to the surface can be observed. It can also be noted that along the detection, there are two peaks in the concentrations that, when compared to Figure 18, lead to the conclusion that the variations in the concentrations of O_3 are directly correlated to the presence of rain, as well as CO_2.

The article Machado et al. [2024] analyzed the evolution of Ozone concentrations throughout rain events. Unfortunately, the article only covers ozone concentrations up to 80m from ground levels. Still, the results from the 80-meter levels can be compared. The article and Figure 19a indicate that at the 80 m level, Ozone concentrations after rain events are higher than before, which should be explained by the injection of Ozone by downdrafts.

Figure 19b presents the behavior of O_3 under the cloud cover of Deep convective clouds during the night. It can be seen that the expected concentrations of O_3 at 150m continue to be higher than at 80m. Other than that it can be noted that before the cloud detection at 80 and 150m the concentrations are decreasing. During the cloud cover, Ozone concentrations at all heights increased considerably, especially at the beginning of the detection. As a result, Ozone concentration after the detection is about 4ppb higher than before. One can note in Figure 20 that during the night, the concentrations of O_3 at 80 and 150m have a trend to decrease, but during the cloud event, the concentrations are

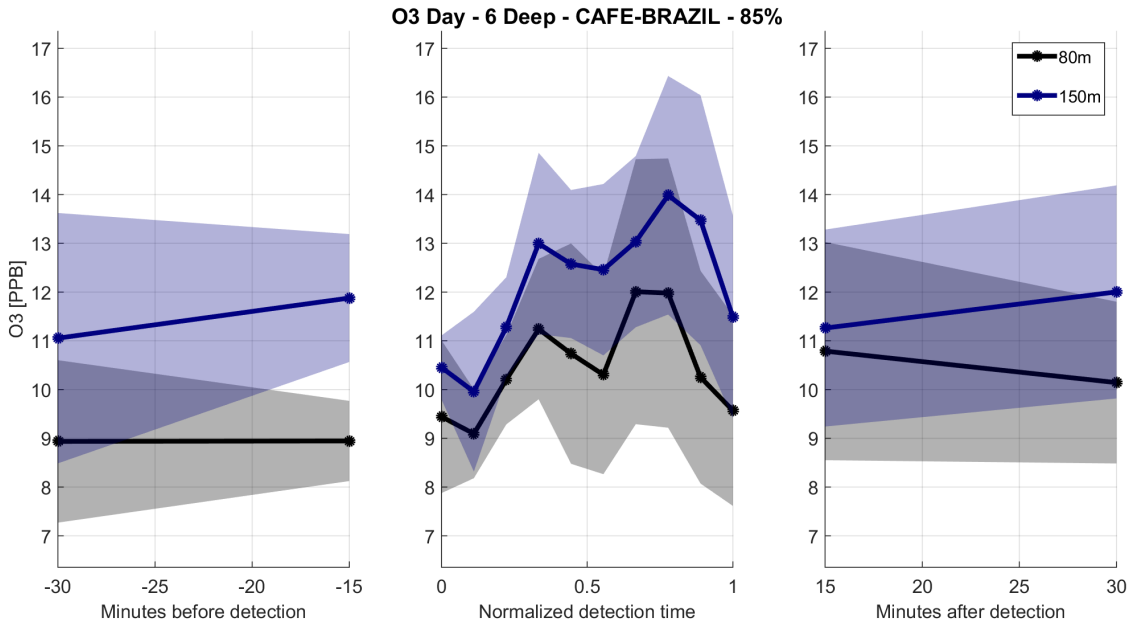

(a)

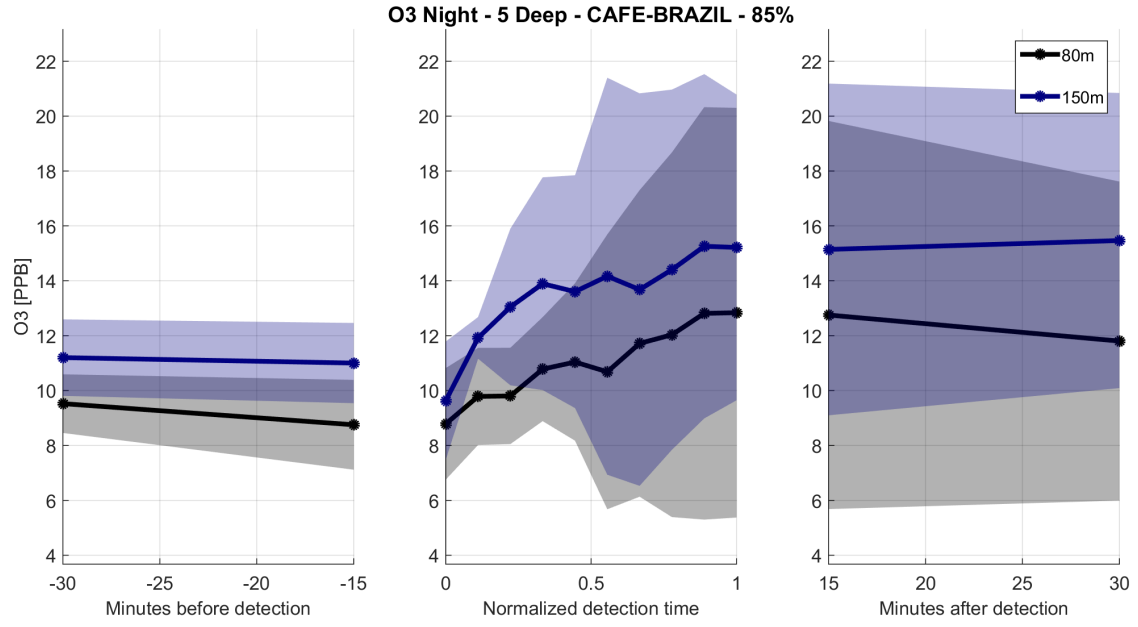

(b)

Figure 19: Evolution of O_3 concentrations from 30 minutes before until 30 minutes after the detection of a deep cloud during: a) the day boundary layer (6 cases); b) the night boundary layer (5 cases). The 2 different curves and their respective confidence intervals represent the evolution of the O_3 concentrations in different heights. The black curve represents the height level of 80m, and the blue curve represents the height of 150m. Day cases are the ones whose detection time is between 8am and 17pm. Night cases are the ones whose detection time is between 20pm and 5am. Ozone measurements were performed using the instrument TEI 49i during the CAFE-BRAZIL campaign.

increasing at all height levels. It indicates that it was caused by the transport of air rich in Ozone from higher altitudes through downdrafts. In addition to that, Figure 18 shows that most of the precipitation in this period has occurred at the very beginning of the detection, which coincides with the moment in which the increase in Ozone is maximum, indicating one more time that the downdrafts should be responsible for the increase in Ozone under the presence of Deep Clouds. Lastly, it is valid to mention that the results from the article Machado et al. [2024] corroborate what was observed in this study: at night at 80 m, Ozone concentration increases during rainfall events.

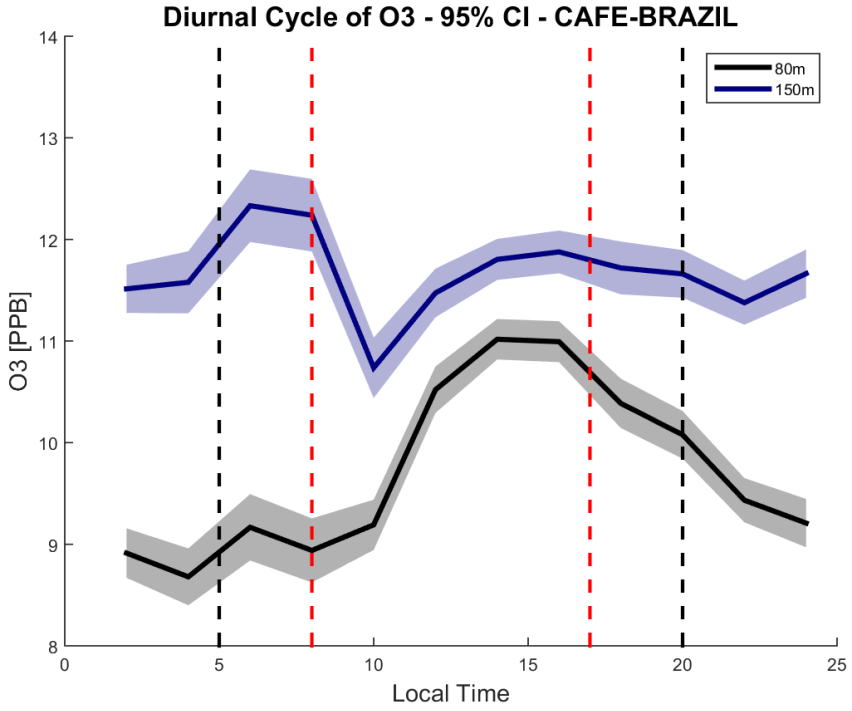

Figure 20: Diurnal cycle of O_3 calculated for the CAFE-BRAZIL campaign in two different heights, each one represented by a different curve. The black curve represents the height level of 80m and the blue curve 150m. The two red vertical dashed lines mark the interval of time defined as the day boundary layer. Outside the two black vertical dashed lines is the period defined as the night boundary layer. Ozone measurements were performed by the instrument TEI 49i.

This section has clarified that Deep clouds indeed impact the concentrations of Ozone and Carbon Dioxide by showing that during the detection of these clouds, the trends in the concentrations can go in the opposite direction of what it would just by the natural diurnal cycle. Now, for a deeper, more complete investigation of how the deep clouds affect the concentrations of these gases, a study case of a Deep cloud will be performed in the next subsection, aiming to clarify the importance of the downdrafts in this process and also trying to characterize how a deep cloud affect the general meteorological conditions in the surface.

4.4.2 A Case study - The relationship between downdrafts and gas concentrations

This section presents a case study of the evolution of meteorological parameters, as

well as the evolution of the concentrations of CO_2 and O_3 under the presence of a deep convection cloud.

The choice of a case study holds great importance. The process involves finding a deep convection case, during which the database is most complete. It is necessary to certify whether the instruments operate correctly and deliver precise and reliable data. Furthermore, the goal is to select a day when interesting events occur. This selection is essential to guarantee that the case study provides insights based on reliable information. Despite the fact the number of deep clouds detected during the CAFE-BRAZIL campaign is considerably larger than during CloudRoots, the deep cloud designated for this case study was detected between 10:42 and 12:54 of the fourteenth of August 2022 during the CloudRoots campaign. That is because the processing of the experimental data from CloudRoots was more advanced by the time this study case was performed, hence the dataset was more complete and which is necessary for a better characterization of the event.

Initially, it was investigated how the selected deep cloud affected the meteorological conditions at the ATTO tower. To do that, it was compared the evolution of a) potential temperature, b) variance of vertical wind speed (W), c) turbulent Kinetic energy, d) specific humidity, e) CO_2 concentrations at 79m, and f) Ozone concentrations at 80m between the deep convective case and an aggregate of shallow cumulus days conditions. The parameters were analyzed inside a window of two hours around the moment of the maximum precipitation rate, as in Machado et al. [2024]. In Figure 21, the blue curves represent the evolution of the parameters during the analyzed case. Meanwhile, the orange curves and their 85% confidence interval represent the average evolution of the parameters among an aggregate of shallow cumulus days. In other words, it represents the average of the parameters' time series within the investigated time window. Still, it's important to note that a day can only contribute to this average if shallow cumulus conditions are predominant and no deep clouds are detected. The daily classification of the predominant cloud conditions in CloudRoots is presented in Vila-Guerau de Arellano et al. [2024]. At last, the green dashed curve represents the absolute difference between the orange (shallow) and blue (deep) curves. To clarify this process, suppose that the maximum rain rate of the selected cloud happened at 11 o'clock. It means that the blue curve shows the evolution of the parameters from 9 until 13 o'clock only on the selected day. In turn, the orange curve depicts the average evolution of the parameters from 9 to 13 o clock, however this average considers exclusively days of predominant shallow convective clouds.

The first meteorological parameter analyzed was the potential temperature. Its evolution is displayed in Figure 21 a). It can be observed that there is a sudden decrease in potential temperature at the moment of the maximum precipitation rate, causing a difference of more than 5 Kelvin between the deep case and the aggregate of shallow cumulus days. Afterwards, the potential temperature gradually increases, reducing the difference. This is expected for the following reasons: abrupt variations in the potential temperature close to the surface indicate injection of air from higher altitudes since all the air in the planetary boundary layer is supposed to be at the same potential temperature, and that makes sense as the moment of maximum precipitation rate should contain strong downdrafts. Other than that, the air from the downdrafts should be colder because rain droplets falling evaporate and consume latent heat, which cools the air. Moving on to Figure 21b), it shows the evolution of the variance of the vertical wind speed. During the deep convec-

tion, the variance reaches its maximum at the moment of maximum precipitation, and it oscillates afterward, decreasing and increasing again. This can be attributed to the strong downdrafts at the moment of the maximum, causing turbulence and, consequently, the increase in the variance of the vertical motion. However, rain usually homogenizes the atmosphere in terms of temperature. Hence, the conditions are typically stable after the rainfall, which explains the decrease in the variance of the vertical motion afterward. The final increase in variance should be related to a reduction in cloud cover after the rain, allowing more radiation to reach the surface and heating it. This, in turn, restores turbulence to normal conditions. Figure 21 c) illustrates the differences in the evolution of Turbulent Kinetic Energy (TKE) under the presence of the Deep cloud and under normal conditions. TKE is the sum of the variance of the wind speed in the three directions, hence high values of TKE can be interpreted as strong turbulence. It can be observed that there is a clear peak in the TKE during the deep case at the moment of Maximum precipitation. Therefore, the analysis of the result from TKE should be similar to the variance of W. The peak of TKE in the moment of maximum precipitation is related to the downdrafts, a vertical air motion from higher to lower altitudes. It is interesting to see the low TKE during the shallow cloud days, which has a nearly constant and low value due to the small vertical motion associated with this cloud type. In addition, once the downdraft reaches the surface, it will spread the air radially around it, causing variance in the two horizontal directions. After the rain, there should be no downdrafts, and as mentioned before, the atmosphere conditions tend to stabilize. Consequently, turbulence will decrease and stabilize around the typical shallow conditions for the analyzed time as observed in the Figure 21 c).

Figure 22 d) presents the evolution of Specific Humidity (q), which, like the other meteorological parameters, was considerably affected by the rain. The blue curve shows that the specific humidity started decreasing about an hour before the maximum precipitation rate, reaching its minimum value 30 minutes post-maximum rain moment. Afterward, it rises again and overcomes the standard values 1 hour and a half after the maximum. At first glance, the fact that the specific humidity declines during the rain might seem unforeseen. However, specific humidity evaluates the amount of water vapor per unit air mass, not liquid water. The downdrafts attached to rain are composed of air masses that have already lost part of their water vapor to condensation, as in the process of rain formation, the amount of liquid water in the parcel increases whilst the water vapor content decreases. Therefore, the air injected by downdrafts is expected to contain a lower amount of water vapor than the air before the rain event, which explains the observed decrease in Q. After the rain, the specific humidity from the studied case overcomes the shallow conditions. This should be caused by the fact the rain will evaporate afterwards increasing the amount of water vapor in the air, consequently specific humidity will increase. The last two panels presented in Figure 21 e) and f) illustrate the evolution of concentrations of CO_2 and O_3. The CO_2 evolutions for both cloud types show a decrease in concentration, but the deep cloud case presents three decreasing steps. One first step before, more intense, a more stable decrease, and another more vigorous decrease after one hour. The impact on the concentrations of Carbon Dioxide is larger before the maximum rain rate and is of the order of 15 ppm. There is a clear gap in the levels of concentrations of CO_2 between the selected case and the average shallow day's conditions, which could be caused by the day-to-day variability of CO_2 instead of being caused by the Deep convection, but this

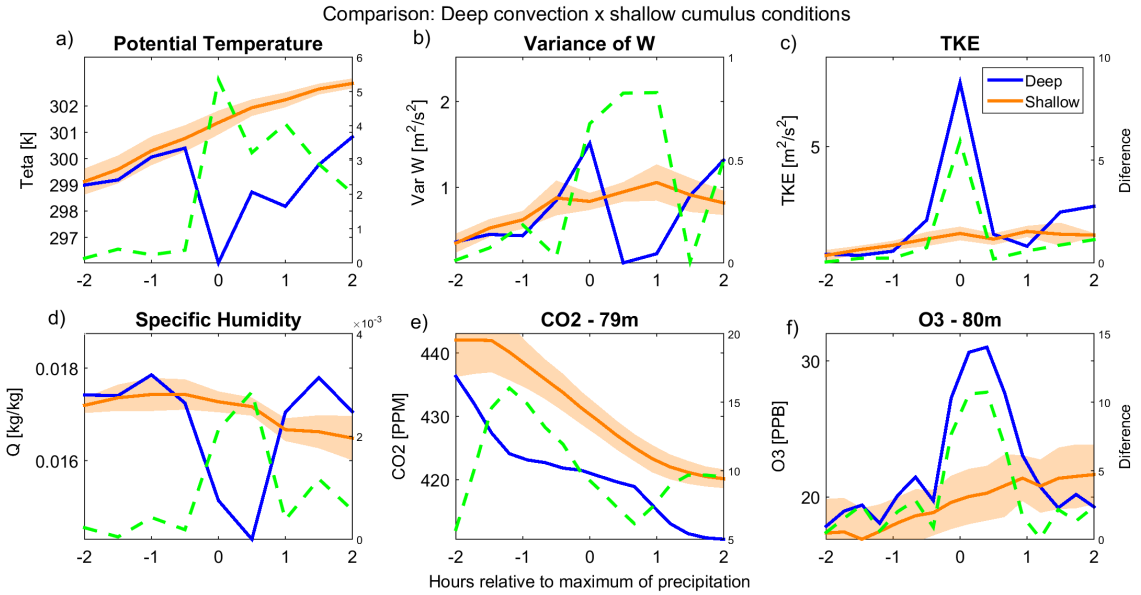

Figure 21: Time series of a) Potential Temperature b) Variance of W c) TKE d) Specific Humidity e) CO_2 f) Ozone within the time window of 2 hours around the moment of maximum precipitation rate of the deep cloud detected at August 14th, 2022. The moment of maximum precipitation was 11 am local time. The blue curve represents the evolution of the parameters during the analyzed case. The orange curves and their 85% confidence interval represent the average evolution of the parameters among an aggregate of shallow cumulus days during the CloudRoots campaign. The green dashed curves represent the absolute difference between the aforementioned curves. All measurements were taken at 80m.

can not be confirmed only with this Figure. Conversely, in Figure 21 f), it can be seen that the Ozone concentrations peaked close to the time of maximum rain rate. The increase of O_3 at the moment of maximum precipitation strongly indicates the injection of ozone-rich air from higher altitudes through the Downdrafts. Nevertheless, the subsequent fall in the ozone levels suggests that the injected air mass either quickly spread, or the ozone quickly reacted to other chemical species as it is a high reactant gas, or even the combination of these two factors. A more complete investigation of the variations of the concentrations related to the presence of downdrafts will be presented in the next paragraphs.

At this point, many hypotheses were put forward regarding the potential role of downdrafts in causing fluctuations in Ozone and Carbon Dioxide concentrations in the presence of Deep clouds and the ozone reaction inside and just above the canopy. Therefore, Figure 22 aims to test this hypothesis by graphically illustrating the evolution of the concentrations of CO_2 and O_3, together with the meteorological parameters that characterize a downdraft: the variance of the vertical wind speed, Turbulent Kinetic Energy, Precipitation and Potential Temperature. The reason for using the variance of the vertical wind speed instead of the actual values of it is that the data of the meteorological parameters are derived from half-hourly averages, and given that downdrafts are not expected to persist for so long at a fixed point at the surface, the average vertical velocity is less relevant than its variance for this study. Nonetheless, as the goal of this investigation is to understand

the variations in the concentrations, Figure 22 illustrates the evolution of the deviation from the profile measured 1 hour before T_i, the moment of the beginning of the detection of the selected Deep cloud. To clarify this process, imagine if at a certain height H, 1 hour before T_i, the concentrations of Ozone are ten ppb, then if 30 minutes later the concentrations at that same height are eight ppb, the graphic will show this value as -2 ppb. This technique facilitates the visualization of variations in the concentrations throughout the analyzed time.

Figure 22 a) and b) illustrate the evolution of deviations of CO_2 from the initial profile. They were divided into 2 different panels because the measurements were taken at the Instant tower until 80 meters and above measured at ATTO; also, the instruments used in the measurements were different. Nevertheless, the combined analyses of both panels are useful to gain important insights on the evolution of CO_2. Next, panel c) depicts the evolution of Ozone, measured at the ATTO tower. Moving on to the right side of this figure, panels d), e), and f) present the evolution of the meteorological parameters. Figure 22 d) is regarding the variance of the vertical wind speed (W), e) the Turbulent Kinetic Energy, and f) the precipitation rate and the potential temperature. The meteorological parameters were measured at the ATTO tower, except for the rain rate, which was measured at the Campina site.

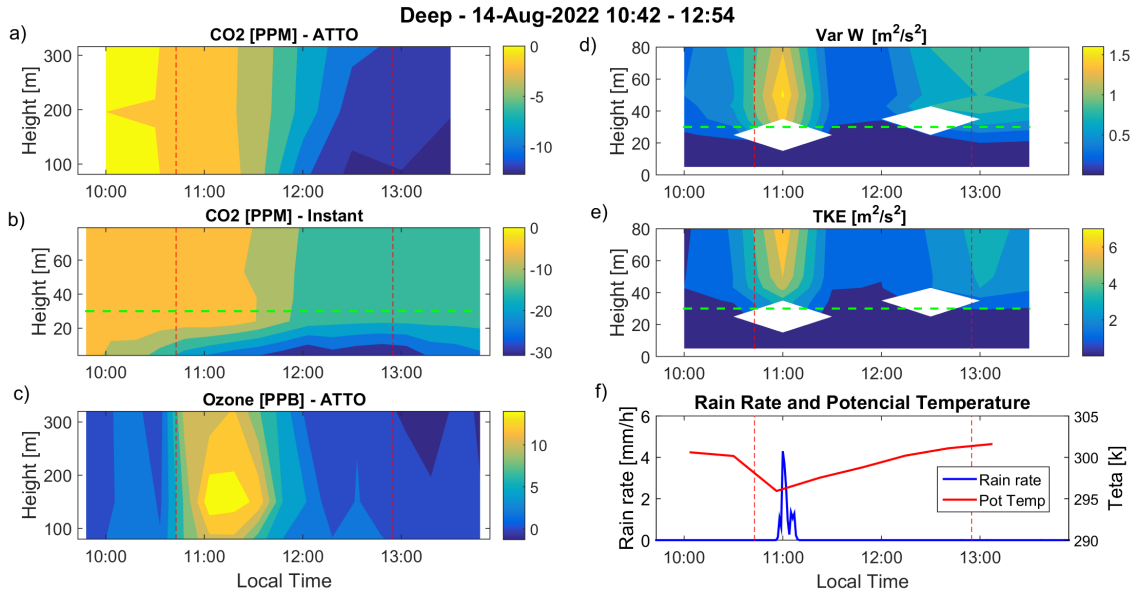

Figure 22: Time evolution of multiple parameters from 1 hour before until 1 hour after the detection of the Deep convection case, during the CloudRoots campaign on the 14th of August 2022. a) CO_2 concentrations at the height levels above 80m at the ATTO tower b) CO_2 concentrations at the height levels below 80m at the Instant tower c) O_3 concentrations from 80 to 320m at the ATTO tower d) Variance of vertical wind speed bellow 80m at the atto tower e) Turbulent Kinetic Energy (TKE) bellow 80m at the atto tower f) Rain rate (blue) at Campina and potential temperature (red) at ATTO. Vertical red dashed lines represent the time window of detection of the cloud. Horizontal green dashed lines represent the canopy height.

It makes sense to start analyzing Figure 22 by the meteorological parameters. It can be noted that it rained for about ten minutes, with the maximum precipitation rate close to 11

o'clock. Simultaneous to the rain, a decrease in potential temperature, an increase in the TKE and the variance of W were observed. These exact conditions are what characterized the Downdraft in this case. Now examining the combined Figure 22 a) and b), one can note that above the canopy height, indicated by the green horizontal dashed line, the CO_2 levels are constantly declining at all heights, which should occur due to the rain effect and the photosynthesis effect working as a sink of CO_2. The decline seems to be accelerated by the downdraft, which will inject air masses from higher altitudes in the PBL. One can note that above 80 m, the CO_2 concentration starts to decline exactly at the time the meteorological variables indicate the dynamic effect of the rain. Other than that, it can be noted that the decrease of CO_2 is maximum at the ground level, which should be explained by the fact that the turbulence generated by the downdraft might allow air penetration from above the canopy inside it. Related to the Ozone, an interesting result can be observed in Figure 22 c) that simultaneously to the downdraft, there is a strong increase of up to 10 ppb in the concentrations of Ozone at all heights, but the maximum concentration is around 150 m. This is strong evidence that the increase in O_3 observed in Figure 10 is caused by the injection of Ozone-rich air from higher altitudes into the planetary boundary layer.

The analysis presented in this section ends the sequence of results that focus on clouds affecting boundary layer conditions. The most important conclusion we could obtain so far is that among the studied cloud types, the deep convective clouds are the ones with the greatest impact on the surface. It was also shown that day and night cases of deep clouds have a distinct impact on the surface concentrations of trace gases if the parameter has a strong diurnal variability such as CO_2. Finally, in this section, it was demonstrated that downdrafts from deep convective clouds, characterized by the presence of rain and turbulence, are one of the factors that are responsible for causing oscillations in the concentrations of at least Carbon Dioxide and Ozone, but possibly several other gases. In the next sections, the results and the discussion will focus on characterizing events of significant variations of the analyzed gases and particles.

4.5 A combined View of Gas and Particle Variation

This session intends to provide an initial view of the different aspects of gas variability and open different scientific questions for further studies. In the future, deeper investigation, specific for each gas and particle, should be done to comprehend this complex system better.

This subsection will present the results regarding significant variations in the concentrations of CO_2, CO, CH_4, O_3, and Black Carbon. The analyses conducted here aim to investigate whether the variations occur independently of rainfall and gain insights into the physical mechanism involved in the oscillations of the gases and particles. Previously, the methodology consisted of first identifying clouds to analyze the concentration's behavior. Now, the approach shifts to first identifying significant variations in the concentrations and later checking whether rainfall coincided with these peaks and trying to understand what are the associated physical processes causing the variations. The peak concentrations were also classified as individual peaks or associated with various simultaneous peaks in the other parameters, in this case corresponding to an oscillation pattern. A secondary objective is to identify cases when most variables oscillate without being in-

fluenced by precipitation, thereby identifying potential "golden cases" for future studies.

The first step is to investigate whether the concentration peaks of the compounds occur exclusively during rainfall events or if they also manifest regardless of precipitation. For this, it is convenient to create a visual representation that allows easy identification of the peaks throughout the analyzed period and indicates whether they occur simultaneously with rain. This last part is especially useful to indentify instances where all analyzed compounds oscillate together, regardless of rainfall. The visual representation developed for this study consists of a chart for each campaign, where the horizontal axis depicts the day. In contrast, the vertical axis comprises five distinct lines, each representing a different chemical compound. The first line with the pink color represents the CO_2 peaks, the second line with the cyan color shows the CH_4 peaks, the third line with the red color is regarding CO, the fourth line with the black color is related to the Black carbon variations, and finally the fifth line with the blue color illustrates the peaks of O_3. This graphical arrangement provides a simple overview of the peak's occurrence over time. In addition, markers denote different variations: rings denote peaks and filled circles represent oscillations. Moreover, the incorporation of green squares symbolizes that the variation in the concentrations happened simultaneously with rain. These markers enable an easy spotting of the cases where peaks or oscillations coincide with rainfall, creating a simple way to analyze whether precipitation is the only factor causing the concentrations to vary. This graphical representation enables the identification of compound peaks and oscillations concerning rainfall and facilitates the identification of concurrent compound peaks across multiple days. Therefore, it serves as a strong visual tool in the present investigation.

Figure 23 illustrates the occurrence of significant variations of the compounds throughout the entire month of August, when the CloudRoots campaign was held. This analysis should be seen as the behavior of the dry season, which is different from the wet season. Initially, each compound will be analyzed individually, and afterward, whether there is a correlation in the variations among the different compounds will be discussed. For CO_2, significant concentration variations can be observed; most of them were classified as peaks (80%), and most occur during non-rain events (70%). The variations are well spread throughout the entire period. The CH_4 peaks are mostly peaks, but oscillations represent 4 out of 9 cases, and the events are also mostly independent of precipitation and spread throughout the month. The CO variations happened within a very short time, concentrated around the twentieth of August, with the first event a peak followed by 3 days of oscillating concentrations. Moving on to the Black Carbon variations, one can note that most variations detected were oscillations, and 5 were around the twentieth of August. The Ozone variations are half oscillations and half peaks; only two of the six variations were related to precipitation. It can be seen that the majority of the variations of O_3 were detected around and after the twentieth of August.

Before attempting to understand the main sources of the variations of the different compounds and explain why some compounds present their variations spread in time, with multiple peaks and oscillations, like CO_2 and CH_4. In contrast, others, like BC, CO, and O_3, have their variations concentrated over a short period; it is important to consider the broader context. August is in the dry season, marked by increased biomass burning across the Amazon. Therefore, it's natural to expect a strong connection between the fluctuations of certain compounds and the fire events. For instance, it can be seen that on all days when significant variations of CO were detected, Black Carbon presented the

same behavior. Knowing that both are biomass-burning products suggests the intensity of the burning in the region should impact the concentrations of BC and CO.

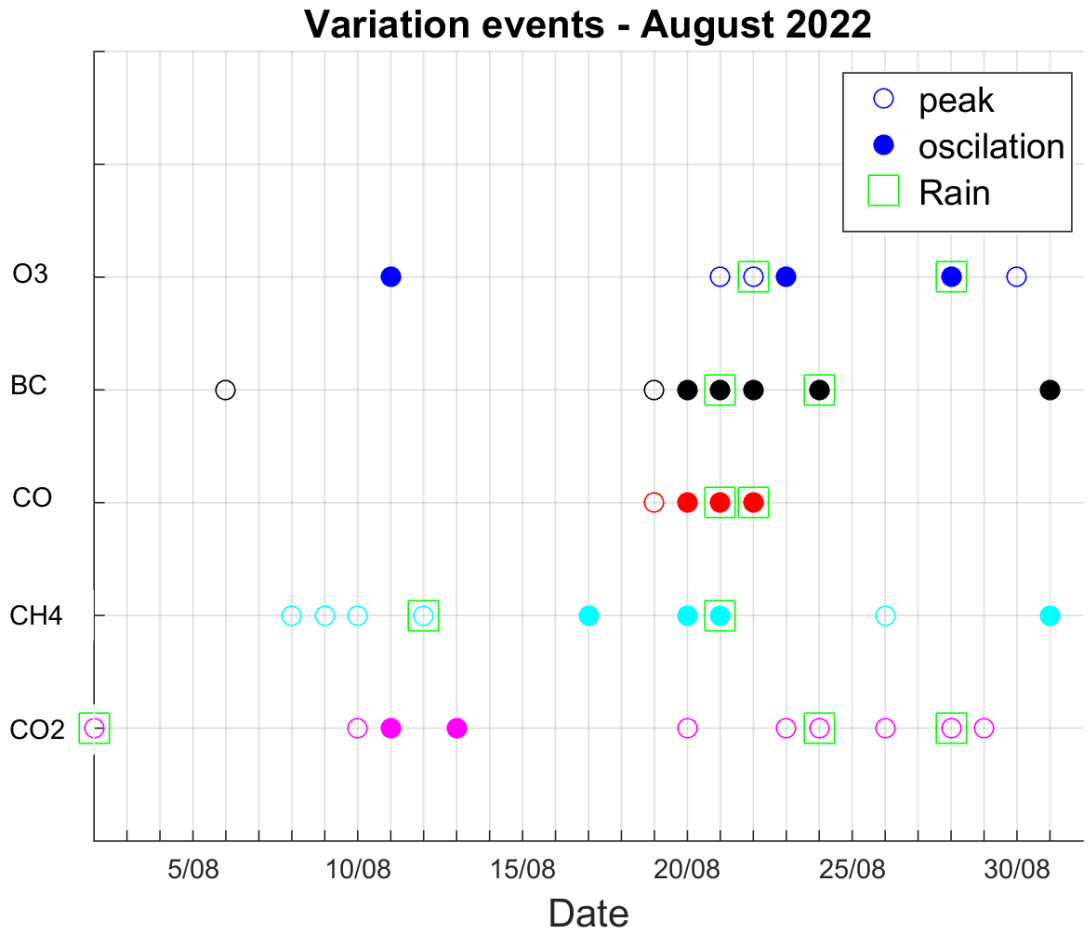

Figure 23: Visual chart on the daily occurrences of significant variations in the concentrations of CO_2 (first line - pink), CH_4 (second line - cyan), CO (third line - red), Black Carbon (fourth line - black) and Ozone(fith line - blue). Variations are divided into two categories: Peaks (marked as rings) and Oscillations (marked as filled circles). In addition, if the variation occurred simultaneously with rainfall, it will be marked with a green square. The analyzed period is the entire month of August 2022, when the CloudRoots campaign was held. All gas concentrations were measured at 80m, and the Black Carbon concentrations were sampled at 320m.

Figure 24 depicts the evolution of the number of fire focus detected in the state of Amazonas throughout August 2022, and the results do not indicate a stronger fire activity during the days that the concentrations of CO and BC present significant variations. Actually, on the days that anticipate the period of variations in BC and CO, the number of fires is not much higher than on other days. It can be seen that the number of fires on the 19th, when the variations on CO were first detected, is less than half of the 13th. It must be mentioned that the region where the ATTO tower is situated is highly preserved, and the number of fires in its surroundings is not expected to be high. Therefore, the wind patterns should be a crucial factor for regulating the concentrations of CO and Black Carbon

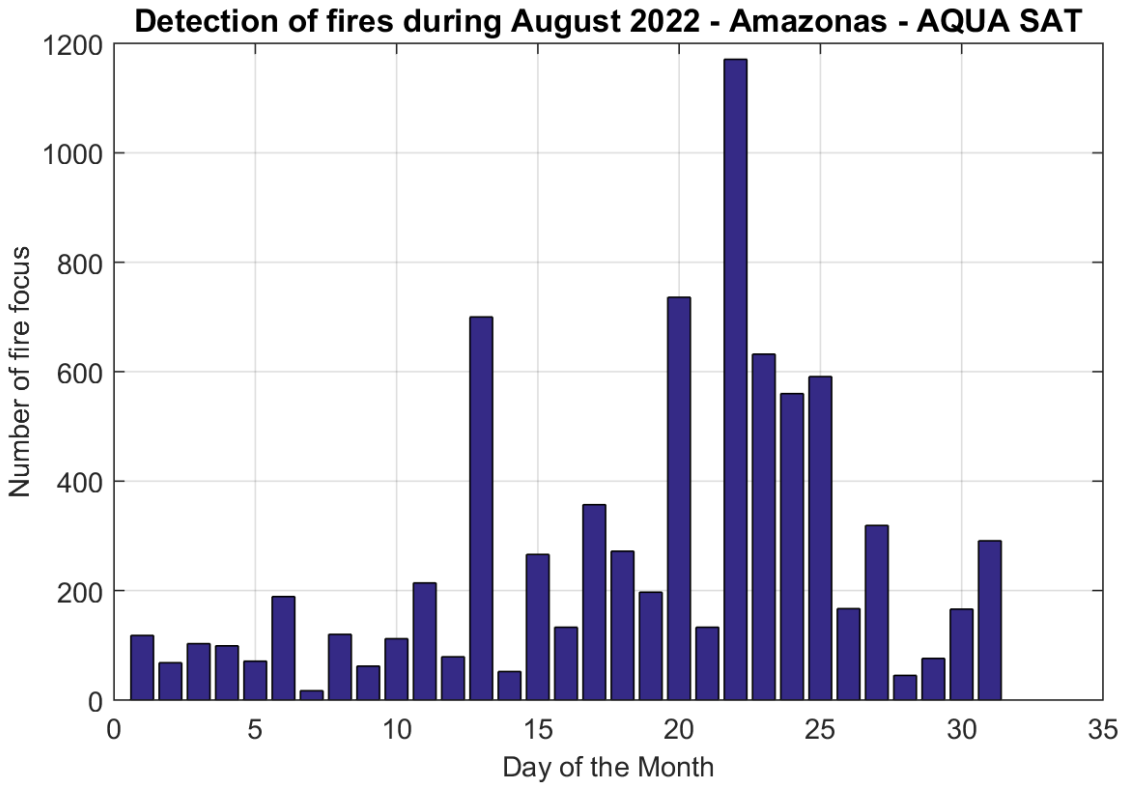

Figure 24: Dayly number of fires detected at Amazonas State by the satellite AQUA during August 2022, when the CloudRoots campaign was held. These data can be accessed at the portal http://terrabrasilis.dpi.inpe.br/queimadas/bdqueimadas/#graficos .

concentrations at ATTO. It might transport polluted air from highly deforested regions or regions with active fires to the ATTO, impacting the concentrations of BC and CO. Figures 26 and 27 present the wind on different days of August 2022, at 700 hPA, the layer around the Amazonian low-level Jet Anselmo et al. [2020]. During most days of the month, the winds move westwards at the entire state of Amazonas, bringing clean air from pristine forests. However, on the 18th, the atmosphere starts to be modified due to the penetration of a squall line and the formation of a vortex located south of the Amazonian, breaking this pattern. On the 19th, the direction of the wind changes to the northwest. This wind pattern transports air directly from the deforestation arch, the most deforested region with intense biomass-burning activity, to ATTO. Hence, this might be an important factor for causing the peaks in Black Carbon and Carbon Monoxide observed on the 19th, which is the first day of the sequence of the 4 days in which significant variations were observed in the concentrations of BC and CO. It is important to mention that this study does not provide enough evidence to conclude whether wind patterns are the only responsible for the observed peaks in CO and BC at ATTO during the dry season. Other factors, such as unforeseen burning nearby or unaccounted-for meteorological parameters, could also contribute. Nonetheless, it does suggest that future research on this topic should prioritize investigating wind patterns, as they likely play a significant role in driving BC and CO concentrations in the region.

Now, regarding the significant variations of CO_2 and O_3, they seem to be directly related to up and downdrafts, which at this point should be expected due to the discussions

from the previous sections. On multiple days, phase oscillations between the two compounds were observed, meaning that when the concentrations of one increase, the other decreases. This process can be explained by the vertical profile of the concentrations of these two gases. Hence, when air from the canopy is transported to the height of 79m, the concentrations of CO_2 are expected to rise and O_3 to decrease. On the other hand, if air from higher altitudes is injected at this level, the reverse process should be observed. An example of this phase variation is illustrated in Figure 25, where it can be seen close to 9 AM, the simultaneous and opposite variation in the concentrations of CO_2 and Ozone.

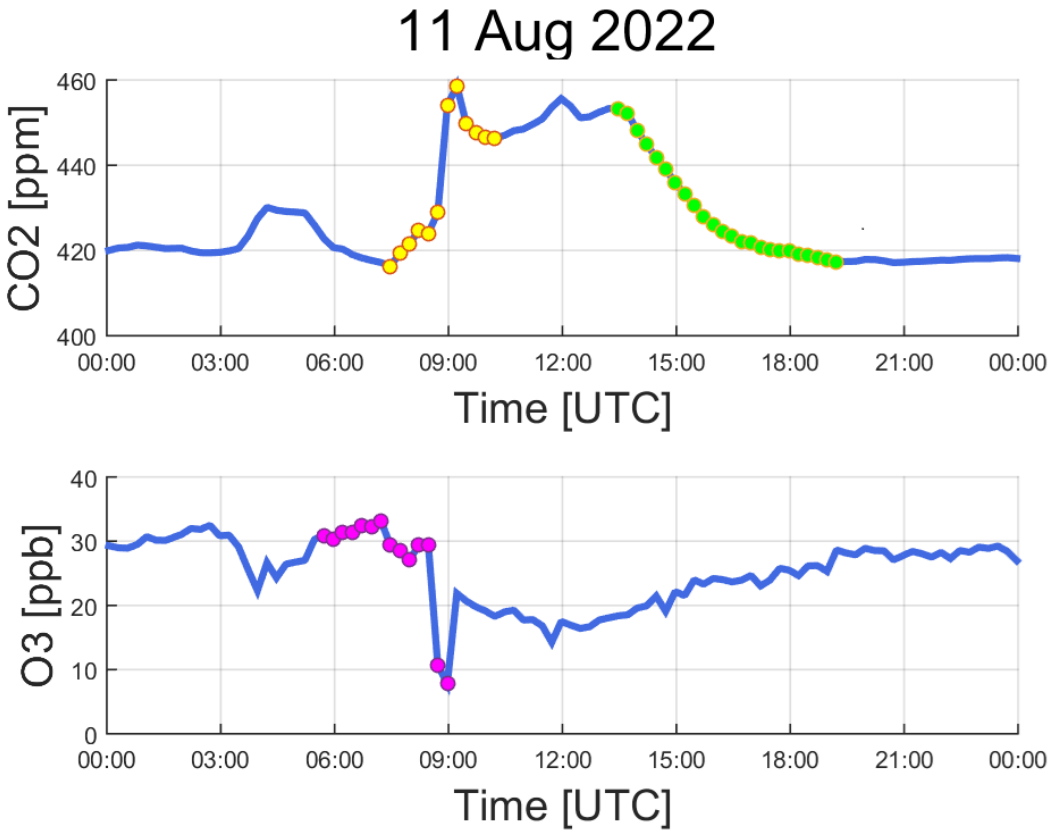

Figure 25: Time series of the concentrations of CO_2 at 79m (illustrated at the upper panel) and O_3 at 80m (illustrated at the panel at the bottom) on the 11th of August, 2022. The colored dots describe the significant variations in the concentrations of these gases. The yellow dots represent peaks, the green ones depict the valleys, and the pink stands for the oscillation. This Figure demonstrates that CO_2 and O_3 concentrations are in phase.

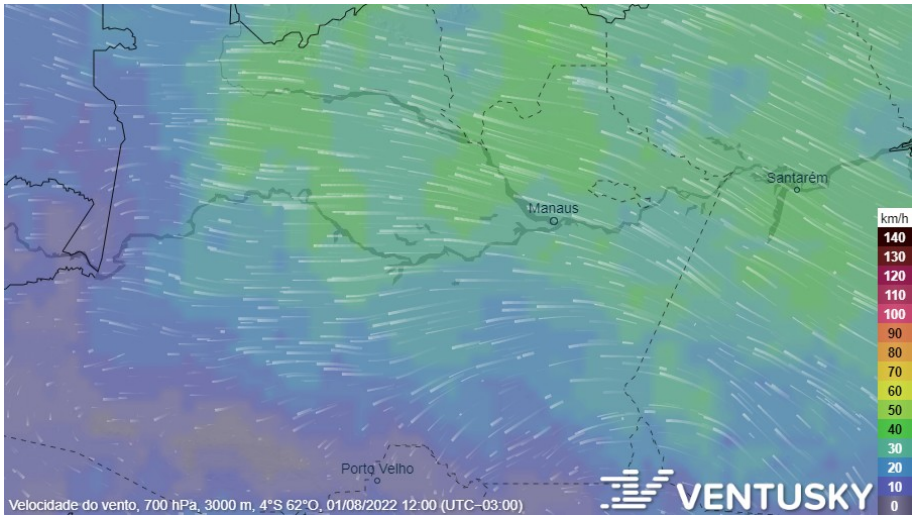

(a)

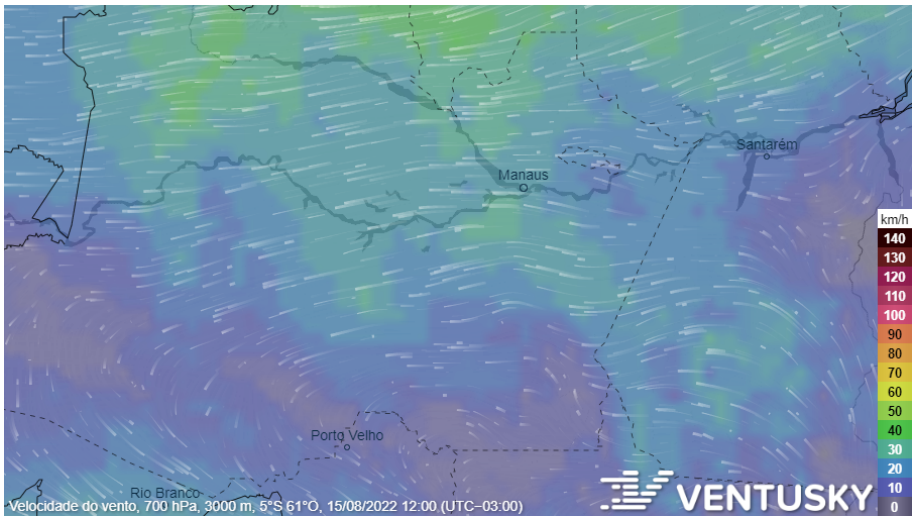

(b)

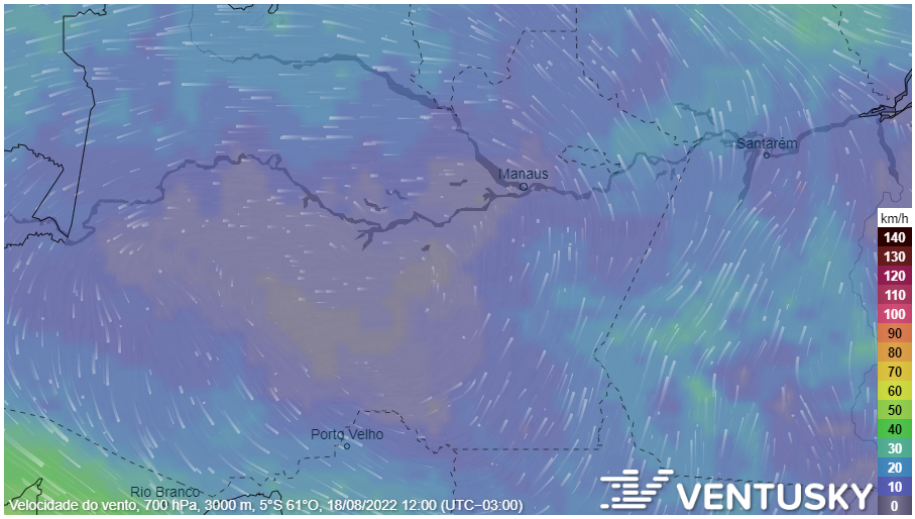

(c)

Figure 26: Illustration of the wind patterns at the Amazonas state throughout August 2022, at 700hpa, 12:00 local time. a) August 1st; b) August 15th; c) August 18th; This images were obtained at at https://www.ventusky.com/?p=-3.9;-56.2;5&l=wind-700hpa&t=20220806/1200 .

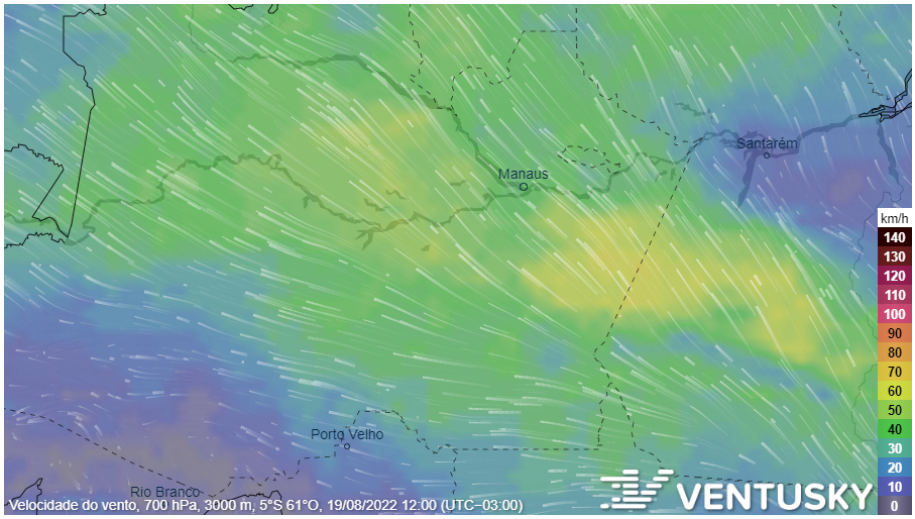

(a)

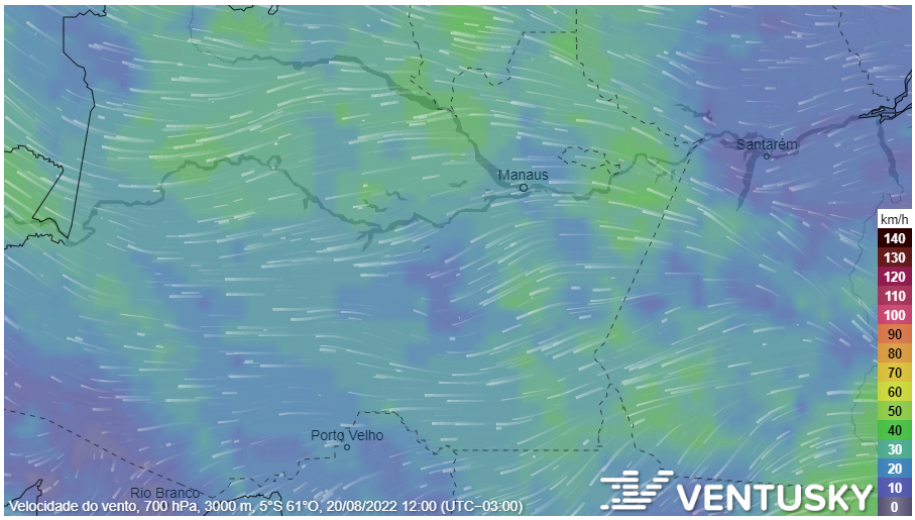

(b)

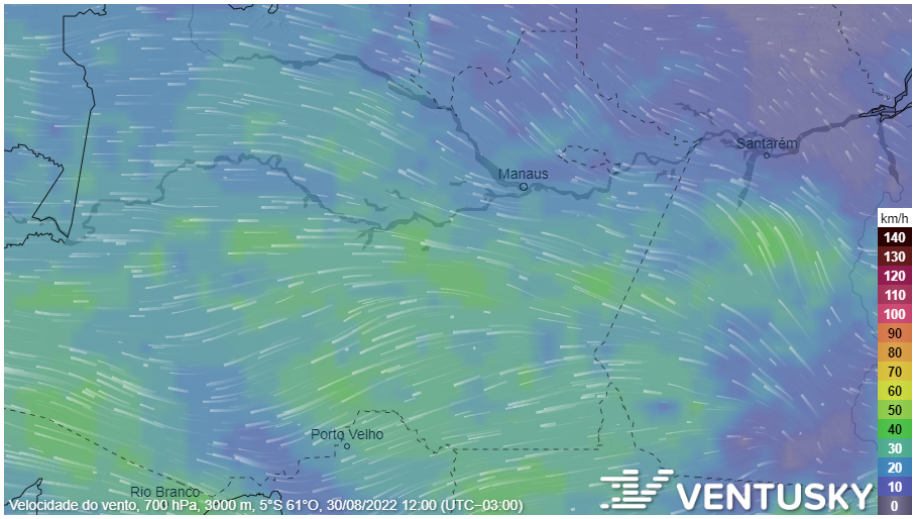

(c)

Figure 27: Illustration of the wind patterns at the Amazonas state throughout August 2022, at 700hpa, 12:00 local time. a) August 19th; b) August 20th; c) August 30th; This images were obtained at at https://www.ventusky.com/?p=-3.9;-56.2;5&l=wind-700hpa&t=20220806/1200 .

Figure 28 illustrates peak concentrations of the compounds throughout December 2022 and January 2023 during the CAFE-BRAZIL campaign. The **CO_2** presents its peaks and oscillations well spread throughout the period. Most of them are associated with rainfall events (75% of the cases), which makes sense since it was already discussed in previous sections that rainfall directly impacts concentrations of CO_2. The **Methane** peaks and oscillations spread well throughout the two months. However, the association with the presence of rain is slightly smaller than for CO_2; only 10 out of 17 variations were simultaneous to rain (60% of the cases). Both gases have a considerable frequency of rain cases. Of course, it is the wet season, where rainy events occur nearly every day, so the peaks cannot be justified only by the occurrence of rain. The analysis requires a more complex evaluation. Regarding the variations of **CO**, it can be noted that they are also well distributed in time, and the correlation with rainfall is less significant than it was for the previous two gases, as only 6 out of 13 peaks and oscillations were detected simultaneously to precipitation. **Black Carbon** peaks and oscillations are concentrated in the first half of the studied period, and their correlation to precipitation is the weakest among all parameters, with only 5 out of 13 peaks being simultaneous to rainfall. At last, **O_3** variations are well distributed throughout the campaign, and its correlation to rain is the strongest among all the 5 compounds. Only 2 out of 18 variations were not related to rainfall, which makes sense as it was demonstrated in previous sections that downdrafts from deep clouds corroborate to increase the concentration of Ozone on the surface.

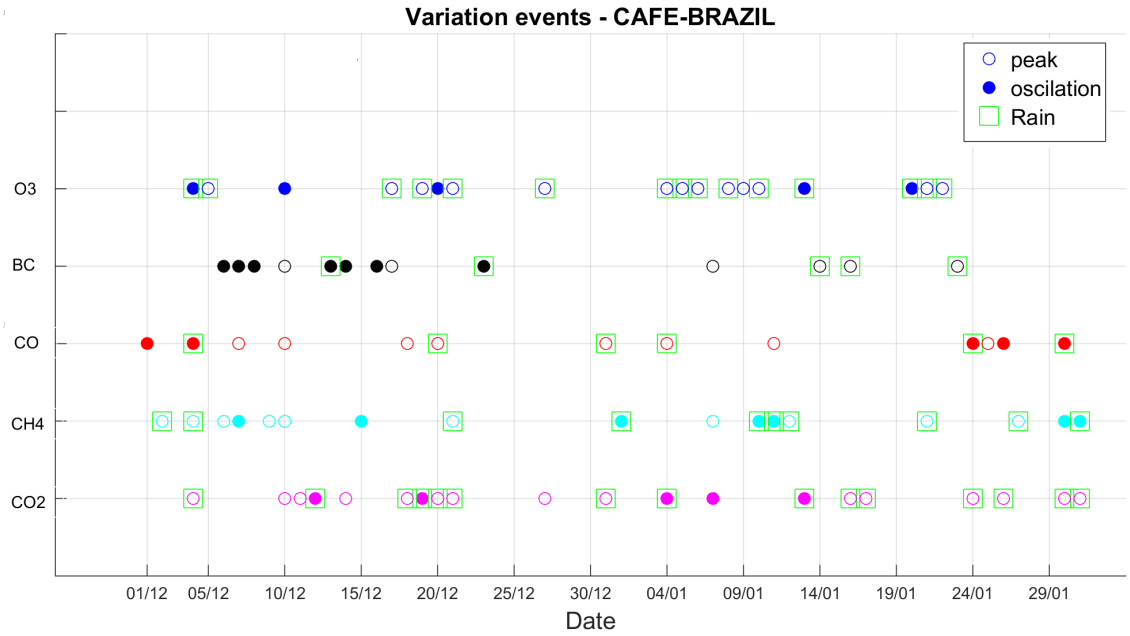

Figure 28: Visual chart on the daily occurrences of significant variations in the concentrations of CO_2 (first line - pink), CH_4 (second line - cyan), CO (third line - red), Black Carbon (fourth line - black) and Ozone(fith line - blue). Variations are divided into two categories: Peaks (marked as rings) and Oscillations (marked as filled circles). In addition, if the variation occurred simultaneously with rainfall, it will be marked with a green square. The analyzed period is from December 2022 to January 2023, when the CAFE-BRAZIL campaign was held. All gas concentrations were measured at 80m, and the Black Carbon concentrations were sampled at 320m.

To understand the main sources for the observed variations, it is important to consider that the measurements were conducted during the wet season, and the Amazonian atmosphere is very clean, mainly in the pristine forests around the ATTO. Previous sections highlighted that rainfall considerably impacts the concentrations of both CO_2 and O_3, and the peaks of both these gases are also correlated to precipitation in most cases. The methane peaks are more complicated to describe, as CH_4 sources are most related to fauna, flora, fungi, and flooded areas from the rainforest. The methane emissions might be indirectly related to rainfall since the emissions are related to the humidity in the soil. The CO variability is different between CloudRoots and CAFE-BRAZIL and appears to have a different forcing. Regarding BC variations, it should be remembered that during the wet season, the main source of Black Carbon in this part of the Amazon is due to long-range air transport. Holanda et al. [2023] shows that around 60% of the BC concentration is from biomass burnings from West Africa in this period. However, the amount of CO from this long-range transport is much lower than that carried in a short range as in the dry season Holanda et al. [2020]. This factor should indicate why, this time, the peaks of CO and BC are not strongly related, and it would make sense if the peaks of CO during the dry season were related to emissions of pollution from Manaus City, located 150km from ATTO. Hence, as the sources of Black Carbon and CO are not local, it is likely that wind patterns are a crucial factor in regulating the concentrations of both compounds.

It can be seen that on the 10th of December, all 5 different analyzed parameters presented significant variations regardless of rain. Figure 29 depicts the concentration of all 5 parameters and the rain rate throughout the day. It is noticeable, however, that not all compounds are simultaneously peaking. CO_2 levels start to rise simultaneously with the Ozone at around 8am, but they reach their maximum earlier, close to 10 am. In comparison, Ozone concentrations continue to increase from 9am to 12pm, together with the observed increase in BC. The two most dislocated increases observed are from CH_4 and CO, which occurred simultaneously between 12 and 15pm.

As briefly discussed in the previous paragraphs, BC during the wet season is driven by long-range transport from African biomass burning and was also associated with the high concentrations of Ozone in the stratified layers of pollution described in Holanda et al. [2020]. Between 9am and 12pm it is observed an increase of the concentrations of both Ozone and Black Carbon. However, at this point, it is unclear how these atmospheric rivers containing high concentrations of BC and Ozone penetrate the boundary layer, especially under clear sky conditions. A plausible explanation for a case like the one displayed in Figure 29, is that at the end of the day, there is a heavy precipitation event associated with deep clouds. It is known that in the surroundings of these convective systems, dynamic features could produce Gravity Waves, which are an alternating pattern of up and downdrafts in the height of the PBL. Consequently, if the gravity waves encounter the atmospheric aerosol rivers, they could inject air masses rich in Black Carbon and Ozone into the boundary layer. That could explain the simultaneous increase in both parameters. However, only this analysis cannot prove the presence of gravity waves controlling the boundary layer gas concentration and oscillation. To demonstrate this hypothesis, it would be necessary to study case by case and include several other meteorological parameters and model simulations. A model simulation for each day would be very useful to support the hypothesis of gravity waves at the moment of the increase in the concentrations. As a initial investigation, it will be presented in the next subsection

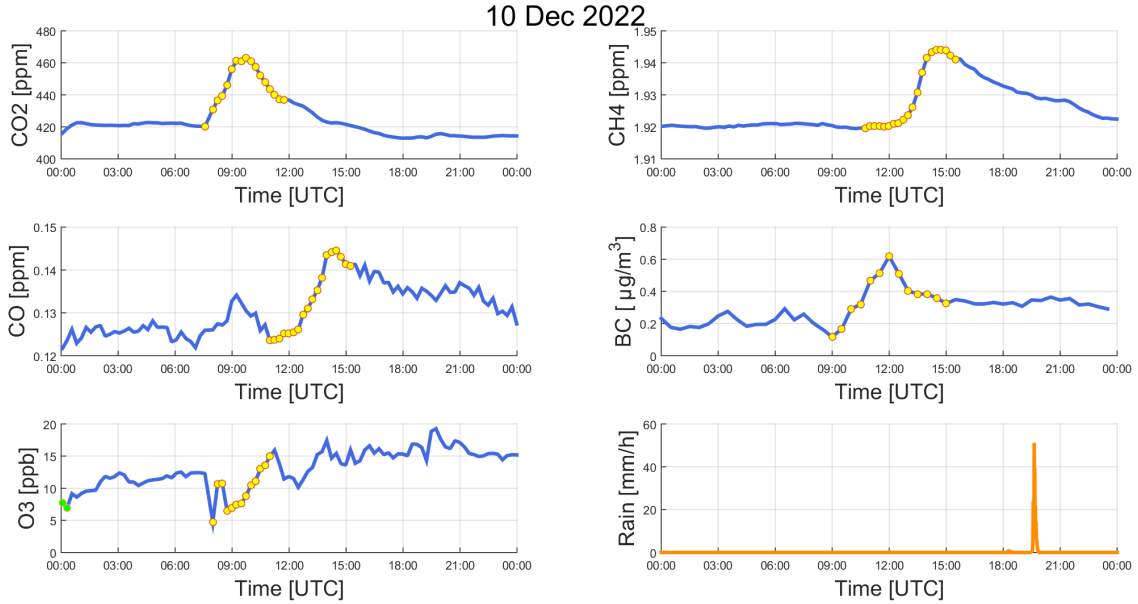

Figure 29: Time series of the concentrations of CO_2, CO and CH_4 at 79m, O_3 at 80m, Black Carbon at 320m and precipitation rate at the 10th of December, 2022. The colored yellow signalize the ocurrance of peaks in the concentrations of these parameters.

a general case study to analyze whether gravity waves exist during mesoscale convection and can contribute to the exchange between the boundary layer and the free troposphere.

4.6 Model Simulations - MesoNH

In this last section, it will be presented and discussed the results from the model simulations using the Mesoscale non-hydrostatic model (MesoNH). See Lac et al. [2018] for a detailed description. The model was run using a horizontal domain of 800km^2 including the ATTO-Campina sites, with a resolution of 200m, and a vertical grid with 130 levels with a spacing varying from 20m near the surface to 200 m at the model top at 20-km altitude. The initial and boundary conditions were provided by European Centre for Medium-Range Weather Forecasts (ECMWF) operational analyses, from which the model was run for 24h, with time steps of 3s. Simulations were performed on the 18th of January of 2023, during the CAFE-BRAZIL campaign. This date was selected through a joint effort to execute a model intercomparison for CAFE-Brazil, with several mesoscale models simulating the same day, aiming to compare their ability to reproduce the observations and determine how close they are to representing the processes at play. However, in this project the goal of the computational analysis was to obtain insights into whether the model reproduces gravitational waves and if these waves produce a dynamic field that can inject air from the free troposphere into the atmospheric boundary layer. The identification of the gravity waves at the height of the PBL involves two parts. The first one is the visual inspection of the map of vertical wind speed in the entire domain of the model at the height of the PBL, and the second part is a statistical analysis based on a wavelet transform focused on the region where the gravity waves were visually spotted.

Figure 30 illustrates the map of vertical wind speed in the full domain at 6:45 UTC.

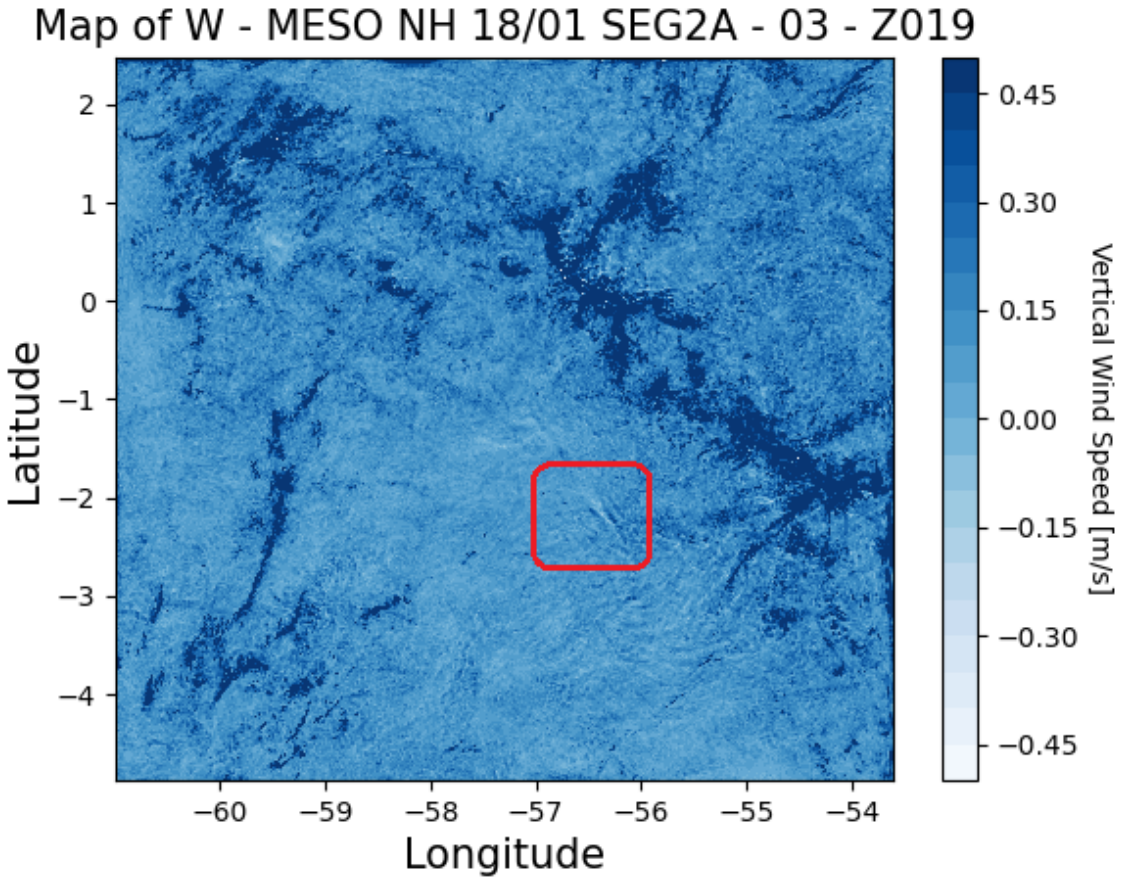

Figure 30: Simulated Vertical wind speed map at PBL height, generated by the MesoNH model, at 6:45 UTC, January 18th, 2023. The red box indicates the region where gravity waves were visually spotted.

There is a large region in this Figure, in which there is a cluster of negative W values. This cluster is the location of a squall line inside the domain. In the surroundings of the squall line, it can be seen some perturbations that have the appearance of wave fronts spreading after a rock falls in the water. These discreet waves are the gravity waves, and the red square delimitates a region in which these perturbations have the exact look of what it is being searched for: a sequence of alternate between up and downdrafts in the radial direction of the squall line.

After visually identifying the gravity waves, it is necessary to use statistical tools to support the analyses, as visual inspections are insufficient and often incorrect. The wavelet analysis fits this investigation, as it is widely used to identify certain types of oscillation frequencies among data series. The most common application of wavelet analyses is to transform a temporal series of data into a map that indicates the predominant oscillation frequencies in each time step. However, in this case, the application of the wavelet transform was adapted to fit the data. After the visual inspection, a fixed longitude where the gravity waves are situated was selected. Instead of applying the wavelet in a temporal series, it was applied in a spatial series of vertical wind speeds in the function of the latitude, and the result of the wavelet is a map that indicates the wavelength of the predominant oscillations for each spatial step. Figure 31 depicts the wavelet analyses

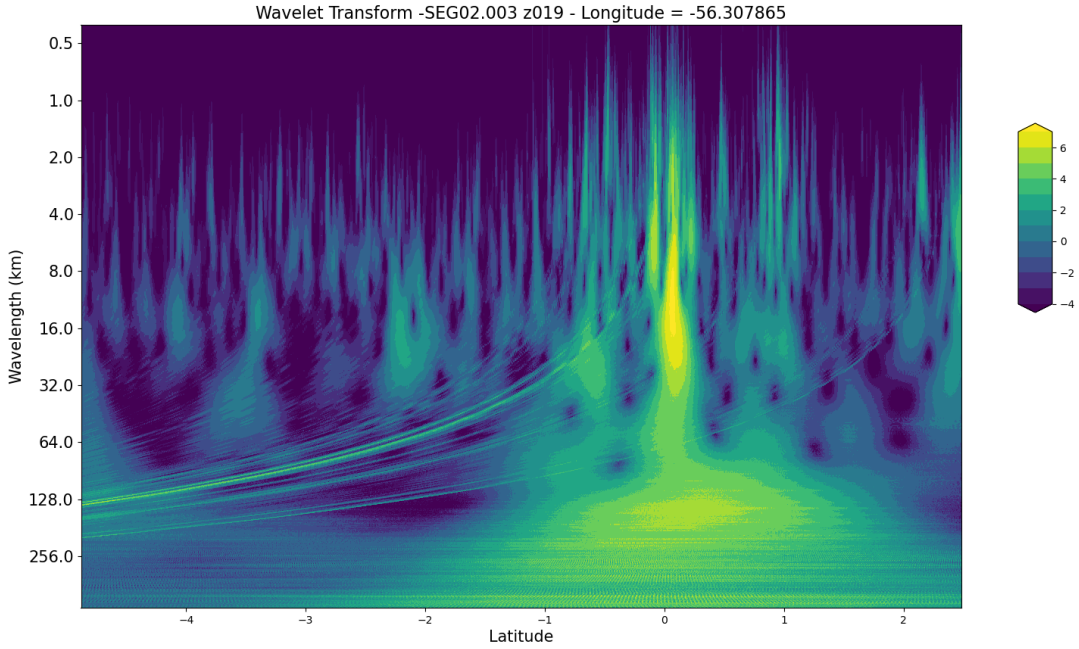

Figure 31: Wavelet Analysis of Latitudinal Distribution of Vertical Wind Speeds (W) at the fixed Longitude -56.3 Degrees. The latitudes are depicted on the horizontal axis and the wavelengths are displaced at the vertical axis.

applied in the latitudinal distribution of W, fixed at the longitude of -56.3 degrees. The red square that denotes the specific gravity wave that is going to be analyzed is situated between -3 and -1 degrees of latitude. In Figure 31, one can note that within this range of latitude, there is a peak of energy in the Wavelet distribution, indicating the presence of oscillations with wavelengths between 8 and 32 km, which is the size scale expected for gravity waves, as described in Kuettner et al. [1987]. The strong peak of energy in the 0-degree latitude is due to the presence of the squall line.

The next step consisted of fixing a latitude, where the gravity waves were visually spotted, and producing a wavelet transform in the longitudinal distribution of the vertical wind speed. Aiming to obtain a different analysis from Figure 31, now different time steps were analyzed. For each time step, a wavelet transform was executed. As wavelengths of the gravity waves should range between 0 and 32km, the energy values of each wavelet transform within that size range were summed. Therefore, in each time step, a longitudinal distribution of the sum of the wavelet transform was produced. Figure 32 illustrates the time evolution of the sum of the wavelet transform ranging between wavelengths from 8 to 64km. A significant energy peak can be seen between the longitudes of -55 and -57 degrees, the same location where the analyzed gravity waves are. Hence, the combination of the analyses in the Figures 30, 31 and 32 indicate the presence of gravity waves situated within the latitudes -1 and -3 degrees and the longitudes -55 and -57 degrees.

Finally, after properly identifying the gravity waves, the main goal of using the model simulations is to investigate whether gravity waves can contribute to the exchange of air

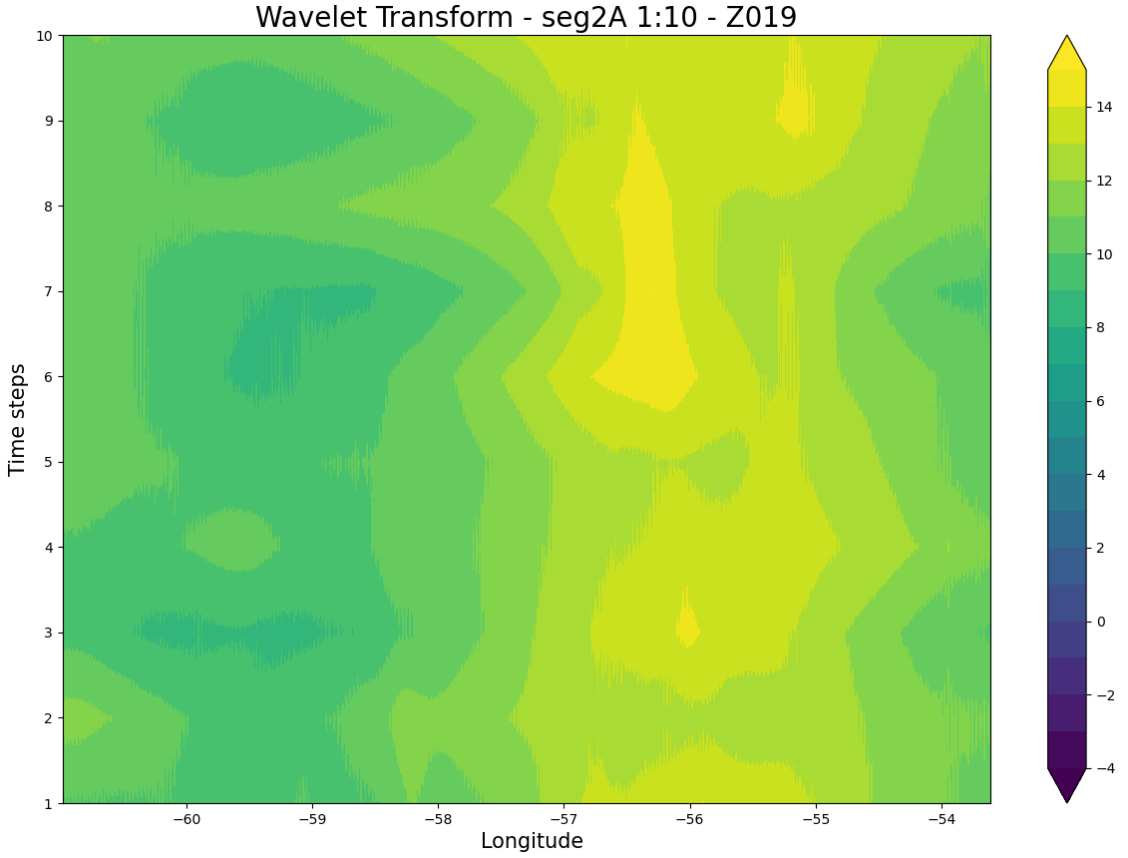

Figure 32: Time series of wavelength integrated Wavelet function of longitudenal Distribution of Vertical Wind Speeds (W) at the fixed latitude of around -2 Degrees. The longitudes are depicted on the horizontal axis and the time steps are displaced at the vertical axis.

masses between the free troposphere and the planetary boundary layer. To do that, the variable called Relative Vapor Transport (RVT), which is related to water vapor mixing ratio at a height level within the PBL, was analyzed in the region where the oscillations were identified. The aim was to check whether altering water vapor mixing ratio patterns can also be seen. Figure 33 depicts the map of the water vapor mixing ratio at 86m meters inside the PBL. The highlighted blue square indicates the region where the gravity waves were identified. Inside the box, strong lines with an alternating pattern between high and low levels of RVT on the bottom part of the square can be seen. However, the oscillations in the water vapor mixing ratio inside the PBL are in a different direction than the gravity waves. On the other hand, there are weaker alternating lines of RVT on the upper section of the square, which are in the same direction as the gravity waves. Therefore, it could be caused by the injection of air with different mixing ratios during the downdraft moments. Despite finding oscillating patterns aligned with the direction of gravity waves and close to their identification region, this study lacks sufficient evidence to confirm the hypothesis definitively. Nonetheless, the analyses presented here give good reasons to explore this topic further, as they suggest that gravity waves do play a role as a mixing agent between the free troposphere and the atmospheric boundary layer.

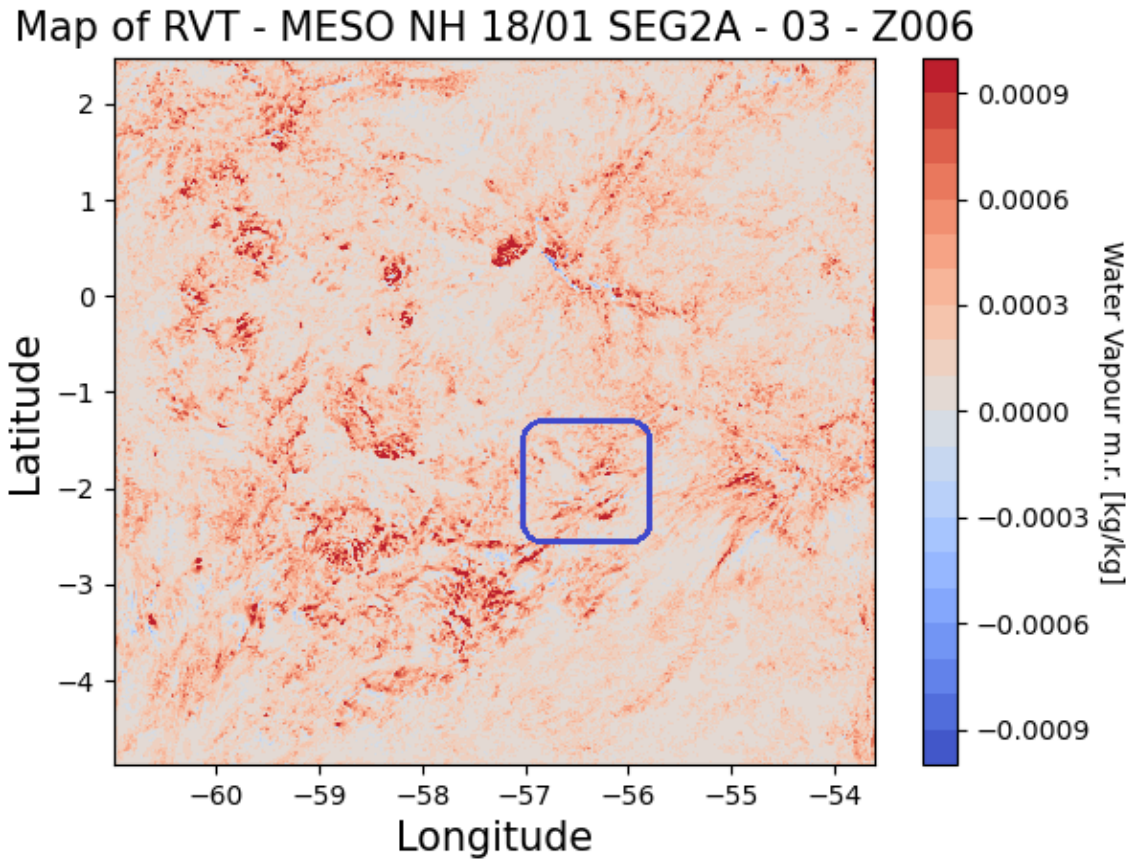

Figure 33: Simulated water vapor mixing ratio map at 86m height, generated by the MesoNH model, at 6:45 UTC, January 18th, 2023. The blue box indicates the region where gravity waves were visually spotted.

5 Conclusion

This study combines multiple measurement data sets from the Amazon Tall Tower Observatory at different heights above and inside the rainforest canopy. Moreover, this study employs the recently established ATTO Campina site, which is equipped with a broad spectrum of radars and in situ measurements. The combination of measurements of the vertical atmospheric and gas profiles and dynamics provides a unique insight into the gas concentration variability in the Amazonian region. Two recent campaigns were used to explore the gas variability: the CloudRoots during the dry season and the CAFE-BRAZIL during the wet season. These campaigns allow us to explore the main features of the dry and wet seasons. This study aims to improve knowledge about the variability of gas concentration during cloud cover events for different cloud types and non-rain events.

Initially, the characteristics of shallow, congestus, and deep clouds were studied. The results were analyzed in two categories: the ones obtained during the CloudRoots campaign (dry season) and the CAFE-BRAZIL campaign (wet season). The results indicate that, in general, these three different cloud types present distinct distributions of the investigated cloud characteristics parameters, which were cloud top height, cloud detection duration, mean vertical velocity of the water droplets in the warm layer, maximum precipitation rate, PWV and day time of the beginning of the detection. A common aspect observed in both campaigns is that Deep clouds have the largest vertical and horizontal extensions (longer detection times), and their water droplets usually fall faster (higher negative vertical velocity values) than the other clouds. These results are reasonable since deep clouds are the ones in the most advanced intensity, reaching, sometimes, the tropopause. Therefore, they should indeed have the biggest extensions, and they are also expected to have the biggest raindrops, which causes their droplets to have the biggest terminal velocities. On the other side of the distributions are the shallow clouds, which are the least developed ones, with the shortest extensions and presenting positive values of droplet mean velocity 9only upward motion). The congestus clouds are situated in the middle of the transition from shallow to deep, as well as their distributions.

Despite a few similarities, there are clear differences between the cloud characteristics analyzed during the dry and the wet season. The differences start with the number of clouds detected in each campaign. During the CloudRoots campaign, only 7 shallow clouds, 32 congestus clouds, and 8 deep clouds were sampled. Meanwhile, during CAFE-BRAZIL, 182 shallow, 148 congestus, and 8 deep clouds were detected. Even though CAFE-BRAZIL lasted for twice as long as CloudRoots, the number of clouds detected during the wet season is much higher than twice the number of clouds detected during the dry season. Consequently, the distributions obtained during the CAFE-BRAZIL hold much more statistical significance than the ones from CloudRoots due to the low number of clouds. It was observed that during the wet season, usually, there is a gradual transition from shallow to deep convection. Shallow clouds are predominant in the morning when the sun comes up. Then, these clouds invigorate until predominant congestus cover is observed in the late morning/ early afternoon. They continue to develop, and in the late afternoon, Deep clouds typically occur. Meanwhile, there are days of shallow and deep cloud conditions during the dry season. On the days in which Deep clouds were observed, the transition was not as smooth as in the wet season, with an abrupt transition from shallow to Deep, and there is no typical time that deep clouds were observed. An in-

teresting factor is a clear distinction in the PWV distribution of the different cloud types. This distinction is not observed during the Wet season. Hence, it can be interpreted as PWV being a crucial factor for activating the transition from shallow to deep during the dry season. However, this does not seem relevant in the wet season as humidity should be abundant all days. Nevertheless, the distribution of the CloudRoots campaign might not be significant to the low cloud population. Hence, a study including more data from the dry season is necessary to confirm whether PWV is a crucial factor in the shallow to deep transition during the dry season. Lastly, results indicate that clouds have a deeper vertical development (higher cloud tops) during the dry season.

After characterizing shallow, congestus, and deep clouds during the dry and wet seasons, the impact of these cloud types on the surface concentrations of trace gases and particles was investigated. The study analyzed the concentrations of CO_2, CO, CH_4, O_3 and BC at 80m, before, during and after the detection of these cloud types. The outcomes of this investigation demonstrated that Deep clouds have the most relevant effect on surface conditions of these parameters. This can be stated since the concentration levels of most of the analyzed gases and particles were the same before and after the detection of shallow and congestus clouds. On the other hand, most of the parameters, but especially CO_2 and O_3, presented clear oscillations during detecting Deep clouds. CO_2 concentrations are highest at the surface and decrease with height, while Ozone levels are lowest at the surface and increase with height. Therefore, variations in the concentrations of these gases should be related to up and downdrafts from Deep clouds. Updrafts should bring air rich in CO_2 from the surface to the 80 m level, causing the CO_2 levels to rise and O_3 to fall. On the other hand, downdrafts should bring air rich in Ozone from higher altitudes to the 80m level, causing O_3 levels to rise and CO_2 fall. To gain further insights on this topic, the deep convection clouds from CAFE-BRAZIL were divided into day and night cases, and their impact on the concentrations of CO_2 and O_3 in different heights was analyzed. After this investigation, it became clear that not only do up and downdrafts play an important role in regulating the concentrations of these gases, but also gust fronts, temperature, and humidity should be considered in causing the variations in the concentration of these gases. In addition, it was demonstrated that the variations of CO_2 under the cloud cover of deep convective clouds are much more pronounced during the night when its concentrations are highest since there is no photosynthesis and the PBL height is lower. Finally, for a detailed investigation on Deep clouds affecting the concentrations of CO_2 and Ozone, a case study was performed on the 14th of August 2022, during the CLoudRoots campaign. The case study demonstrated that it considerably impacts surface weather conditions. In addition a moment of downdraft was identified during the cloud detection, when it was raining, turbulence levels were high and a potential temperature decrease was observed. Simultaneously to the occurrence of the downdraft, a significant increase in O_3 concentrations and a decrease in CO_2 was observed, corroborating the initial hypothesis.

The next part of this study consisted of a general view of significant variations in the concentrations of CO_2, CO, CH_4, O_3, and BC at 80 during the dry and wet seasons.

The findings from the analysis performed during the dry season suggest that besides the few rain events, wind synoptic patterns drive the day-to-day variability of CO and Black Carbon. The ATTO tower is situated in a highly preserved rainforest region. However, during the dry season, the Amazon is marked by intense biomass burning activity in

the region of the arch of deforestation, situated in the southern parts of the Amazon going from the state of Maranhão until Acre. CO and BC are biomass burning tracers, hence the main sources of these compounds at ATTO in this period should be transport of air from the arch of deforestation. This hypothesis was corroborated by the fact that the wind pattern was transporting air from the arch in the direction of ATTO in the first of the only 4 subsequent days of significant variations in CO concentrations during August 2022. In addition, it was observed that during the dry season, the majority of the significant variations among all compounds happened during non-rain days. Also, results indicated that CO_2 and o_3 variations were mostly caused by up and downdrafts.

The results obtained during the wet season were different from the dry season in many aspects. First, it was observed that most of the peaks and oscillations happened simultaneously with rainfall. However, it can not be interpreted for all cases as a relationship of causality since during the wet season, it rains every day, and the variations could be happening simultaneously to rain regardless of it. The only compounds in which the rainfall should indeed cause the variations are CO_2 and especially O_3, as demonstrated by the investigation of the impact of deep clouds on the concentrations of these gases. Regarding the significant variations of BC, Holanda et al. [2023] showed that its main source during the wet season is the long-range transport from biomass burnings in West Africa. It was hypothesized that gravity waves generated by deep convection could play a role in injecting the black carbon present in the Atmospheric rivers at the free troposphere into the planetary boundary layer, and that could be the cause for some of the significant variations of BC during the wet season. This study could not test this hypothesis directly. Still, it used model simulations to gain insight into whether gravity waves can inject air from the free troposphere into the PBL and vice versa, and that analysis will discussed in the next paragraph.

The last part of this study involved using model simulations from MesoNH to investigate the potential role played by gravity waves in the exchange between the free troposphere and the PBL. The model was run on January 18th, a day selected for a future model intercomparison, aiming to evaluate its capability of reproducing the system accurately. In this case, a propagating mesoscale squall line produced gravity waves of around 32 km spatial scale, producing a series of up and down movements changing the water vapor mixing rations inside the PBL.

This study describes the variability of trace gases forced by weather events, demonstrating some processes and creating hypotheses about other potential sources of trace gas variability near the surface. I will evaluate and test this hypothesis during my further studies.

6 Bibliography

References

M. O. Andreae, O. C. Acevedo, A. Araùjo, P. Artaxo, C. G. G. Barbosa, H. M. J. Barbosa, J. Brito, S. Carbone, X. Chi, B. B. L. Cintra, N. F. da Silva, N. L. Dias, C. Q. Dias-Júnior, F. Ditas, R. Ditz, A. F. L. Godoi, R. H. M. Godoi, M. Heimann, T. Hoffmann, J. Kesselmeier, T. Könemann, M. L. Krüger, J. V. Lavric, A. O. Manzi, A. P. Lopes, D. L. Martins, E. F. Mikhailov, D. Moran-Zuloaga, B. W. Nelson, A. C. Nölscher, D. Santos Nogueira, M. T. F. Piedade, C. Pöhlker, U. Pöschl, C. A. Quesada, L. V. Rizzo, C.-U. Ro, N. Ruckteschler, L. D. A. Sá, M. de Oliveira Sá, C. B. Sales, R. M. N. dos Santos, J. Saturno, J. Schöngart, M. Sörgel, C. M. de Souza, R. A. F. de Souza, H. Su, N. Targhetta, J. Tóta, I. Trebs, S. Trumbore, A. van Eijck, D. Walter, Z. Wang, B. Weber, J. Williams, J. Winderlich, F. Wittmann, S. Wolff, and A. M. Yáñez Serrano. The amazon tall tower observatory (atto): overview of pilot measurements on ecosystem ecology, meteorology, trace gases, and aerosols. *Atmospheric Chemistry and Physics*, 15(18):10723–10776, 2015. doi: 10.5194/acp-15-10723-2015. URL `https://acp.copernicus.org/articles/15/10723/2015/`. 1

Evandro M Anselmo, Courtney Schumacher, and Luiz AT Machado. The amazonian low-level jet and its connection to convective cloud propagation and evolution. *Monthly Weather Review*, 148(10):4083–4099, 2020. 4.5

Evandro M Anselmo, Luiz AT Machado, Courtney Schumacher, and George N Kiladis. Amazonian mesoscale convective systems: Life cycle and propagation characteristics. *International Journal of Climatology*, 41(7):3968–3981, 2021. 4.1

Paulo Artaxo, Luciana V. Rizzo, Joel F. Brito, Henrique M. J. Barbosa, Andrea Arana, Elisa T. Sena, Glauber G. Cirino, Wanderlei Bastos, Scot T. Martin, and Meinrat O. Andreae. Atmospheric aerosols in amazonia and land use change: from natural biogenic to biomass burning conditions. *Faraday Discuss.*, 165:203–235, 2013. doi: 10.1039/C3FD00052D. URL `http://dx.doi.org/10.1039/C3FD00052D`. 1

D. Atlas, R. C. Srivastava, and R. S. Sekhon. Doppler radar characteristics of precipitation at vertical incidence. *Reviews of Geophysics*, 11(1):1–35, 1973. doi: https://doi.org/10.1029/RG011i001p00001. URL `https://agupubs.onlinelibrary.wiley.com/doi/abs/10.1029/RG011i001p00001`. 4.1

Roman Bardakov, Joel A Thornton, Ilona Riipinen, Radovan Krejci, and Annica ML Ekman. Transport and chemistry of isoprene and its oxidation products in deep convective clouds. *Tellus B: Chemical and Physical Meteorology*, 73(1):1–21, 2021. 1

Roman Bardakov, Radovan Krejci, Ilona Riipinen, and Annica ML Ekman. The role of convective up-and downdrafts in the transport of trace gases in the amazon. *Journal of Geophysical Research: Atmospheres*, 127(18):e2022JD037265, 2022. 1

Yuval Ben-Ami, Ilan Koren, Yinon Rudich, P Artaxo, ST Martin, and MO Andreae. Transport of north african dust from the bodélé depression to the amazon basin: a case study. *Atmospheric Chemistry and Physics*, 10(16):7533–7544, 2010. 1

Thiago S Biscaro, Luiz AT Machado, Scott E Giangrande, and Michael P Jensen. What drives daily precipitation over the central amazon? differences observed between wet and dry seasons. *Atmospheric Chemistry and Physics*, 21(9):6735–6754, 2021. 4.1

WH Brune, PJ McFarland, Eric Bruning, S Waugh, D MacGorman, DO Miller, JM Jenkins, X Ren, J Mao, and J Peischl. Extreme oxidant amounts produced by lightning in storm clouds. *Science*, 372(6543):711–715, 2021. 1

Micael A Cecchini, Luiz AT Machado, Jennifer M Comstock, Fan Mei, Jian Wang, Jiwen Fan, Jason M Tomlinson, Beat Schmid, Rachel Albrecht, Scot T Martin, et al. Impacts of the manaus pollution plume on the microphysical properties of amazonian warm-phase clouds in the wet season. *Atmospheric Chemistry and Physics*, 16(11):7029–7041, 2016. 1

Sudip Chakraborty, Bin Guan, Duane E Waliser, Arlindo M da Silva, Sophie Uluatam, and Peter Hess. Extending the atmospheric river concept to aerosols: Climate and air quality impacts. *Geophysical Research Letters*, 48(9):e2020GL091827, 2021a. 1

Sudip Chakraborty, Bin Guan, Duane E Waliser, Arlindo M da Silva, Sophie Uluatam, and Peter Hess. Extending the atmospheric river concept to aerosols: Climate and air quality impacts. *Geophysical Research Letters*, 48(9):e2020GL091827, 2021b. 1

Cléo Quaresma Dias-Júnior, Rayonil Gomes Carneiro, Gilberto Fisch, Flávio Augusto F D'Oliveira, Matthias Sörgel, Santiago Botía, Luiz Augusto T Machado, Stefan Wolff, Rosa Maria N dos Santos, and Christopher Pöhlker. Intercomparison of planetary boundary layer heights using remote sensing retrievals and era5 reanalysis over central amazonia. *Remote Sensing*, 14(18):4561, 2022. 4.4.1

G Fisch, John Tota, LAT Machado, Maria Assunção Faus da Silva Dias, RF Da F. Lyra, CA Nobre, AJ Dolman, and JHC Gash. The convective boundary layer over pasture and forest in amazonia. *Theoretical and Applied Climatology*, 78:47–59, 2004. 4.4.1

Marco A Franco, Florian Ditas, Leslie A Kremper, Luiz AT Machado, Meinrat O Andreae, Alessandro Araújo, Henrique MJ Barbosa, Joel F de Brito, Samara Carbone, Bruna A Holanda, et al. Occurrence and growth of sub-50 nm aerosol particles in the amazonian boundary layer. *Atmospheric Chemistry and Physics*, 22(5):3469–3492, 2022. 1

Marco Aurélio de Menezes Franco. *Vertical transport, growth processes, and aerosol characterization in Amazonia*. PhD thesis, Universidade de São Paulo, 2021. 3.1.1

Meredith Galanter, Hiram Levy, and Gregory R Carmichael. Impacts of biomass burning on tropospheric co, no x, and o3. *Journal of Geophysical Research: Atmospheres*, 105 (D5):6633–6653, 2000. 4.3

Luciana V Gatti, Luana S Basso, John B Miller, Manuel Gloor, Lucas Gatti Domingues, Henrique LG Cassol, Graciela Tejada, Luiz EOC Aragão, Carlos Nobre, Wouter Peters, et al. Amazonia as a carbon source linked to deforestation and climate change. *Nature*, 595(7867):388–393, 2021. 1

Scott E Giangrande, Zhe Feng, Michael P Jensen, Jennifer M Comstock, Karen L Johnson, Tami Toto, Meng Wang, Casey Burleyson, Nitin Bharadwaj, Fan Mei, et al. Cloud characteristics, thermodynamic controls and radiative impacts during the observations and modeling of the green ocean amazon (goamazon2014/5) experiment. *Atmospheric Chemistry and Physics*, 17(23):14519–14541, 2017. 3.2.1

Alice Henkes, Gilberto Fisch, Luiz Augusto Toledo Machado, and Jean-Pierre Chaboureau. Morning boundary layer conditions for shallow to deep convective cloud evolution during the dry season in the central amazon. *Atmospheric Chemistry and Physics Discussions*, 2021:1–29, 2021. 1, 4.2

Bruna A Holanda, Mira L Pöhlker, David Walter, Jorge Saturno, Matthias Sörgel, Jeannine Ditas, Florian Ditas, Christiane Schulz, Marco Aurélio Franco, Qiaoqiao Wang, et al. Influx of african biomass burning aerosol during the amazonian dry season through layered transatlantic transport of black carbon-rich smoke. *Atmospheric Chemistry and Physics*, 20(8):4757–4785, 2020. 1, 4.5, 4.5

Bruna A Holanda, Marco A Franco, David Walter, Paulo Artaxo, Samara Carbone, Yafang Cheng, Sourangsu Chowdhury, Florian Ditas, Martin Gysel-Beer, Thomas Klimach, et al. African biomass burning affects aerosol cycling over the amazon. *Communications Earth & Environment*, 4(1):154, 2023. 1, 4.5, 5

IPCC. *Climate Change 2022: Impacts, Adaptation and Vulnerability*. Summary for Policymakers. Cambridge University Press, Cambridge, UK and New York, USA, 2022. ISBN 9781009325844. 1

Izzet Karakurt, Gokhan Aydin, and Kerim Aydiner. Sources and mitigation of methane emissions by sectors: A critical review. *Renewable energy*, 39(1):40–48, 2012. 1

Thomas Karl, A Guenther, A Turnipseed, G Tyndall, Paulo Artaxo, and S Martin. Rapid formation of isoprene photo-oxidation products observed in amazonia. *Atmospheric Chemistry and Physics*, 9(20):7753–7767, 2009. 1

Joachim P. Kuettner, Peter A. Hildebrand, and Terry L. Clark. Convection waves: Observations of gravity wave systems over convectively active boundary layers. *Quarterly Journal of the Royal Meteorological Society*, 113(476):445–467, 1987. doi: https://doi.org/10.1002/qj.49711347603. URL `https://rmets.onlinelibrary.wiley.com/doi/abs/10.1002/qj.49711347603`. 4.6

Christine Lac, Jean-Pierre Chaboureau, Valéry Masson, Jean-Pierre Pinty, Pierre Tulet, Juan Escobar, Maud Leriche, Christelle Barthe, Benjamin Aouizerats, Clotilde Augros, et al. Overview of the meso-nh model version 5.4 and its applications. *Geoscientific Model Development*, 11(5):1929–1969, 2018. 3.2.4, 4.6

L. A. T. Machado, J. Kesselmeier, S. Botia, H. Van Asperen, A. C. de Araújo, P. Artaxo, A. Edtbauer, R. Ferreira, H. Harder, S. Jones, C. Q. Dias-Júnior, G. G. Haytzmann, C. A. Quesada, S. Komiya, J. Lavric, J. Lelieveld, I. Levin, A. Nölscher, E. Pfannerstill, M. Pöhlker, U. Pöschl, A. Ringsdorf, L. Rizzo, A. M. Yáñez Serrano, S. Trumbore, W. I. D. Valenti, J. Vila-Guerau de Arellano, D. Walter,

J. Williams, S. Wolff, and C. Pöhlker. How rainfall events modify trace gas concentrations in central amazonia. *submitted to EGUsphere*, 2024:1–28, 2024. doi: 10.5194/egusphere-2023-2901. URL `https://egusphere.copernicus.org/preprints/2024/egusphere-2023-2901/`. 4.4.1, 4.4.1, 4.4.1, 4.4.2

Luiz A. T. Machado, Gabriela R. Unfer, Sebastien Brill, Stefanie Hildmann, Christopher Pöhlker, Yafang Cheng, Jonathan Williams, Harder Hartwig, Meinrat O. Andreae, Paulo Artaxo, Joachim Curtius, Marco A. Franco, Micael A. Cecchini, Achim Edtbauer, Thorsten Hoffmann, Bruna Holanda, Théodore Khadir, Radovan Krejci, Leslie A. Kremper, Yunfan Liu, Bruno B. Meller, Mira L. Pöhlker, Carlos A. Quesada, Akima Ringsdorf, Ilona Riipinen, Susan Trumbore, Stefan Wolff, Jos Lelieveld, and Ulrich Pöschl. Frequent nanoparticle bursts in the amazon rainforest. *submitted to Nature*, 2023. 4.4.1

Luiz AT Machado, Alan JP Calheiros, Thiago Biscaro, Scott Giangrande, Maria AF Silva Dias, Micael A Cecchini, Rachel Albrecht, Meinrat O Andreae, Wagner F Araujo, Paulo Artaxo, et al. Overview: Precipitation characteristics and sensitivities to environmental conditions during goamazon2014/5 and acridicon-chuva. *Atmospheric Chemistry and Physics*, 18(9):6461–6482, 2018a. 1, 4.1

Luiz AT Machado, Alan JP Calheiros, Thiago Biscaro, Scott Giangrande, Maria AF Silva Dias, Micael A Cecchini, Rachel Albrecht, Meinrat O Andreae, Wagner F Araujo, Paulo Artaxo, et al. Overview: Precipitation characteristics and sensitivities to environmental conditions during goamazon2014/5 and acridicon-chuva. *Atmospheric Chemistry and Physics*, 18(9):6461–6482, 2018b. 4.1

Luiz AT Machado, Marco A Franco, Leslie A Kremper, Florian Ditas, Meinrat O Andreae, Paulo Artaxo, Micael A Cecchini, Bruna A Holanda, Mira L Pöhlker, Ivan Saraiva, et al. How weather events modify aerosol particle size distributions in the amazon boundary layer. *Atmospheric Chemistry and Physics*, 21(23):18065–18086, 2021. 1

Luiz Augusto T Machado and Henri Laurent. The convective system area expansion over amazonia and its relationships with convective system life duration and high-level wind divergence. *Monthly weather review*, 132(3):714–725, 2004. 4.1

Yadvinder Malhi, Daniel Wood, Timothy R Baker, James Wright, Oliver L Phillips, Thomas Cochrane, Patrick Meir, Jerome Chave, Samuel Almeida, Luzmilla Arroyo, et al. The regional variation of aboveground live biomass in old-growth amazonian forests. *Global Change Biology*, 12(7):1107–1138, 2006. 1

Scot T Martin, Paulo Artaxo, Luiz Augusto Toledo Machado, Antônio Ocimar Manzi, Rodrigo Augusto Ferreira de Souza, C Schumacher, Jian Wang, Meinrat O Andreae, HMJ Barbosa, J Fan, et al. Introduction: observations and modeling of the green ocean amazon (goamazon2014/5). *Atmospheric Chemistry and Physics*, 16(8):4785–4797, 2016. 1

Wiro Maria Liduina Meijninger. *Surface fluxes over natural landscapes using scintillometry*. Wageningen University and Research, 2003. 3.1.4

Janaina P Nascimento, Henrique MJ Barbosa, Alessandro L Banducci, Luciana V Rizzo, Angel Liduvino Vara-Vela, Bruno B Meller, Helber Gomes, Andre Cezar, Marco A Franco, Milena Ponczek, et al. Major regional-scale production of o3 and secondary organic aerosol in remote amazon regions from the dynamics and photochemistry of urban and forest emissions. *Environmental Science & Technology*, 56(14):9924–9935, 2022. 1

Carlos Afonso Nobre, Diane Wickland, and Pavel Kabat. The large scale biosphere-atmosphere experiment in amazonia (lba). *Concise Experimental Plan. INPE, C. Paulista, SP, Brazil*, 1996. 1

HG Ouwersloot, J Vilà-Guerau de Arellano, BJ H. van Stratum, MC Krol, and J Lelieveld. Quantifying the transport of subcloud layer reactants by shallow cumulus clouds over the amazon. *Journal of Geophysical Research: Atmospheres*, 118(23):13–041, 2013. 1

Mira L Pöhlker, Florian Ditas, Jorge Saturno, Thomas Klimach, Isabella Hrabě de Angelis, Alessandro C Araùjo, Joel Brito, Samara Carbone, Yafang Cheng, Xuguang Chi, et al. Long-term observations of cloud condensation nuclei over the amazon rain forest–part 2: Variability and characteristics¡? xmltex\break?¿ of biomass burning, long-range transport, and pristine¡? xmltex\break?¿ rain forest aerosols. *Atmospheric Chemistry and Physics*, 18(14):10289–10331, 2018. 1

VLRD Ramanathan, RD Cess, EF Harrison, P Minnis, BR Barkstrom, E Ahmad, and D Hartmann. Cloud-radiative forcing and climate: Results from the earth radiation budget experiment. *Science*, 243(4887):57–63, 1989. 1

Eneas Salati, Attilio Dall'Olio, Eiichi Matsui, and Joel R Gat. Recycling of water in the amazon basin: an isotopic study. *Water resources research*, 15(5):1250–1258, 1979. 1

Gilvan Sampaio, Carlos Nobre, Marcos Heil Costa, Prakki Satyamurty, Britaldo Silveira Soares-Filho, and Manoel Cardoso. Regional climate change over eastern amazonia caused by pasture and soybean cropland expansion. *Geophysical Research Letters*, 34 (17), 2007. 1

Luiz F Sapucci, Luiz AT Machado, Eniuce Menezes de Souza, and Thamiris B Campos. Global p ositioning s ystem precipitable water vapour (gps-pwv) jumps before intense rain events: A potential application to nowcasting. *Meteorological Applications*, 26(1): 49–63, 2019. 4.2

Thomas F Stocker, Dahe Qin, Gian-Kasper Plattner, M Tignor, Simon K Allen, Judith Boschung, Alexander Nauels, Yu Xia, Vincent Bex, and Pauline M Midgley. Climate change 2013: The physical science basis. Technical report, 2013. 1535 pp. 1

Gabriela Rosalino Unfer. An observational study about aerosols and their mutual interactions with cloud components in the atto/amazon region. Master's thesis, Instituto Nacional de Pesquisas Espaciais (INPE), São José dos Campos, 2023. URL `http://urlib.net/ibi/8JMKD3MGP3W34T/48T8J9S`. 3.1.3

J Vilà-Guerau de Arellano, Xuemei Wang, X Pedruzo-Bagazgoitia, Martin Sikma, Anna Agustí-Panareda, Souhail Boussetta, Gianpaolo Balsamo, LAT Machado, T Biscaro, P Gentine, et al. Interactions between the amazonian rainforest and cumuli clouds: A large-eddy simulation, high-resolution ecmwf, and observational intercomparison study. *Journal of Advances in Modeling Earth Systems*, 12(7):e2019MS001828, 2020. 1

J. Vila-Guerau de Arellano, O. K. Hartogensis, H. de Boer, R. Moonen, R. Gonzalez Armas, M. Janssens, G. A. Adnew, D. J. Bonell Fontas, S. Botía, S. P. Jones, H. van Asperen, S. Komiya, V. S. de Feiter, D. Rikkers, S. de Haas, L. A. T. Machado, C. Q. Dias-Junior, G. Giovanelli Haytzmann, W. I. D. Valenti, R. C. Figueiredo, C. S. Farias, D. H. Hall, A. C. S. Mendonça, F. A. G. da Silva, J. L. Marton da Silva, R. Souza, G. Martins, J. N. Miller, W. B. Mol, B. Heusinkveld, C. C. van Heerwaarden, F. A. F. D'Oliveira, R. R. Ferreira, R. Acosta Gotuzzo, G. Pugliese, J. Williams, A. Ringsdorf, A. Edtbauer, C. A. Quesada, B. Takeshi Tanaka Portela, E. Gomes Alves, C. Pohlker, S. Trumbore, J. Lelieveld, and T. Rockmann. Cloudroots-amazon22: Integrating clouds with photosynthesis by crossing scales. *submitted to Bulletin of the American Meteorological Society*, 2024. 3.1.5, 3.2.2, 4.3, 4.4.2

RL Walterscheid, G Schubert, and DG Brinkman. Small-scale gravity waves in the upper mesosphere and lower thermosphere generated by deep tropical convection. *Journal of Geophysical Research: Atmospheres*, 106(D23):31825–31832, 2001. 1

Manfred Wendisch, Ulrich Pöschl, Meinrat O Andreae, Luiz AT Machado, Rachel Albrecht, Hans Schlager, Daniel Rosenfeld, Scot T Martin, Ahmed Abdelmonem, Armin Afchine, et al. Acridicon–chuva campaign: Studying tropical deep convective clouds and precipitation over amazonia using the new german research aircraft halo. *Bulletin of the American Meteorological Society*, 97(10):1885–1908, 2016. 1

E Williams, D Rosenfeld, N Madden, J Gerlach, N Gears, L Atkinson, N Dunnemann, G Frostrom, M Antonio, B Biazon, et al. Contrasting convective regimes over the amazon: Implications for cloud electrification. *Journal of Geophysical Research: Atmospheres*, 107(D20):LBA–50, 2002. 4.1

J Winderlich, H Chen, A Höfer, C Gerbig, T Seifert, O Kolle, C Kaiser, JV Lavrič, and M Heimann. Continuous low-maintenance co 2/ch 4/h 2 o measurements at the zotino tall tower observatory (zotto) in central siberia. *Atmospheric Measurement Techniques Discussions*, 3(2):1399–1437, 2010. 3.1.2

Hongbin Yu, Mian Chin, Tianle Yuan, Huisheng Bian, Lorraine A Remer, Joseph M Prospero, Ali Omar, David Winker, Yuekui Yang, Yan Zhang, et al. The fertilizing role of african dust in the amazon rainforest: A first multiyear assessment based on data from cloud-aerosol lidar and infrared pathfinder satellite observations. *Geophysical Research Letters*, 42(6):1984–1991, 2015. 1

Xuebin Zhang, Hui Wan, Francis W Zwiers, Gabriele C Hegerl, and Seung-Ki Min. Attributing intensification of precipitation extremes to human influence. *Geophysical Research Letters*, 40(19):5252–5257, 2013. 1

Yizhou Zhuang, Rong Fu, José A Marengo, and Hongqing Wang. Seasonal variation of shallow-to-deep convection transition and its link to the environmental conditions over the central amazon. *Journal of Geophysical Research: Atmospheres*, 122(5):2649–2666, 2017. 1

7 Appendix

A typical cloud classification during the wet season is well represented by Figure 34. In the morning, particularly between 8:00 am and 12:00 pm, shallow clouds are present. The altitude of their cloud bases is rising throughout this period. This process reflects the ascending PBL during the morning hours, attributed to the warming of this atmospheric layer by the sun's radiation. In the early afternoon (12:00 - 15:00), Congestus clouds are predominant. In this period, water droplets are continuously detected from the cloud tops until the ground, which at first sight might suggest that the cloud is raining or that there is a fog event. This phenomenon is common in the region during the morning but not in the afternoon . The correct interpretation of the droplets being detected until the ground height is the presence of rain in these clouds. Another phenomenon observed in this period is the increasing cloud top height caused by convection, boosted by the sun. In the late afternoon 16:00, there is a Deep convection cloud, representing the final stage of the life cycle of a convective cloud. In the Deep cloud is the presence of rain, like in the congestus observed earlier. It can be seen several white spots in the middle of the cloud are caused by signal attenuation due to severe rain, usually associated with deep convection clouds.

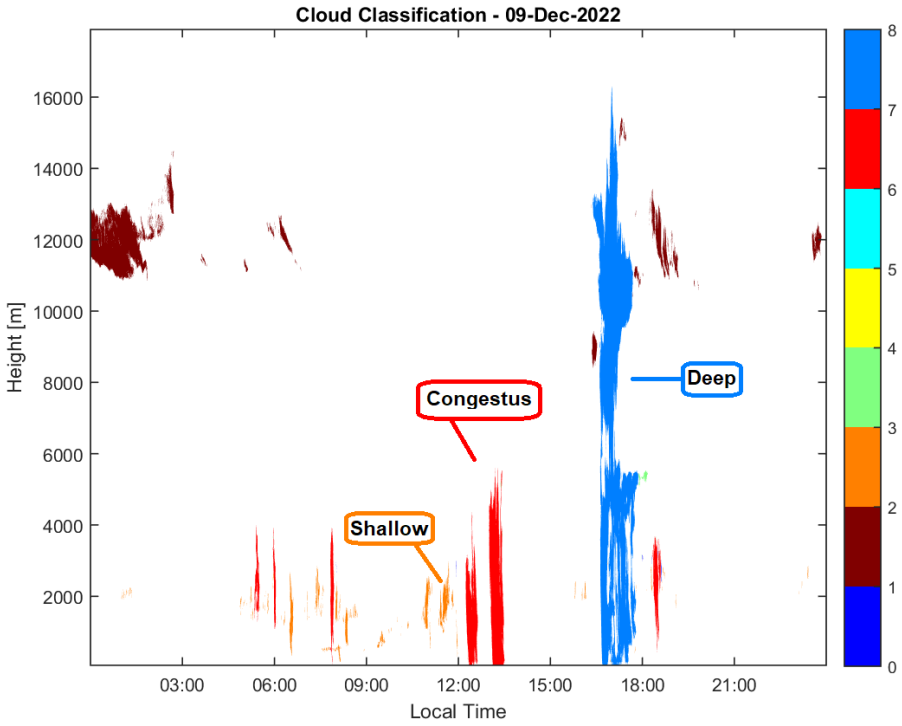

Figure 34: Cloud classification on December 9th, 2022, during the CAFE-BRAZIL campaign at the Campina site.

During the dry season, there is not a clear convection pattern, such as in the wet period. On the one hand, there are days in which no clouds are observed, on the other hand there are days when the same convection pattern from the wet season is observed.

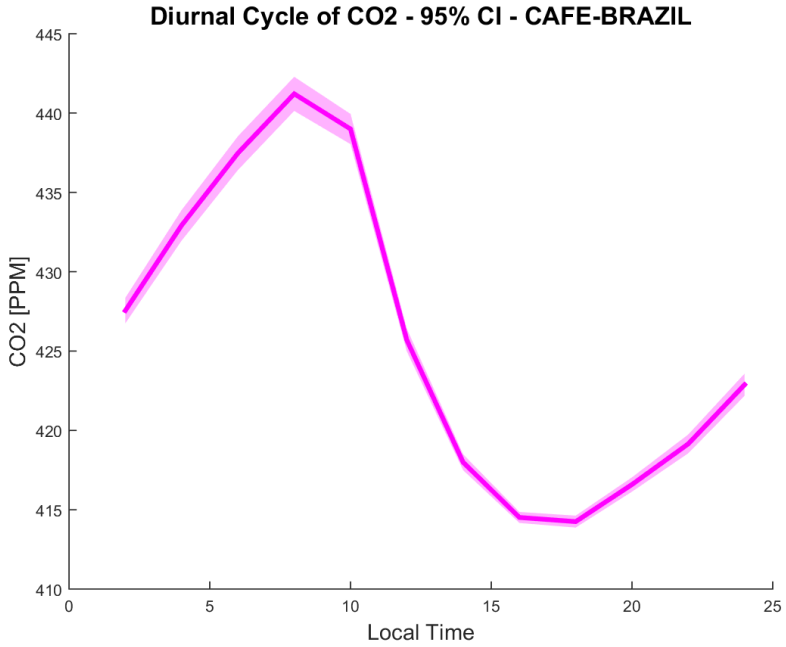

Figure 35: Diurnal cycle of CO_2 calculated during the CAFE-BRAZIL campaign.

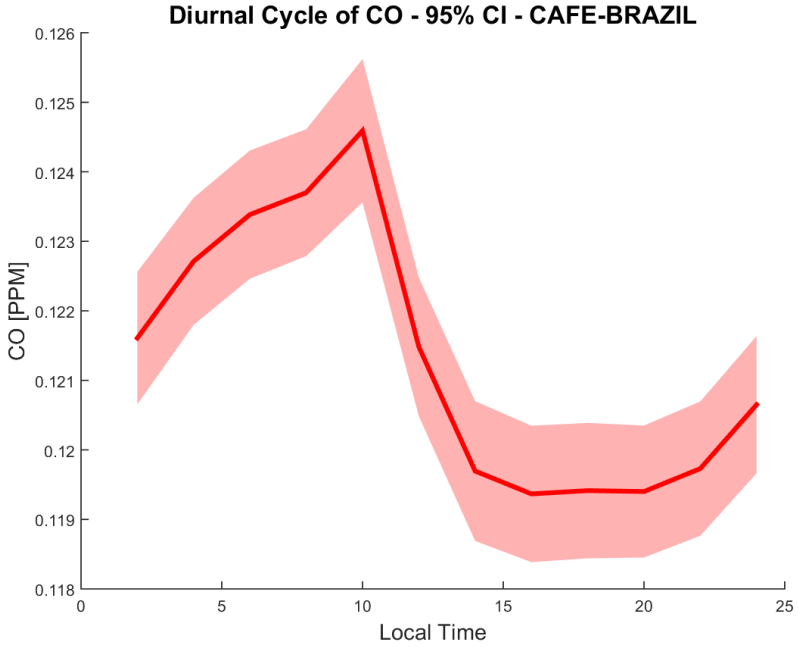

Figure 36: Diurnal cycle of CO calculated during the CAFE-BRAZIL campaign.

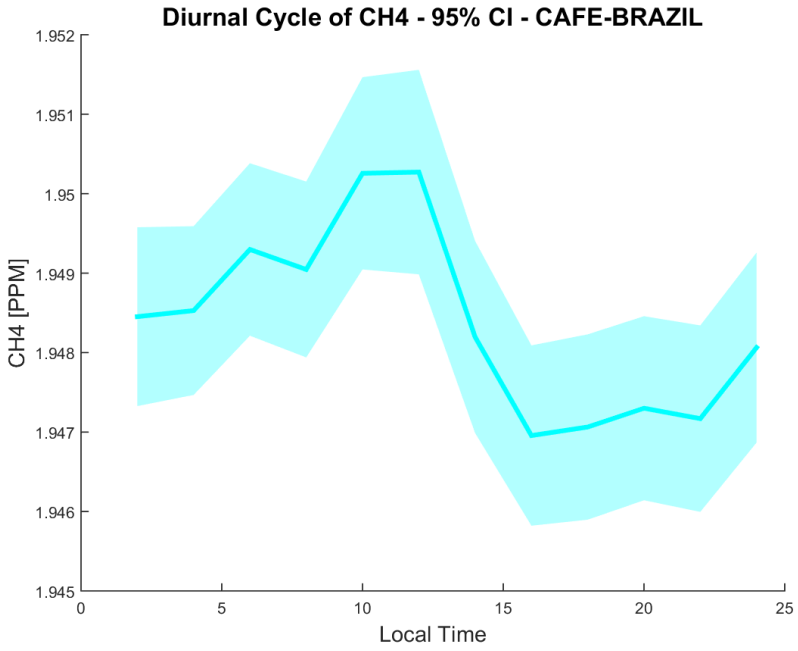

Figure 37: Diurnal cycle of CH_4 calculated during the CAFE-BRAZIL campaign.

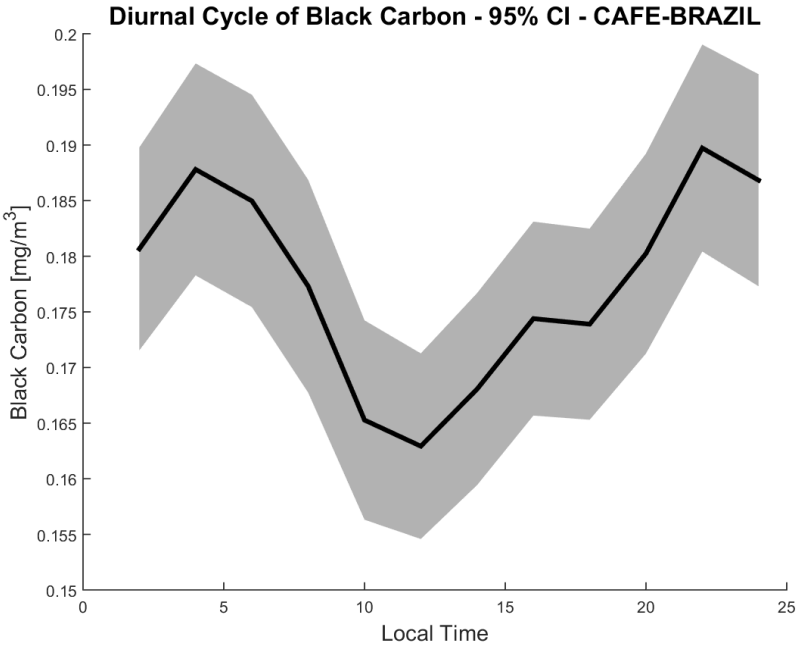

Figure 38: Diurnal cycle of black carbon calculated during the CAFE-BRAZIL campaign.

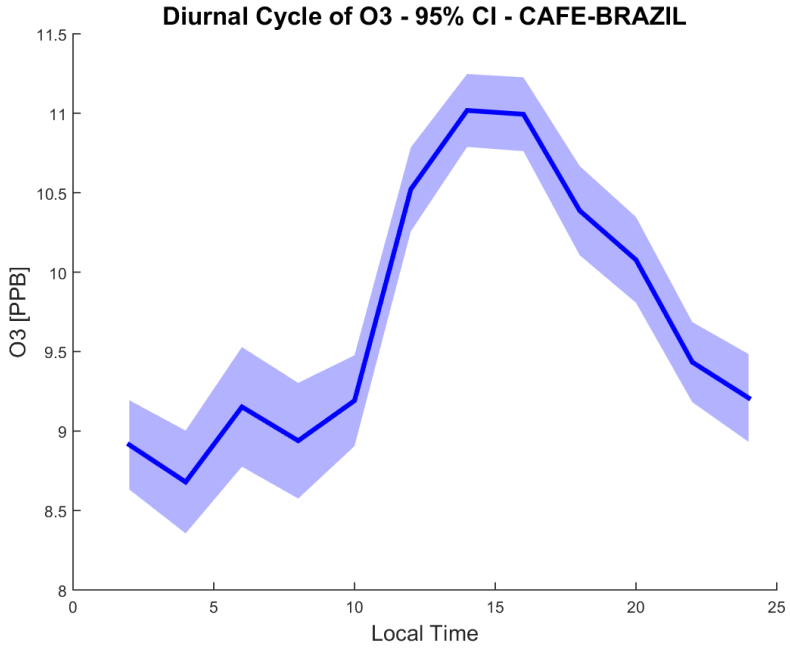

Figure 39: Diurnal cycle of O_3 calculated during the CAFE-BRAZIL campaign.